



UNIVERSITY OF BIRMINGHAM

PERFORMANCE OF FUEL CELLS A STUDY ON IP-SOFC AND DMFC

BY

ANTONY DAVID MEADOWCROFT

Thesis submitted in accordance with the requirements of
The University of Birmingham for the degree of
MASTER OF RESEARCH

School of Chemical Engineering
College of Engineering and Physical Sciences
University of Birmingham
September 2010

UNIVERSITY OF
BIRMINGHAM

University of Birmingham Research Archive

e-theses repository

This unpublished thesis/dissertation is copyright of the author and/or third parties. The intellectual property rights of the author or third parties in respect of this work are as defined by The Copyright Designs and Patents Act 1988 or as modified by any successor legislation.

Any use made of information contained in this thesis/dissertation must be in accordance with that legislation and must be properly acknowledged. Further distribution or reproduction in any format is prohibited without the permission of the copyright holder.

2.1.2	Cathode.....	20
2.1.2.1	LSM or New Material.....	20
2.1.3	Interconnects.....	21
2.1.3.1	Metal.....	22
2.1.3.2	Ceramic.....	23
2.2	SOFC Degradation.....	24
2.2.1	SOFC Losses from theoretical efficiency.....	24
2.2.2	SOFC Accelerated Aging.....	25
3	IP-SOFC.....	29
3.1	Project Aims.....	29
3.2	Experimental.....	29
3.2.1	Durability testing.....	31
3.3	Results.....	32
3.4	Analysis and conclusions.....	32
4	DMFC- Jenny 600S.....	36
4.1	Introduction.....	36
4.2	Project Aims.....	36
4.3	Experimental.....	36
4.3.1	Conditions Testing.....	37
4.3.2	Signature testing.....	40

CONTENTS

1	Introduction.....	1
1.1	Global Warming.....	1
1.1.1	CO ₂ Emissions.....	1
1.1.2	Government Targets.....	2
1.2	Power Generation.....	2
1.2.1	Power Plants.....	2
1.2.2	Renewables.....	3
1.2.3	Fuel Cells.....	4
1.2.3.1	Current Fuel Cell Technology.....	5
1.2.3.2	SOFC.....	6
1.2.3.2.1	IP-SOFC.....	7
1.2.3.3	DMFC.....	9
2	SOFC Literature Review.....	13
2.1	SOFC Materials.....	13
2.1.1	Anode.....	13
2.1.1.1	Pure Metallic.....	15
2.1.1.2	Yttria stabilised zirconia – nickel anodes.....	16
2.1.1.3	Ceria-rare earth anodes.....	19

4.4	Results.....	42
4.5	Analysis	42
4.6	Conclusions	47
5	Project Summation	50
5.1	Industrial Relevance.....	50
5.2	Presentation of Findings	51
5.2.1	Conferences	51
5.2.2	Reports.....	51
6	References	52
7	Appendices	i
7.1	Appendix i – IP-SOFC.....	i
7.1.1	Test Conditions	i
7.1.2	Power output	ii
7.1.3	I-V and Power Curves.....	iii
7.2	Appendix ii –DMFC.....	v
7.2.1	– Voltage response to load	v
7.2.2	Thermal response to load	xiv
7.2.3	Thermal imaging	xxii
7.2.4	Acoustic signature.....	xxviii
7.2.5	Fuel consumption	xxx

7.2.5.1	Regular Fuel, Steady State, Ambient Conditions.....	xxx
7.2.5.2	Desert Fuel, Steady State, Ambient Conditions	xxxi
7.2.5.3	Steady state, ambient conditions, Fuel Comparison.....	xxxi
7.2.5.4	Regular Fuel, Transient State.....	xxxiii
7.2.5.5	Regular Fuel, Idle State, Ambient Conditions.....	xxxiii
7.3	Appendix iii –Poster	xxxiv

TABLE OF FIGURES

Figure 1-i Rolls Royce IP-SOFC manufacture and bundling [22]	7
Figure 1-ii Rolls Royce IP-SOFC tube with anode gas manifold	7
Figure 1-iii Schematic of IP-SOFC operation	8
Figure 1-iv Schematic of DMFC	9
Figure 2-i Porosity of Ni-YSZ anodes, related to initial cermet porosity [46].....	17
Figure 2-ii Anode conductivity by nickel content [43]	18
Figure 2-iii Characteristic IV Curve, showing characteristic losses	25
Figure 3-i Reduction technique used for tube 1	30
Figure 3-ii Reduction technique used for tube 2	30
Figure 4-i. Experimental set up for environmental testing.	38
Figure 4-ii. Experimental set up for altitude testing (pressure).	39
Figure 7-i Test conditions for IP-SOFC over test lifetime.....	i
Figure 7-ii Power output from tube 2 at 1A over 801 hours	ii
Figure 7-iii “Smoothed” power output from tube 2 at 1A over 801 hours	ii
Figure 7-iv IV and power curves for tube 1. From left to right downward sloping lines use left axis, upwards sloping lines use right axis.	iii

Figure 7-v IV and power curves for tube 2. From left to right downward sloping lines use left axis, upwards sloping lines use right axis.	iii
Figure 7-vi IV and power curves for tube 2. From left to right downward sloping lines use left axis, upwards sloping lines use right axis.	iv
Figure 7-vii Highlighting the difference in voltage at maximum current density in tube 2	iv
Figure 7-viii. Voltage response to 5W AT AH	v
Figure 7-ix. Voltage response to 15W, AT AH, over 2 hours.	vi
Figure 7-x. Voltage to response 25W AT AH, over 2 hours.	vi
Figure 7-xi. Voltage to response Transient cycle AT AH, over 2 hours.....	vii
Figure 7-xii. Voltage to response when idle AT AH, over 20 hours.	vii
Figure 7-xiii. Voltage to response to 25W, AT AH, over 2 hours, using desert fuel.	viii
Figure 7-xiv. Voltage to response to 15W, AT AH, over 2 hours, using desert fuel.	viii
Figure 7-xv. Voltage to response to 5W, AT AH, over 2 hours, using desert fuel.	ix
Figure 7-xvi. Voltage to response to 10W, 25W, and idle, AT LH, over 12 hours.....	ix
Figure 7-xvii. Voltage to response to transient cycle, AT LH, over 10 hours.	x
Figure 7-xviii. Voltage to response to transient cycle, AT LH, over 2 hours.	x
Figure 7-xix. Voltage to response to 5W, 15W and 25W, AT HH, over 10 hours.	xi
Figure 7-xx. Voltage to response to transient cycle, AT HH, over 8 hours.	xi

Figure 7-xxi. . Voltage to response to 25W, 15W and 5W, HT LH, over 3 hours. Using desert fuel.	xii
Figure 7-xxii. . Voltage output when idle, HT LH, over 17 hours. Using desert fuel.....	xii
Figure 7-xxiii. Voltage to response to transient cycle, HT HH, over 20 hours. Using desert fuel.	xiii
Figure 7-xxiv. Voltage to response to 5W and 15W, HA2500 (pressure), over 2 hours.....	xiii
Figure 7-xxv. Voltage response to 25W, HA2500, over 15 minutes.....	xiv
Figure 7-xxvi. Voltage response to 25W, HA4000, over 15 minutes.	xiv
Figure 7-xxvii. Thermal response to load at 25W, AT AH, over 2 hours.....	xv
Figure 7-xxviii. Thermal response to load at 15W, AT AH, over 2 hours.	xv
Figure 7-xxix. Thermal response to load at 5W, AT AH, over 2 hours.....	xvi
Figure 7-xxx. Thermal response to transient cycle, AT AH, over 28 hours.....	xvi
Figure 7-xxxi. Thermal response to transient cycle, AT AH, over 2 hours.	xvii
Figure 7-xxxii. Thermal response when idle, AT AH, over 20 hours.	xvii
Figure 7-xxxiii. Thermal response to load at 25W, AT AH, over 2 hours. Using desert fuel..	xviii
Figure 7-xxxiv. Thermal response to load at 15W, AT AH, over 2 hours. Using desert fuel..	xviii
Figure 7-xxxv. Thermal response to load at 5W, AT AH, over 2 hours. Using desert fuel.....	xix
Figure 7-xxxvi. Thermal response to load at 10W, 25W and idle, AT LH, over 12 hours.	xix

Figure 7-xxxvii. Thermal response to transient cycle, AT LH, over 2 hours..... xx

Figure 7-xxxviii. Thermal response to load at 5W, 15W and 25W, AT HH, over 10 hours. See Figure 7-xix..... xx

Figure 7-xxxix. Thermal response to transient cycle, AT HH, over 8 hours. xxi

Figure 7-xl. Thermal response to load at 25W, 15W and 5W, HT LH, over 4 hours. Using desert fuel. See Figure 7-xxi..... xxi

Figure 7-xli. Thermal response when idle, HT LH, over 20 hours. Using desert fuel..... xxii

Figure 7-xlii. Thermal response to transient cycle, HT HH, over 20 hours. Using desert fuel. xxii

Figure 7-xliii. Thermal image of Jenny 600S before application of load.....xxiii

Figure 7-xliv. Thermal image showing peak temperature of Jenny 600S after application of 5W.....xxiv

Figure 7-xlv. Thermal image showing peak temperature of Jenny 600S after application of 15W.....xxv

Figure 7-xlvi. Thermal image showing peak temperature of Jenny 600S after application of 25W. (Orientation 1).....xxvi

Figure 7-xlvii. Thermal image showing peak temperature of Jenny 600S after application of 25W. (Orientation 2).....xxvii

Figure 7-xlviii. Thermal image showing Jenny 600S as thermally invisible after cooling. ...xxviii

Figure 7-xlix. Sound levels recorded for background and Jenny 600Sxxix

Figure 7-l. Sound levels recorded for background and calculated for Jenny 600S.xxix

Figure 7-li. Sound levels calculated for Jenny 600S with background noise set as baseline..xxx

Figure 7-lii. Hourly volumetric consumption of fuel. Desert fuel consumption measured 2 ways.xxxii

Figure 7-liii. Volumetric consumption of fuel per kilowatt hour. Desert fuel consumption measured 2 ways.xxxii

Figure 7-liv. Volumetric consumption of pure methanol per kilowatt hour. Desert fuel consumption measured 2 ways.xxxiii

TABLE OF TABLES

Table 1-1. Electricity produced from renewable energy in the UK [9].....	4
Table 1-2. The 6 types of fuel cells and their component parts (most common)	5
Table 4-1. Definition of HA2500 (pressure)	39
Table 4-2. Definition of depleted oxygen altitude simulation	39
Table 4-3. Testing modes evaluated for voltage output	40
Table 4-4. Testing modes with measured thermal signature.....	41
Table 4-5. Test conditions and modes evaluated for fuel consumption	42
Table 4-6. Rough average temperature (excl purge) when active.	45
Table 7. Regular fuel consumption in ambient conditions.....	xxx
Table 8. Desert fuel consumption in ambient conditions	xxxi
Table 9. Conversion of desert fuel consumption into pure methanol consumption.	xxxi
Table 10. Comparison of energetic efficiencies of regular and desert fuels	xxxi
Table 11. Regular fuel consumption in transient state	xxxiii
Table 12. Regular fuel consumption when idle	xxxiii

NON DISCLOSURE

The work carried out on the DMFC unit, Jenny 600S, was done as part of a confidential work agreement with industry. This document should be in no way reproduced or circulated.

ABSTRACT

As the effects of climate change are increasingly recognised interest has been renewed in the development of clean electricity generation methods. The Solid oxide fuel cell, (SOFC) offers electrical conversion at up to 60% efficiency making it a desirable technology. Rolls Royce Fuel Cell Systems (RRFCS) is one company currently researching and developing SOFC for power generation on the MW scale. The RRFCS SOFC has unique geometry amongst fuel cells. Two RRFCS SOFC tubes have been studied for degradation utilising differing reduction technique. It has been found that deviating from a standard reduction profile alters the performance of the fuel cell.

Direct methanol fuel cells (DMFC) are being developed for the replacement or charging of batteries. Their advantage is using methanol as a fuel which is both more convenient than hydrogen and more energy dense than lithium ion batteries. One of the companies currently developing DMFC, smart fuel cell (SFC) has developed DMFC solutions for the recreational vehicle market. As well as leisure solutions military units have been developed, one such unit, Jenny 600S has been assessed for use in the field and results are presented in this thesis.

ACKNOWLEDGEMENTS

The following people merit acknowledgement for their contributions.

- My Supervisor, Waldemar Bujalski
- Bruno Pollet
- Kevin Kendall
- Richard Greenwood
- Artur Majewski
- Aman Dhir
- John Wedderburn
- All those at the centre for hydrogen and fuel cell research
- Anna & Robert Meadowcroft

DEFINITION OF ACRONYMS

Acronym	Definition
CCS	Carbon Capture And Storage
SOFC	Solid Oxide Fuel Cell
IP-SOFC	Integrated Planar Solid Oxide Fuel Cell
mT-SOFC	Micro Tubular Solid Oxide Fuel Cell
MCFC	Molten Carbonate Fuel Cell
PAFC	Phosphoric Acid Fuel Cell
PEMFC	Proton Exchange Membrane Fuel Cell
GM	General Motors
DMFC	Direct Methanol Fuel Cell
APU	Auxiliary Power Unit
MEA	Membrane Electrode Assembly
YSZ	Yttria Stabilised Zirconia
LSM	Strontium Doped Lanthanum Manganate
DOT	Department Of Transport
BOP	Balance Of Plant
TPB	Triple Phase Boundary
CTE	Coefficient Of Thermal Expansion
LSGM	Lanthanum Strontium Gadolinium Manganate
EMF	Electromotive Force
UPS	Uninterruptible Power Supply
OCV	Open Circuit Voltage
AMI	Advanced Measurements Incorporated
GDUK	General Dynamics United Kingdom
UOB	University Of Birmingham
SFC	Smart Fuel Cell
AT	Ambient Temperature
HT	High Temperature
RH	Relative Humidity
AH	Ambient Humidity
HH	High Humidity
LH	Low Humidity
HA2500	High Altitude (2500 M)
HA4000	High Altitude (4000 M)
DI	De Ionised

1 INTRODUCTION

1.1 Global Warming

1.1.1 CO₂ Emissions

Global warming is now considered a scientific fact; whilst some still dispute the key causes of global warming it is the consensus of the scientific community that global warming is a man made phenomenon [1]. The cause of the temperature increases lies with the introduction of greenhouse gasses into the atmosphere. Most famous of these greenhouse gasses is carbon dioxide; however other compounds such as methane, and surprisingly water have a larger warming effect per molecule than carbon dioxide [2]. The excess level in the atmosphere of these three molecules comes directly from the combustion of fossil fuels. Globally a natural cycle ensures that the level of carbon above ground is moderated, however this cycle takes hundreds of thousands of years to self moderate, the mining and burning of fossil fuels is done at a rate far faster than carbon sequestration. The use of fossil fuels releases green house gasses CO₂ and H₂O in roughly equal amounts, and to lesser extent lower hydrocarbons such as methane and ethane. The water released by use of fossil fuel is often overlooked because the water cycle is seen to be responsive, as the atmosphere has saturation limits for water. The CO₂ however is a problem, research, especially in Mauna Loa, over the last 50 years has shown a marked increase of atmospheric CO₂ levels whilst other studies have shown an increase in global temperature [3]. The importance of the research is twofold, firstly the length

of the study, and secondly, the location, Mauna Loa is found in the central pacific, possibly as far away from an industrial city as is possible in a non-polar location. The upward trend in CO₂ here shows that the effect is truly global.

1.1.2 Government Targets

As the damage to the environment from greenhouse gas emissions was acknowledged by an increasing number of scientists, activists and politicians action began to be taken. The Kyoto agreement was made between 187 nations. This agreement saw industrialised member nations agree to cut CO₂ levels by 5.2% of 1990 levels by 2010 [4]. Now the agreement is coming to a close and many individual nations are looking to reduce their CO₂ emissions of their own accord, the UK for instance plans to cut CO₂ levels by 80 % by 2050 [5].

1.2 Power Generation

As the UK had seen a dramatic decline in industry the CO₂ contributions have steadily fallen from this sector, leaving transportation and power generation as the biggest contributors to CO₂ emissions. There is currently a large incentive to look towards technologies that reduce the carbon footprint in both of these sectors; this report however will focus on the power generation side of the problem.

1.2.1 Power Plants

The power profile of the UK currently sees the majority of our power being produced from fossil fuels, through coal and gas power stations [6]. Coal and gas fired power stations tend to have efficiencies in the region of 30-50 % and emit CO₂ at a rate of 4.4 g / kWh (midpoint coal and gas) [7]. If the UK is to reach the 80% cuts in CO₂

emission by 2050, then it is clear that a radical rethink on the countries power source must be implemented. The system which least affects the national power infrastructure is to simply “clean up” these plants, using systems such as carbon capture and storage (CCS). CCS works by harvesting CO₂ from the exhaust of the power station, this CO₂ is then stored indefinitely, with most plans utilising underground geological traps [8].

A more pressing issue for the UK government than the carbon footprint of our fossil fuel fired power plants is the energy supply and security. As the UK is no longer a net exporter of fossil fuels, we must now depend on the supply of these fuels from other countries. Most oil and gas is produced in politically unstable regions, vastly reducing the security of the supply.

The combination of a commitment to CO₂ reduction and the security of the fuel supply create a situation where the viability of coal and gas power plants is increasingly low. Governments and energy suppliers, the world over are now looking more seriously at alternative sources.

1.2.2 Renewables

The renewable sector makes up only 3.0% of all UK power usage. However in electricity production this percentage is much higher, at 6.6%. Of this there are 3 main sectors, biomass, hydroelectric and wind. Table 1-1 shows how the use of renewable has increased over the last four years [9].

Table 1-1. Electricity produced from renewable energy in the UK [9].

	GWh				
	2005	2006	2007	2008	2009
Generation : Renewables Obligation basis					
Wind:					
Onshore (1)	2,501	3,574	4,491	5,792	7,564
Offshore (2)	403	651	783	1,305	1,740
Solar photovoltaics	8	11	14	17	20
Hydro:					
Small scale (1)	444	478	534	568	598
Other hydro including refurbished large scale	1,542	1,969	1,912	1,926r	2,016
Biomass:					
Landfill gas	4,290	4,424	4,677	4,757	4,952
Sewage sludge digestion	466r	447r	502r	547r	638
Co-firing with fossil fuels	2,533	2,528	1,956	1,613	1,806
Animal Biomass (3)	468	434	555	587	620
Plant Biomass (4)	382	363	409	568	1,109
Total biomass	8,138r	8,196r	8,098r	8,072r	9,126
Total renewables generation on an obligation basis (5)	13,036r	14,879r	15,833r	17,680r	21,063

Each method of energy production sees its own range of costs and benefits. Each comes with significant carbon footprint, however once constructed each works to become carbon neutral and eventually carbon negative. Biofuel combustion does, in its own right, release large quantities of CO₂ into the atmosphere, but as the carbon content of this fuel is not mined, the carbon comes from the rapid carbon cycle, so emissions are still seen to be “green”[9].

1.2.3 Fuel Cells

All of the power sources previously highlighted, with the exception of solar, have required mechanical energy to create electricity. Fuel cells however, like solar, generate electricity directly through electrochemical means, with no moving parts [10]. Whilst solar energy utilises photons, fuel cells utilise an easily oxidised fuel. The fuel cell is made of 3 key component parts, an anode, where a fuel source is oxidised, an electrolyte through which ions may pass, but not electrons, and cathode, where oxygen, often from ambient air, is reduced [11]. The flow of electrons is passed

around an external circuit, from the anode to the cathode, completing the circuit and delivering power.

1.2.3.1 Current Fuel Cell Technology

The actual materials of the fuel cell vary by type, of which 6 are recognised as most common and these are described below.

Table 1-2. The 6 types of fuel cells and their component parts (most common).

	Polymer Electrolyte	Direct Methanol	Solid Oxide	Molten Carbonate	Phosphoric Acid	Alkaline
Operating Temperature	80-120	50-120	500-1000	650-1000	150-250	80
Anode Material	Carbon (Pt catalyst)	Carbon (Pt and Rh catalyst)	Ceramic (YSZ) (Ni catalyst)	Nickel	Transition metals (Pt catalyst)	Carbon (Pt catalyst)
Cathode Material	Carbon (Pt catalyst)	Carbon (Pt catalyst)	Ceramic (LSM)	Nickel oxide	Transition metals (Pt catalyst)	Carbon (Pt catalyst)
Electrolyte Material	Polymer (Nafion)	Polymer (Nafion)	Ceramic (YSZ)	MC salt in ceramic matrix	Phosphoric Acid	Sodium Hydroxide (aq)

As well having very different material make up the cost and efficiency of each type of fuel cell varies greatly too. Due to the differences in performance and the availability of fuel, only higher temperature fuel cells are currently viable for large scale power production; Solid Oxide Fuel Cells (SOFC), Phosphoric Acid Fuel Cells (PAFC) and Molten Carbonate Fuel Cells (MCFC). The application of SOFC will be discussed in chapter 1.2.3.2.

Alkaline fuel cells saw success in early fuel cell development, being used to power cars and provide onboard water and power on space missions [10]. PAFC see use in stationary power, and have been deployed as such within the US military [12].

PEMFC is currently the best publicised of all fuel cells, owing to their application in motor vehicles. Many of the world's major car manufacturers including Mercedes, Honda, Toyota and GM are looking into PEMFC powered electronic cars, the most famous model being the Honda FCX Clarity [13]. Our group looks at the application and development of a PEMFC automotive solution through our fleet of microcab vehicles [14]. The application of DMFC will be discussed in chapter 1.2.3.3

1.2.3.2 SOFC

SOFCs require inexpensive catalysts and are able to utilise fuel supplies which are rich in carbon, such as landfill or natural gas [15]. The use of these fuels results in emissions of water and carbon dioxide. These are the same emissions as produced by conventional power stations. Per unit fuel fed into an SOFC the emitted gas will have the same carbon footprint as it would have done had it been fed into a gas fired power station. The advantage of the fuel cell is twofold here, whilst per unit fuel inputted it will produce the same CO₂ emissions it will produce none of the NO_x or sulphur containing emissions of its conventional counterpart [16]. A further benefit of SOFC comes in the form of the quantity of emissions; this is because SOFC systems are much more efficient than thermal power plants. SOFC units have been shown to reach 60% electrical efficiency [17]. Resultant emissions are 17% lower than a gas powered plant. The useful heat gained from cogeneration means that SOFC may see useful application in distributed power [18]. As SOFC has no moving parts other than for gas management, they are much quieter than a standard cogeneration plant [16]. SOFC power is also much more scalable, with work looking into both kW and MW systems [19],[20]. This means that individual buildings or communities may be able to

install an SOFC unit which delivers both baseline electrical and thermal power requirements.

1.2.3.2.1 IP-SOFC

IP-SOFC is a hybrid between tubular and planar SOFC [21]. The design sees several membrane electrode assemblies (MEA) screen printed onto either side of a rectangular tube, as shown in Figure 1-i. Each cell is connected by screen printed interconnects. All areas not covered by MEA or interconnect are covered in a sealant glass. The charge collection comes in the form of Pt wires at each end of the tube. This design of tube is designed to have a current output of 50W.

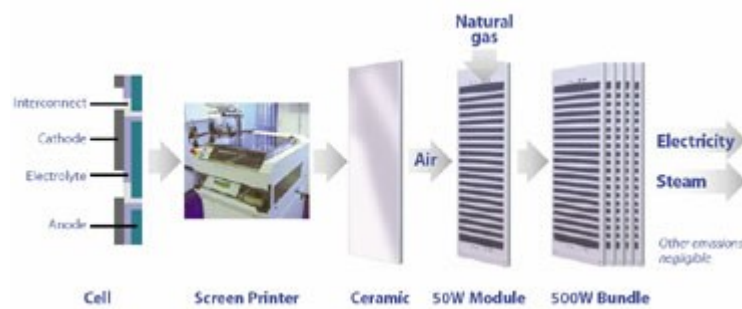


Figure 1-i Rolls Royce IP-SOFC manufacture and bundling [22]

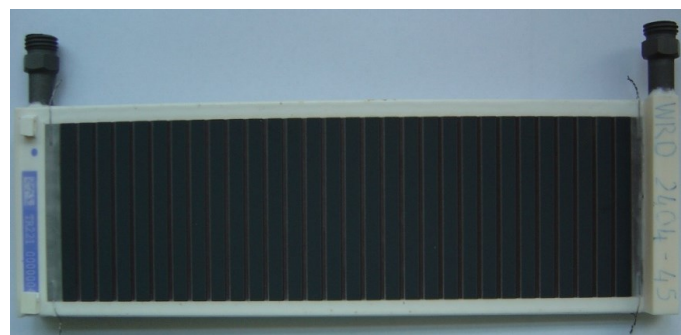


Figure 1-ii Rolls Royce IP-SOFC tube with anode gas manifold

The IP-SOFC works by feeding fuel through the centre of the tube, where it diffuses through the ceramic wall and meets the screen printed anode. Here the fuel combines with oxide ions that have been produced by the cathode on the outside of

the tube. Whilst the exact composition of the components is kept as knowhow, the cells are made from YSZ-Ni/YSZ/LSM, an industrially standard arrangement.

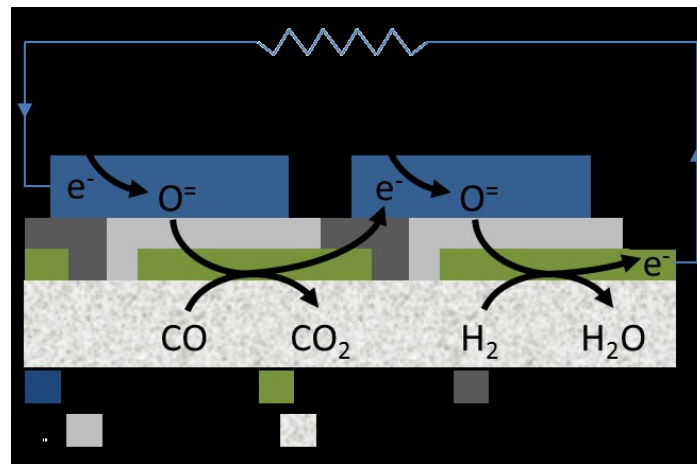


Figure 1-iii Schematic of IP-SOFC operation

The Rolls Royce design has, in theory, many advantages over either tubular or planar designs. The tube design does not require the same level of sealant demands as planar fuel cells, nor does it suffer from long current paths due to a long distance to an interconnect, this is a problem in tubular fuel cells [21]. As each component is thinner than in other fuel cells thermal expansion mismatches should also be better accommodated. Other major problems such as applying compression and gas management are also greatly simplified.

Rolls Royce has earmarked this technology for multi megawatt production, especially for use in the US where grid stability is still issue, as highlighted by the blackouts on the east coast in 2003 [23]. For this reason the tubes have been made to be easily stackable. The gas manifold shown in Figure 1-ii is only for single tube testing purposes, in a system, multiple tubes will be stacked on top of each other connected by their gas manifolds and the platinum interconnect wires found at either end of the

tube. This approach will create modular stacks of tubes which will allow easily scalable systems. For the multi MW production that Rolls Royce has envisaged this system is run under pressure which allows for combination with a gas turbine, leading to superior efficiency [23].

1.2.3.3 DMFC

Whilst other fuel cells are named on the basis of their electrolyte, DMFCs are named after their fuel type. DMFCs share the same electrolyte as PEMFCs, most commonly nafion [11]. PEMFC is only able to utilise 99.999% pure hydrogen as a fuel, DMFC may also utilise this fuel but is usually run using methanol and less commonly, ethanol. The difference between the fuel cell types that allows for the use of a carbon rich fuel is in the anodic electrocatalysts. Whilst PEMFC uses Pt as its electrocatalyst both anodically and cathodically, DMFCs utilise a mixture of Pt and Ru electrocatalyst on the anode side [24]. In both types of fuel cell the catalyst is found impregnated into a carbon cloth or paper which has been bonded to the electrolyte.

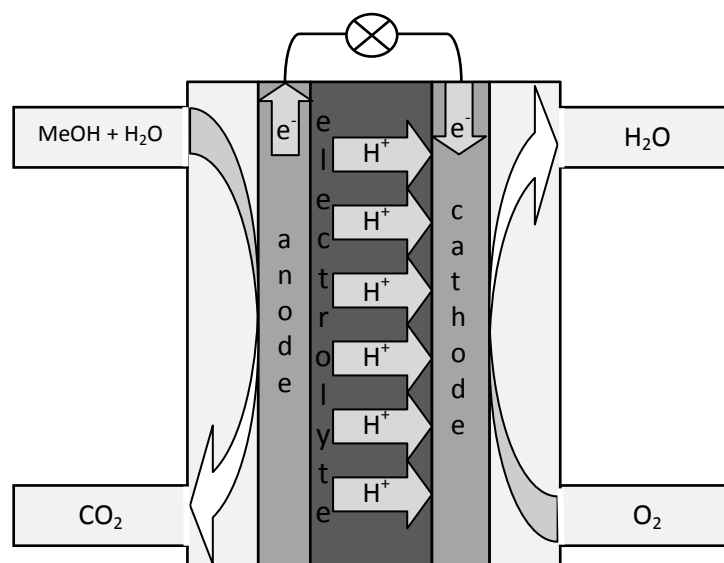


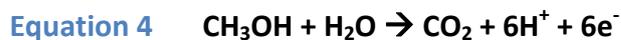
Figure 1-iv Schematic of DMFC

On a DMFC anode a solution of methanol in water is applied, usually at 1-2 M [25]. The methanol reacts on the surface of platinum being oxidised as in Equation 1 down to four protons, four electrons and a carbon monoxide molecule, which is adsorbed to the surface of the platinum. In a regular PEMFC this would act as a poison, however as shown in Equation 2 ruthenium is able to split water into a proton, an electron and a hydroxyl radical which is adsorbed to the surface of Ru [26].

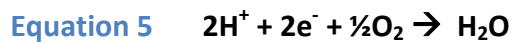
Electrocatalytic anodic reactions



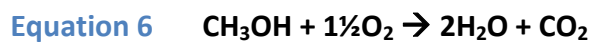
Overall anode reaction



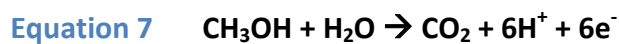
Electrocatalytic cathodic reaction



Overall reaction



Electrolytic cathode reaction



Electrolytic anode reaction



Overall electrolytic reaction



Should the Ru and Pt be in close proximity then Equation 3 may proceed. This reaction sees the adsorbed carbonyl and the adsorbed hydroxyl groups combine to emit another proton and electron and evolve carbon dioxide [27]. The protons travel through the electrolyte and with them drag through water molecules, typically 2.5 water molecules per proton in a nafion, which combines to create a water requirement of 15mol per mol methanol [28]. A water requirement this high limits anodic methanol concentration to 3M. The high water content at the anode also works to prevent a phenomenon unique to the DMFC, fuel crossover. The chemistry of nafion as an electrolyte allows the passage of very few compounds, protons and water have already been mentioned, a third compound that may pass through nafion is methanol. As the methanol active electrocatalyst, platinum is found on both the anode and the cathode, methanol crossover results in the formation of protons and electrons on the cathode side, as in Equation 4. Methanol oxidised on the cathode side may react with oxygen without having to push electrons through the external circuit [10]. This leads to a reduction in the cell potential and therefore efficiency of the fuel cell. If the fuel cell is run in reduced oxygen conditions, for example when the cathode is flooded, the fuel cell may act electrolytically, with crossed over methanol being oxidised on the cathode side as in Equation 7, then the resultant protons being pushed through the nafion, before being converted to hydrogen on the cathode as in Equation 8 [27]. The evolution of hydrogen on the cathode poses problems with fuel management and safety. Methanol crossover has a further outcome. The interaction between methanol and nafion is exothermic, therefore this effect may be used to

raise the fuel cell to operational temperature, this will aid in cold starting the fuel cell in practical operations, for instance in winter [29].

Despite the problems of crossover and the great expense of the fuel cell itself DMFC has many potential applications. The applications for these fuel cells are often in markets where the use of hydrogen is impractical or the use of high temperature fuel cells untenable. The market where DMFC currently sees commercial success is leisure APU. In this market recreational vehicles for example in the USA, where new noise legislation increasingly prohibits use of petrol generators, are supplied with a DMFC of up to 90W. This fuel cell trickle charges the on board batteries and requires no user interaction, other than to replenish methanol supplies. DMFC has also been developed for use in the military, and one such product is tested in chapter 4. The use of DMFC as a replacement for phone and laptop batteries has led to a successful lobby by industry to the US Department of Transport (DOT) to allow methanol as hand luggage [30]. The DOT now allows methanol cartridges up to 200 ml, this is double the allowance of any other liquid [31].

2 SOFC LITERATURE REVIEW

2.1 SOFC Materials

Since the discovery of the ionic conductivity of Yttria stabilised Zirconia (YSZ) by W. Nernst in the 1890's it has remained the primary component of the solid oxide fuel cell [32],[33]. Whilst many improvements have been made since the construction of the first SOFC in 1937, the components would still be recognisable to those the material scientists of 70 years ago used [34].

2.1.1 Anode

The anode environment plays host to the electrochemical conversion of a fuel, commonly hydrogen or methane into water and carbon dioxide. Methane fuel is converted into hydrogen, carbon monoxide, carbon dioxide and pure carbon.

Equation 10	Steam reforming	$\text{CH}_4 + \text{H}_2\text{O} \rightarrow \text{CO} + 3\text{H}_2$	ΔH^0 206 kJ/mol
Equation 11	Reforming	$\text{CH}_4 + \text{CO}_2 \rightarrow 2\text{CO} + 2\text{H}_2$	ΔH^0 247 kJ/mol
Equation 12	Shift reaction	$\text{CO} + \text{H}_2\text{O} \rightarrow \text{CO}_2 + \text{H}_2$	ΔH^0 -41 kJ/mol
Equation 13	Pyrolysis	$\text{CH}_4 \rightarrow \text{C}_{\text{solid}} + 2\text{H}_2$	ΔH^0 75 kJ/mol
Equation 14	Boudouard reaction	$2\text{CO} \rightarrow \text{C}_{\text{solid}} + \text{CO}_2$	ΔH^0 -173 kJ/mol
Equation 15	Electro-oxidation (CO)	$\text{CO} + \text{O}^- \rightarrow \text{CO}_2 + 2\text{e}^-$	ΔH^0 -283 kJ/mol
Equation 16	Electro-oxidation (H₂)	$\text{H}_2 + \text{O}^- \rightarrow \text{H}_2\text{O} + 2\text{e}^-$	ΔH^0 -242 kJ/mol
Equation 17	Electro-oxidation (CH₄)	$\text{CH}_4 + 4\text{O}^- \rightarrow \text{CO}_2 + 2\text{H}_2\text{O} + 8\text{e}^-$	ΔH^0 -802 kJ/mol

The creation of pure carbon from methane is the most thermodynamically favoured of all the reactions and the reaction which engineers strive most to avoid [35]. Whilst

it has been shown that modest carbon deposition, coking, increases the conductivity of mT-SOFC, excessive coking leads to the blockage of electrochemical sites, and eventually to the blockage of pores, reducing tortuosity and therefore reducing triple phase boundary area [36]. It is possible to avoid coking through using a steam / carbon ratio greater than two [37]. Carbon deposition is a reversible process; Equation 18 shows the steam gasification reaction which promotes the removal of deposited carbon. The removal of deposited carbon is not entirely reversible, and using a great excess of steam may re-oxidise the anode and corrode interconnect materials [38]. Consequently rather than work to remove deposited carbon effort is made to reduce deposition.



From a fuel maximisation standpoint Equation 10 and Equation 11 are the most desirable. Both of these reactions act to cool the fuel cell which acts to reduce the requirement of active cooling. Further benefit is the lack of any coking agents, for this reason reformers are included in some systems as BOP[38].

The electrochemical reactions shown in Equation 15 and Equation 16 take place on regions where the three phases of the reaction meet, the electronic, the ionic and the gaseous phases. This point is known as the triple phase boundary (TPB). As no one component of the anode is able to carry multiple phases the triple phase boundary occurs at places where electrolyte, charge carrier and gasses meet [38]. The reaction then proceeds on the surface of this boundary. As the surface area of the TBP increases per unit area of electrolyte more fuel may be oxidised, and therefore the available current density also increases.

With most current SOFC cells being anode supported it is vital that the anode provides structural integrity to the cell . The mechanical stability of the anode requires a thick layer of anode material. Competing directly with the need for strong mechanical strength is the need for very high porosity, for gas must be able to travel to electrochemically active regions. As well as the need for gas access and mechanical strength an anode must also provide electrical conductivity, ionic conductivity, whilst being inert with respect to other cell components [39]. The chemical inertness as well as the strength combine to give another requirement of the anode, long term stability at operational temperature, >10,000 hours in most practical applications [40].

An ideal anode would have 40,000 hours stability, tolerance to vapour borne impurities as well as well matched CTE to the cathode and electrolyte [41].

2.1.1.1 Pure Metallic

The simplest anode, and indeed an approach attempted at great lengths during early fuel cell development sees the anode as a single phase porous metal layer over an electrolyte, here the TPB lies on the border of the electrolyte. Many materials were chosen for use, mainly transition metals and graphite [34]. Whilst deployed successfully in other applications none of the materials were able to work as an anode for any length of time. Materials such as platinum, an excellent electro catalyst, suffered from spalling, whilst iron and graphite suffer from oxidative corrosion [42]. Cost and agglomeration prevent the usage of cobalt and nickel respectively [15].

2.1.1.2 Yttria stabilised zirconia – nickel anodes

The failure to produce a pure single phase anode led to the development of 'cermets'. A cermet is used to combine the properties of the ceramic and the metallic components. Cermets are advantageous over metallic anodes for several reasons, the most important of which possibly being the extension of the TPB [15]. By combining the ionic conductivity of the ceramic with the electrical conductivity of the metal it is possible to build up a structured TPB away from the electrolyte [15]. For the cermet to be an effective there must be long connected paths of ceramic from the electrolyte to the TPB and connective paths of metal from the TPB to the current collector. The porosity of the structure must also be high enough to allow effective gas transport [40] [43].

Currently the cermet of choice for SOFC anodes, especially those operating above 700 °C is Ni within YSZ [11]. The main reason for the use of nickel in the cermet over other metals is cost [43]. Nickel is both abundant and cheap. There are several other advantages to nickel, firstly, thermal expansion; the nickel YSZ cermet has a closely matched CTE to the most common electrolyte material YSZ, owing largely to the high YSZ content of the anode [43]. The porosity of nickel based anodes is easily made higher than 30% as shown in Figure 2-i, leading to a high degree of tortuous pores, this level of porosity permits facile transport of both fuel to, and exhaust away from, the triple phase boundary [44],[45].

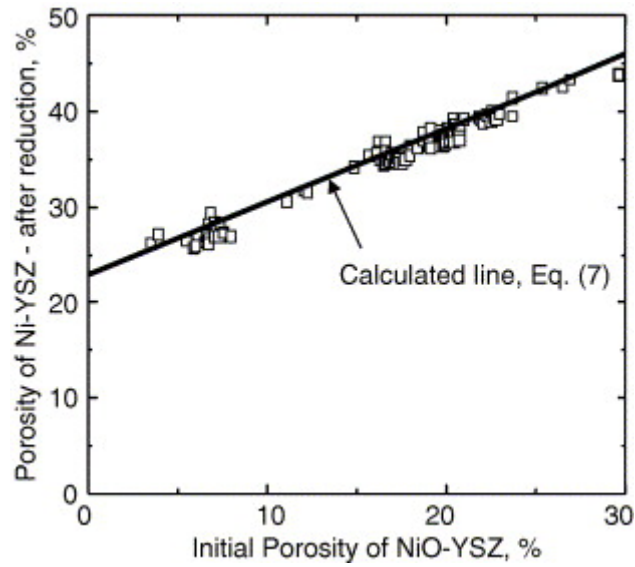
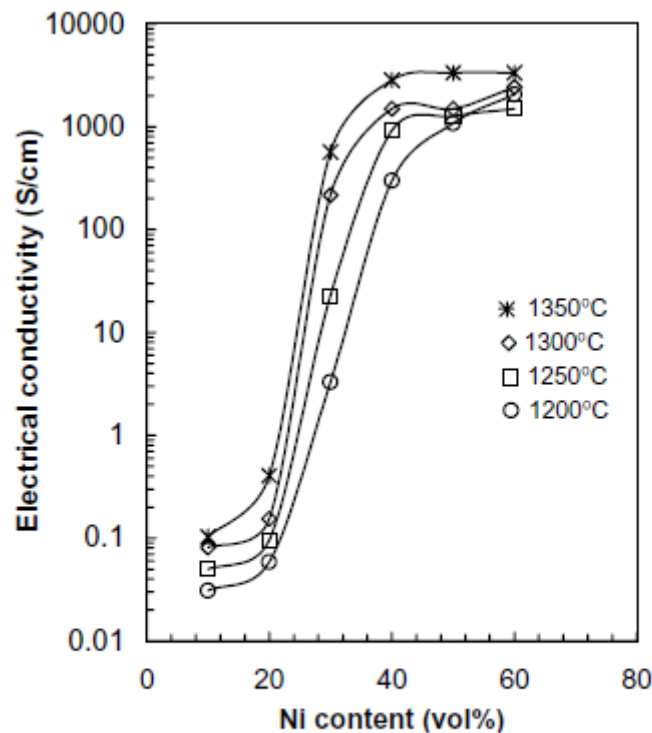


Figure 2-i Porosity of Ni-YSZ anodes, related to initial cermet porosity [46].

The electrical conductivity of the anode increases with nickel content, as nickel is the only electron carrier in the anode. The transition from being electronically isolating to conducting happens at a critical point which occurs at around 30% Ni, shown in Figure 2-ii. This point represents the level of nickel which allows for continuous 'wires' to form between triple phase boundaries and the current collector [43].



Variation of electrical conductivity measured at 1000 °C as a function of nickel concentration of Ni/ZrO₂(Y₂O₃) cermet fired at different temperatures

Figure 2-ii Anode conductivity by nickel content [43]

The anode is fabricated from slurry of nickel oxide in YSZ with binders. Nickel oxide, and not nickel metal is used for two reasons, firstly the fine nickel powders that would be required for fabrication have significant health risks, and industrial processing would become costly [47]. Secondly, the porosity of the structure is improved with use of nickel oxide. NiO is mixed, often as a 50-50 (molar) mixture with YSZ and this mixture is then formed into the anode using one of many fabrication techniques. The tube is then sintered at high temperature to set the ceramic. On first use the anode will be reduced through being exposed to fuel at operational temperature. The fuel reduces the NiO to pure Ni. The reduction process reduces the

volume of the NiO particles by 40% and this reduction in volume sees the porosity of the structure increase as in Figure 2-i [46].

The role of the YSZ in the anode is more than just to provide ionic conductivity but also to provide the mechanical stability for the electrode, as well as mechanical scaffold to the electrode as a whole YSZ acts as a micro-structural support for Ni particles [43]. This prevents nickel agglomeration, which will be discussed in Chapter 2.2.

2.1.1.3 Ceria-rare earth anodes

Ceria has the ability to conduct both ions and electrons; this means that the anode can be a pure ceramic material [48]. The mixed conductivity simplifies the TPB, as the entire gas/ceria interface is the TPB. The ceria anode is currently the anode of choice for low temperature SOFC applications <800 °C [43].

Ceria is able to offer the mixed conductivity due to the transition of some Ce^{4+} ions to Ce^{3+} ions in reducing environments. This creates both oxygen vacancies and electron holes. The detriment of this process comes from the expansion of the material that accompanies the reduction of Ce^{4+} [43]. The expansion may lead to destructive cracks forming at the anode.

The reduction triggered expansion of the material which can be prevented through doping. Doping Ceria with cations such as Gd^{3+} , Sm^{3+} or Y^{3+} can act to prevent the expansion whilst providing the vacancies required for conductivity. It has been found that 40-50% substitution of Ce^{4+} with Gd^{3+} should provide a structurally stable conductive ceramic [43]. This anode is further improved in several ways. In the case

of a YSZ based electrolyte being used an anchoring YSZ layer can be laid down to support a thin anode layer [43].

One of the key advantages of Ceria as an electrode is the ability to perform reaction shown in Equation 17) i.e. the direct oxidation of methane with negligible coking [49]. This however proceeds with slow kinetics, and cell performance is improved if a ceria / transition metal cermet is used. Studies have been conducted using Ni, Ru, Pt and others showing encouraging improvements [50].

2.1.2 Cathode

The cathode surface plays host to the electrochemical reduction of oxygen ambient air. The role of the cathode is to receive electrons from the external circuit and use them to reduce oxygen from the air into oxide ions. The cathode must, as with other cell components have a CTE compatible with the other components, good ionic conductivity and, as it is the case with the anode, the cathode must also have good electronic conductivity [51]. As few cells designs are cathode supported cathodes are often made to be thin, to minimise resistance.

2.1.2.1 LSM or New Material

The most common material used for anodes is strontium doped lanthanum manganate (LSM). LSM used for cathodes often has the composition $\text{La}_{0.8}\text{Sr}_{0.2}\text{MnO}_3$. This composition works well as is thermally compatible with the electrolyte YSZ, and performs the electrochemical reaction required adequately [51]. The performance of the electrode can be enhanced through the formation a mixed ceramic, with YSZ. The

improvement in electrode performance stems from the low ionic conductivity of LSM and the high ionic conductivity of YSZ [51].

There are many alternative materials available for cathode use e.g. the Gd containing LSGM offers improved ionic conductivity [51]. Co containing ceramics, such as LSCF offer superior oxide conductivity, due to the large number of oxide vacancies introduced into the crystal structure [51]. The thermal expansion of Co containing cathodes is not compatible with YSZ electrolytes, therefore buffer layers must be used [51].

2.1.3 Interconnects

The role of the interconnect in the SOFC varies depending on the fuel cell geometry. The primary function of the interconnect in all geometries is to act as a charge collector which completes the SOFC circuit, and it is where an external load may be applied [52]. In mT-SOFC the role of the interconnect usually ends here, in some cases the interconnect serves to act as a manifold or stack structure [53].

In the case of planar cells the interconnect has a much greater purpose. Here not only must the interconnect provide structural support to the stack but also to separate the fuel and cathode gasses meaning that the material should be gas tight [52].

The rigour of having to provide structure to the stack, electrical conductivity, gas tightness whilst being chemically inert with respect to the ceramic materials of the cell reduces the number of possible materials available to use for the interconnect plate [15].

2.1.3.1 Metal

The use of metal interconnects is desirable for the commercialisation of SOFC. The benefits come primarily for cost, not only from the price of the materials, but from the cost of processing [15]. The interconnect must both collect current whilst providing gas distribution to both the anode and cathode. The formation of accurate and complex gas distribution requires processing which is expensive in ceramics; however metals may be pressed or machined into shape, which is potentially much cheaper and scalable processes [54].

Several factors hinder the effective use of metallic interconnects. These include thermal expansion compatibility, oxide formation and chemical interaction with cell components [54].

At high temperature the use of many metal alloys for interconnects is prohibited due to the formation of non-conductive oxides on the interconnect surface in the presence of oxygen at high temperature. This is especially the case with low Cr containing metals [55]. These metal oxides reduce stack performances in two key ways, firstly the oxides are electronically insulating [55]. Thus reducing the charge collection ability of the interconnect plate. Secondly the oxide layers tend to spall away from the surface of the metal [56].

The chemical interaction between the cell components and the interconnect needs to be avoided. The most common chemical interaction is found on the cathode side; here chromium evaporating from steel poisons the electrocatalytic activity [54]. The use of metals which do not contain chromium has been tested, including nickel.

However the requirement to be chemically stable in both reducing and oxidising environments, coupled with a CTE that is incompatible with YSZ at high temperature, made nickel unsuitable for use as an interconnect material [15].

The use of chromium in steels is essential to prevent the formation of rust in the presence of steam, a product of the anodic reaction. As a result specialist steels such as Crofer-22 have been developed which whilst containing Cr do not suffer from Cr evaporation [57]. Other approaches see the use of protective layers to protect against Cr evaporation [54].

2.1.3.2 Ceramic

Ceramic interconnects offer superior thermal expansion properties over metallic ones, as well as having better chemical compatibility with the cell components [15].

Ceramic components are however much harder to process as the construction of gas distribution and current collection channels is a demanding task in ceramics. The connection of ceramic interconnect plates to each other, and to sealants is also challenging (something that can be relatively easily done by welding with metallic interconnects) .

Despite the problems associated with ceramic materials they are commonly used especially at temperatures above 900 °C where the thermal expansion of metals increases. The ceramics used tend to be perovskite structures such as lanthanum or yttrium chromite [58],[59]. The conductivities of these materials increase with temperature, preventing use at lower temperature [10].

2.2 SOFC Degradation

For commercial success the SOFC must deliver longevity as well as efficiency. As shown throughout this review there are many factors preventing the longevity of the fuel cell. This section will seek to identify and explain how degradation is measured and defined before describing methods of accelerated aging.

2.2.1 SOFC Losses from theoretical efficiency

The SOFC open circuit voltage is governed by the Nernst equation, Equation 19 [11]. This equation governs the deviance from the standard cell voltage, at open circuit, which for the oxidation of hydrogen is 1.18 V. The Nernst equation shows us that the theoretically available voltage drops with temperature, so for operation at 800 °C a voltage of 0.99 is the theoretical ideal, for a cell operating at lower temperature, for instance 650 °C a Nernst voltage of 1.03 V exists.

Equation 19 Nernst Equation

$$E = E_0 + \frac{RT}{nF} \ln \frac{P_{H_2O}}{P_{H_2} \sqrt{P_{O_2}}}$$

When current is drawn from a fuel cell the voltage output tends to drop. Figure 2-iii shows how the voltage drops according to current drawn; the initial losses are related to activation energies, as the drawing of load forces the chemical reaction to proceed. The losses across the majority of the load profile are due to the resistive losses in the fuel cell. Each cell component will have electronic and ionic resistance which lead to the linear section of the IV-Curve. Finally as the current drawn rises the mass transfer of reactants exceeds the limits of the electrode and voltage is lost.

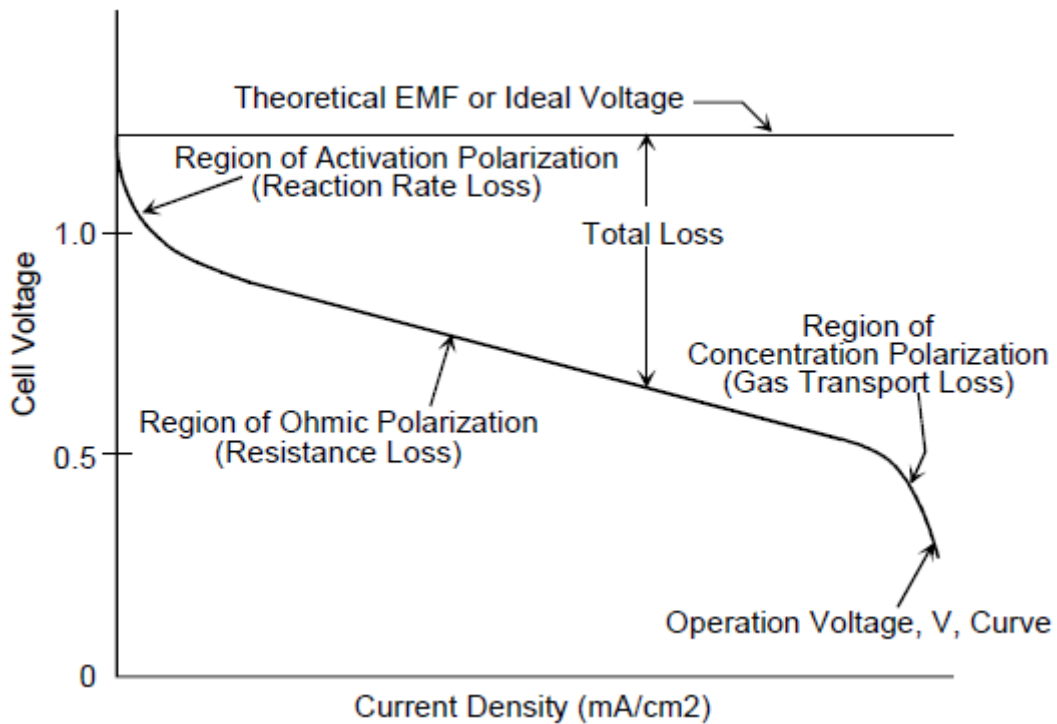


Figure 2-iii Characteristic IV Curve, showing characteristic losses

The efficiency of a fuel cell can be measured in several ways, however the most convenient way to measure the efficiency of an SOFC is through Equation 20, where μ_f is fuel utilisation and V_c is the cell voltage. The fuel utilisation is simply represented by Equation 21.

Equation 20 Efficiency
$$\eta = \mu_f \frac{V_c}{1.23} 100\%$$

Equation 21 Fuel utilisation
$$\mu_f = \frac{\text{mass of fuel reacted in cell}}{\text{mass of fuel input to cell}}$$

2.2.2 SOFC Accelerated Aging

As a fuel cell is operated over an extended period of time the performance steadily decreases, and the process involved is assigned as aging, and is usually measured in % loss in performance parameter (voltage under defined load, as an example) per

1000h. For commercial use as stationary power the fuel cell must have a life of over 40,000 hours, with only slight loss of power and this means that degradation rates lower than 0.1% per thousand hours should be sought [60].

SOFC cells and stacks may fail in many ways, some of these failure mechanisms are steady degradations whilst others are sudden failures.

A common and steady route of degradation is nickel agglomeration in the anode. The nickel particles, which require close contact for electrical conductivity will pool at high temperature [61]. The pooling of nickel breaks the connection between electrolyte and current collector, halting the electrochemical reaction on the surface. Careful control of the cermet microstructure is therefore essential to avoid nickel mobility [62].

Other common failure modes come from thermal mismatch [15]. Here materials expand at different rates, the initial response of the material is to bend, but planar cells under compressive pressure may not bend, and instead crack. The cracking of an electrode leads to reduced activity, whereas an electrolyte crack may destroy the cell. The passage of gasses through the electrolyte leads to two possible scenarios, combustion of the fuel at the point of fracture or the short circuiting of the fuel cell, as the entire electrochemical process may occur at either the anode or cathode without need for oxide conduction. Failure of interconnects or seals may have the same effect.

Another possible outcome of thermal mismatch is delamination; here ceramic layers separate from each other, reducing the contact area between electrode and electrolyte thus reducing performance.

A more sudden reduction of performance comes from redox cycle of nickel on the anode [63]. Nickel reduces in volume by 40% on reduction from nickel oxide, but will increase in volume by 70% on re-oxidation. This is because the nickel oxide particles formed will be porous. The increase in volume places mechanical stress on the ceramic support, and the anode will become rapidly ineffective.

Corrosive failure due to the oxidation or spalling of an interconnect plate may be observed as a more gradual degradation [54]. As will the evaporation of chromium from an interconnect plate [56].

The thermal and mechanical failures of the fuel cell may be expedited by using accelerated aging techniques. By subjecting a fuel cell to rapid cycles of load, thermal shock or redox conditions the failure mode of the fuel cell may become apparent more rapidly [64].

In many cases, especially for stationary power SOFC, the system is designed to be used as an uninterruptable power supply (UPS) [65]. Here the fuel cell is unlikely to undergo any thermal cycling, however it is not unreasonable to assume that maintenance, component failure or supply cut-out will cause shut down of the stack, often more rapidly than is recommended. The heating and cooling of a stack is known as thermal cycling. Thermal cycling induces stress on the ceramic materials in the cell. The structure of the fuel cell has been locked in place during the sintering process, at

>1200 °C and this means that at lower temperatures the material is under most stress. The differences in material CTE's makes the stress greater over a thermal gradient [66]. Thermal cycling often leads to cracks and delamination of cell materials.

The cut off of fuel supply may result in a relatively high partial pressure of oxygen on the anode side and this oxygen may oxidise the nickel component of the anode, forming NiO, which is of greater volume than the scaffold around it. This leads to destruction of the anode [63].

Current cycling is demanding for the electrocatalyst, throughout the lifetime of a stack the drawn load will vary. Rapid cycling from OCV to the design point current will amplify any electrochemical defects [67].

3 IP-SOFC

3.1 Project Aims

Work has previously been conducted within our group into the performance of previous generation of IP-SOFC which focused around the ten cell tube design. This work looked at the degradation of the 30 cell tube in conditions mimicking those already published as well as under altered initial anode reduction conditions.

3.2 Experimental

The durability testing has been conducted in order to assess baseline degradation of the fuel cell. We have tested two tubes simultaneously. By running two experiments in tandem, environmentally isolated systems, we have been able to alter one variable, reduction technique, as shown in Figure 3-i and Figure 3-ii. All previous work with the Rolls Royce IP-SOFC tube had been conducted under the terms of the now expired Real-SOFC project. This meant following stringent reaction procedures, and a prescribed reduction profile. Previous results have shown an initial sharp degradation in performance (unpublished results, W. Bujalski, A. Majewski) and it was postulated that this was due to hasty initial anode reduction process employed creating an inefficient anode, where the rapid reduction causes, as with rapid crystallisation, small nickel particles in the anode structure. Whilst small particles have a large surface area, and therefore a greater region of triple phase boundary, if these particles do not interconnect there will be no passage of electrons throughout the electrode. Without efficient passage of electrons the current density will drop off very

quickly. A slower more controlled reduction may allow the formation of nickel particles with a defined particle size and distribution on reduction from nickel oxide.

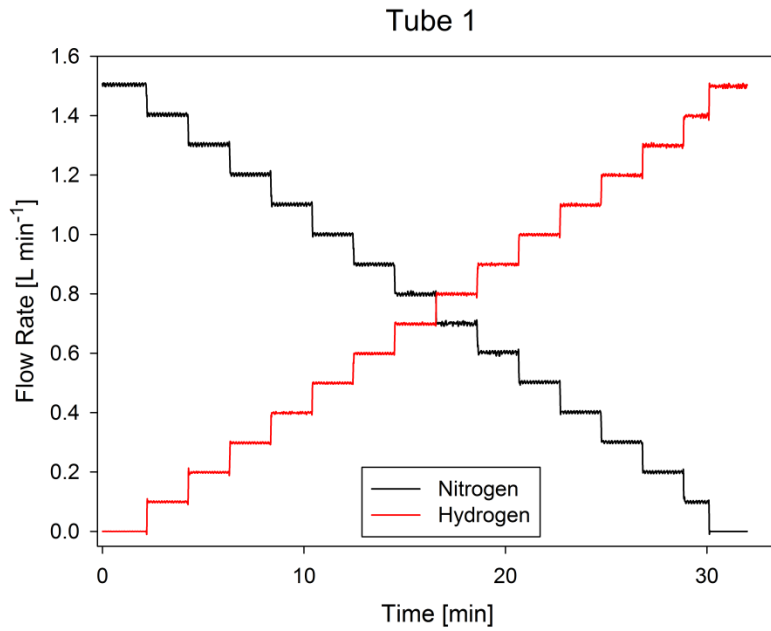


Figure 3-i Reduction technique used for tube 1

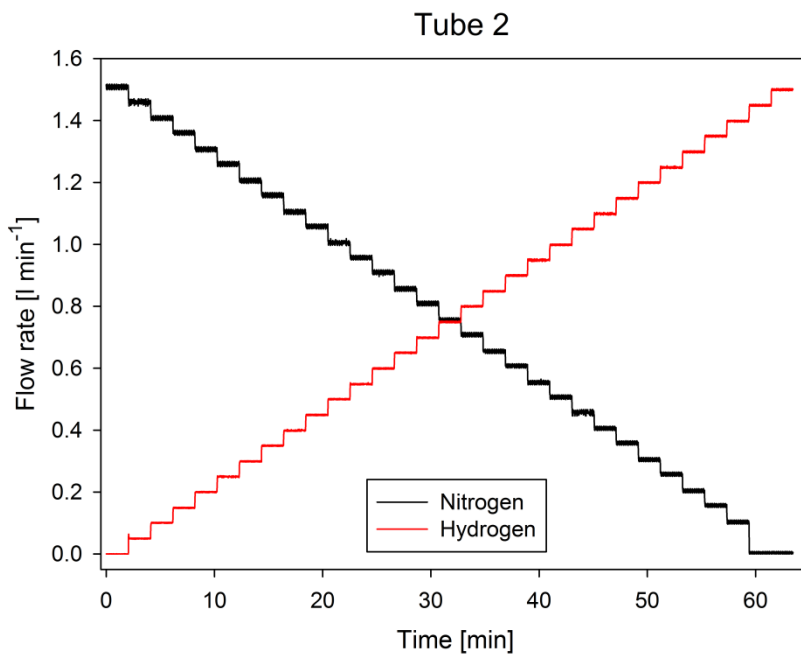


Figure 3-ii Reduction technique used for tube 2

3.2.1 Durability testing

Using an Advanced Measurements Inc. (Canada) made fuel cell testing rig, the fuel cell tube was purged of atmospheric gasses with nitrogen to prevent unwanted chemistry as the tube is heated. The tube is heated in furnace, in the absence of gasses to 900 °C at 1 °C a minute from room temperature. At 900 °C the temperature is stabilised. The tube is fed with nitrogen gas and 3% humidity before gradual introduction of hydrogen and removal of nitrogen until there is 1.5 L min⁻¹ of hydrogen flowing. This process reduces the NiO in the tube to Ni. Our experiments have used two profiles, one where the flow rate of hydrogen increases by 0.1 Lmin⁻² the other by 0.05 L min⁻², referred to from here on in as reduction methods 1 and 2, respectively (with the tubes referred to as tube 1 and 2 accordingly using the same naming system).

Once reduced, the fuel cell is operated without load to allow the fuel cell to stabilise. At this point the tube is said to be primed, an I-V curve is taken by initially increasing the applied current load at 0.1 A every 40 seconds from 0 to 1.8 volts and back down to 0 A again, in order to assess the initial characteristics of the tube and to establish a reference point from which data analysis can be started. The tube is then allowed to cool to room temperature, at this point the experiment starts. After the initial reduction management of the gasses is important to avoid re-oxidisation of the anode as redox reactions would lead to delamination of the ceramic and nickel materials due to the stresses of thermal and chemical expansion. At all temperatures below 400 °C a safe gas mixture of 95% nitrogen and 5% hydrogen is used, as the ceramic is not ion conductive at these temperatures the hydrogen acts solely to

protect against oxidation. At temperatures above 400 °C the inlet gas is hydrogen carrying 3% humidity.

The tube was reheated to 900 °C at 1°C min⁻¹, and stabilised without load for one hour and at this point an IV curve was taken, IV curve 2, in the results that follow. After this the load drawn from the fuel cell was increased at a rate of 0.05 A min⁻¹, to 1A, at this point durability testing was said to have commenced with the first second of load taken at 1A given value T0, making IV curves 1 and 2 precede T0. The load was held at a constant 1A for 36 h before being lowered to 0A at 0.05 A min⁻¹. Another IV curve was taken, and the process repeated. After 9 and 17 cycles the tube was cooled to room temperature and restarted. These breaks allowed time for data analysis to occur and visual inspection of the tube in the test box.

A total of 801 hours at 1A were recorded.

3.3 Results

Results, in the form of tables and charts can be found in Appendix i – IP-SOFC, raw data can be found on the accompanying CD.

3.4 Analysis and conclusions

Figure 7-i shows the profile of the complete durability experiment, for tube 2, clearly showing the restarts and the IV curves and the tubes reaction to these. At each start up and shut down the tube voltage is seen to increase, this is an effect of the YSZ electrolyte. As the ceramic changes temperature so does the ion conductivity, changing the voltage. IV curves, denoted by spikes in the current loading are reacted to, by the tube with lower voltage; this change in voltage in relation to applied load is

one of the evaluative methods used later in these results. It can also be noted that the voltage output of the tube at 1A remains largely stable, and that there is a wide range of temperatures within the test box. The temperature variance comes from the exothermic reactions of the fuel cell, air is fed to the bottom of the box at a relatively low temperature, as this air flows up and past the fuel cell it is heated causing a gradient of 35 °C across the test box.

The voltage of the tube, and therefore power output under a load of 1 A was evaluated. Figure 7-ii shows the raw power output of the tube at 1A over the test duration. This data is difficult to read meaningfully, therefore it has been smoothed using a moving average method, Figure 7-iii, where each point is the average of the 10 data points that preceded it which has the effect of tightening the dataset, making trends easier to evaluate. The second figure, Figure 7-iii, also switches to a percentage scale, where t_0 is arbitrarily set to 100%.

It is clear to see that the first 120 hours of operation the output of tube 2 increases, by 1.5 %. This increase in performance then levels out and the power output remains stable until the tube is restarted after 267 hours. Once the tube is restarted a clear fall in performance is seen, but once again as the test progresses the performance of the tube increases, with the initial 60-100 hours showing the sharpest rise in performance, however, this test doesn't run long enough to show a clear plateau before restart. The next restart shows the same trend, an initial drop in performance from the end of the last test and continued improvement in performance throughout the test and, this time levelling out after around 100 hours. The gaps clearly evident in Figure 7-ii and Figure 7-iii correspond to the IV curves taken.

The results are unusual in comparison to other results we have seen in the lab, where the initial performance of other tubes drop by 4% over the first 50 hours of operation before entering into a steady rate of degradation at 0.13% every 100 hours.

Tube 1, run in tandem to this experiment experienced problems with the stability of its electronic load controller; this problem means that valid analysis of results is impossible.

By looking at the IV curves it is possible to see how the tube performs transiently, by plotting subsequent IV curves, transient performance as a function of time can be assessed. Figure 7-iv shows the performance of tube 1 at cycles 1, 9, 10, 17, 18 and 25. Figure 7-v shows the same data this time for tube 2. The cycles were chosen to reflect the start and finishing values for each test sequence, and to show the discontinuation that occurs as a result of the restart, as highlighted previously. Tube 1 shows classical degradation, in that the first I-V curve taken shows the highest power density, expressed as the highest voltage at the highest current density. This gradually decreases throughout the first test, then after the restart a sharp decrease in performance is observed from cycle 9 to 10. The second restart has less of an effect, however by cycle 25 the performance is considerably lower than at cycle 18, showing considerable degradation throughout the 3rd durability testing session. In contrast tube 2 has cycle 1 as the lowest performing IV curve, with 9 being the best, after each restart there is degradation from the previous experiment, but during each session the

performance of the tube increases, so that the power density of the tube at cycle 25, under 1.8 A is higher than at cycles 1, 10 or 17.

Tube 2 can be looked at more closely, as in Figure 7-vii, This figure highlights the difference in voltage of the tube at 1.8A, (i.e. $\sim 0.3 \text{ Acm}^{-2}$). Here the trend is clear, the tube loses performance immediately after each restart, throughout each session the tube increases its measured performance, although the effect of being restarted stays with the tube and each test session sees peak performance lower than the previous session. Cycles 2 and 7 showed the worst and best performance respectively.

The improvement in performance across each test in tube 2 is in stark contrast to both previous results and to tube 1 [64], [68]. As each tube underwent identical test procedures, bar only the reduction step, it is postulated that the reduction technique itself has altered the microstructure of the anode. This process may have extended the initial priming mechanism, or created a structure which takes a long time to become activated at each restart. The accumulation of thermal stress and localised delamination may explain the sharp reduction in performance after each full restart. Without many more sample tubes this single result is very hard to extrapolate.

4 DMFC- JENNY 600S

4.1 Introduction

Direct methanol fuel cells are currently seeing commercial success in the leisure industry. One company reaping many of the rewards of this technology are Smart Fuel Cell AG (SFC). As well as products designed for the public market SFC also make DMFC units for military purposes, Jenny 600S being one example. Jenny 600S is a man portable DMFC unit that provides 600 Wh_e a day. As soldiers carry many electrical items on a modern mission they must also carry many batteries if they wish to spend any time away from base. Jenny 600S seeks to reduce the burden of the soldier by acting as a portable power source utilising a fuel 15 times more power dense than lithium ion batteries.

4.2 Project Aims

The project aims to assess the battle readiness of Jenny 600S. The tests carried out by our facility aim to compare baseline performance of Jenny 600S in ambient British conditions to more demanding simulated environments, imitating the most demanding environments a soldier may be deployed in.

4.3 Experimental

The evaluation of Jenny 600S for battle readiness involved evaluation of several key parameters. These parameters are thermal signature, acoustic signature, fuel consumption and response to load. These test parameters were tested in varying conditions of low and high and ambient humidity as well as at ambient and high

temperature. The unit has two fuel types which will also be evaluated. The regular fuel is suitable for operation between -20 °C and +35 °C, whilst the desert fuel, containing 40 % water and 60 % methanol, is suitable for temperatures between 10 °C and 55 °C.

In each test thermocouples were placed around the unit, with one being placed at the exhaust, one on the body, at previously identified hot-spot and a third in ambient air. The unit was electronically evaluated using the evaluation cable supplied. This allowed connection to an external load, Array 3710A and to a computer, from where properties could be evaluated.

4.3.1 Conditions Testing

For control of temperature and humidity an environmental chamber was used (see Figure 4-j). The chamber was programmable and had a resolution of 0.1 °C and 1% RH, with a controllable minimum of 10% RH. This chamber was unable to simulate altitude. For these tests Jenny 600S was placed in the centre of the chamber and turned on. Thermocouples were placed inside the chamber and the load was connected by the evaluation cable. The test instrumentation was kept outside the chamber and cables ran from inside to outside the chamber to control load and read thermocouples.



Note 1

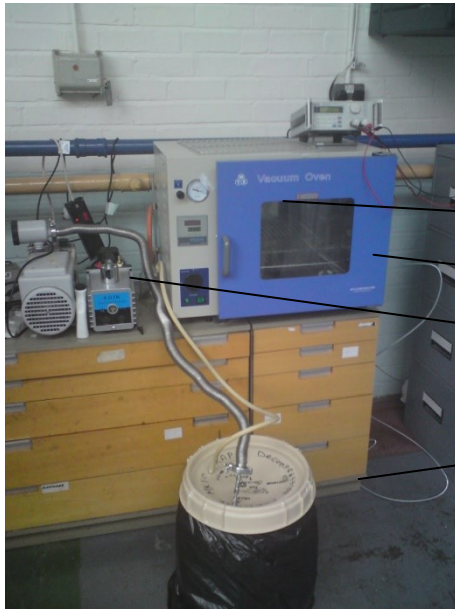
- Circulation fan
- Environmental chamber
- Jenny 600S
- Exhaust thermocouple

Figure 4-i. Experimental set up for environmental testing.

For the control of altitude two experimental methods were required, a reduced pressure method and a depleted oxygen method. The reduced pressure method saw Jenny placed inside a 30 dm³ hypobaric chamber with a 25 dm³ pre-chamber (see Figure 4-ii). The pre chamber was connected to a vacuum pump and then connected to the main chamber via a valve. The use of a pre chamber is required due to the low volume of the chamber. A pre chamber allows for rapid decompression, as the pre chamber can be evacuated first, then by opening the valve, the main chamber can be rapidly evacuated to the required pressure. The rapid decompression is essential as Jenny 600S requires oxygen from the ambient air in order to function. As the unit is switched on, and hence consuming oxygen, when the chamber is sealed it is essential to evacuate quickly to avoid too rapid consumption of the ambient oxygen. Sealing requirements permitted only the evaluation cable to be used in these tests. No thermal signature can be evaluated.

Table 4-1. Definition of HA2500 (pressure)

Mode	Pressure
HA2500 (pressure)	643 mbar



Note 2

- Array 3710A
- To computer
- Vacuum gauge
- Hypobaric chamber
- Vacuum pump
- Pre-chamber

Figure 4-ii. Experimental set up for altitude testing (pressure).

A second method saw Jenny 600S placed in a depleted oxygen chamber. This chamber had a volume of 5 dm³. The chamber covered the lower half of Jenny 600S, and therefore the air inlets, and not the exhaust. The chamber was fed with two air streams, which were mixed in a small chamber, air and nitrogen. The level of air and nitrogen was varied to simulate altitude.

Table 4-2. Definition of depleted oxygen altitude simulation

Mode	Air (dm ³ /pm)	Nitrogen (dm ³ /pm)
HA2500	7.5	2.5
HA4000	6	4

4.3.2 Signature testing

The response to load is measured by monitoring the voltage output of Jenny 600S, this is done through the evaluation cable. The black and red connections are linked to an electronic load, and then to a computer. The voltage response is measured by two methods, firstly through a National instruments computer, utilising Labview software. Labview software is used because of its flexibility and easy programmability; this input however provides no information about the load drawn. A second recording method, through the electronic loads own software records both power and voltage response. The hardware required to record this data was not available throughout the entire testing period.

Table 4-3. Testing modes evaluated for voltage output

Mode	Fuel	25W	15W	5W	Transient	Idle
Ambient	Regular	✓	✓	✓	✓	✓
Ambient	Desert	✓	✓	✓		
AT LH	Regular	✓			✓	✓
AT HH	Regular	✓	✓	✓	✓	
HT LH	Desert	✓	✓	✓		✓
HT HH	Desert	✓			✓	✓
HA2500	Regular	✓				
HA4000	Regular	✓				

The thermal characteristics were measured in two ways. Firstly by thermocouple, 3 thermocouples were used; one monitoring the exhaust temperature, the hottest and most thermally detectable region of the unit, a second thermocouple was placed on the body in a position identified as a hot-spot in preliminary tests. The third thermocouple was placed away from the unit to measure local conditions, therefore establishing the temperature of the unit above local conditions. The second measurement of thermal characteristics utilised a thermal imaging camera, (FLIR

T400, EPSRC). Jenny 600S was positioned in an enclosure lined with non-reflective lining. The camera was positioned 1 m away. Images were recorded at 30 s intervals. Table 4-4 shows modes tested.

Table 4-4. Testing modes with measured thermal signature.

Mode	Fuel	25W	15W	5W	Transient	Idle
Ambient	Regular	✓ 	✓ 	✓ 	✓	✓
Ambient	Desert	✓	✓	✓		
AT LH	Regular	✓			✓	✓
AT HH	Regular	✓	✓	✓	✓	
HT LH	Desert	✓	✓	✓		✓
HT HH	Desert				✓	✓

✓ Measured by thermocouple  Measured by thermal imaging camera

The acoustic footprint was recorded using a Marantz PMD660 with a microphone. The recordings were made at a distance of 1m, as per convention. The Marantz PMD 660 records sound with IEC – A weighting, this weights the sounds recorded to accentuate sounds the human ear is sensitive to. The sounds are recorded on a negative scale, the zero point being unknown, due to effects from the external microphone and gain built into the unit. The recording was made in a pair, firstly 10 minutes of background noise was recorded, and secondly one hour of operational noise was recorded. The recording was then checked for sounds unrelated to the experiment, for instance a large truck passed the building causing a spike in noise, and were excluded.

As Jenny 600S has on-board mixing and service fluid chambers measuring fuel consumption is not as simple as measuring the difference in mass of the cartridge both before and after the test. Jenny and the cartridge are weighed separately then the unit as a whole. The fuel consumption stated below refers to the difference in

the whole unit weight (Unit mass change method). The measurement of fuel cartridge mass difference is used when the mass changes dramatically during the test (Cartridge mass change method). Attempts were made to measure the mass of the unit during the test; however the cables and thermocouples, used to draw load and measure thermal characteristics, influenced this measurement too greatly to provide any reliable conclusions.

The following test conditions were evaluated by this method. The measurements highlighted (*) are calculated fuel consumption based on previous experiments.

Table 4-5. Test conditions and modes evaluated for fuel consumption

Mode	Fuel	25W	15W	5W	Transient	Idle
Ambient	Regular	✓	✓	✓	✓	✓
Ambient	Desert	✓	✓	✓		
AT LH	Regular				✓*	

Due to the method of testing (see Conditions Testing) it was not possible to measure fuel consumption under most non-ambient conditions.

4.4 Results

Results figures can be found in Appendix ii –DMFC

4.5 Analysis

The output voltage clearly has three phases. There is the battery dominated phase, the fuel cell dominated phase and the purge phase, (see Figure 7-viii). During the purge phase power draw is higher than in the battery phase as pumps are being driven to purge the cell. The most stable power output comes from the battery mode, where the voltage response to load is flat, irrespective of operating conditions.

The fuel cell output voltage tends to be higher than battery voltage by 0.4 V running at 29.8 V nominal output. The output voltage in these tests is not controlled by SMBUS. The stability of the fuel cell mode output remains steady across all conditions, with fluctuations in output voltage occurring more under partial load within the first hour of testing. The least stable output comes during the purge phase, as the power manager handles residual power from the stack, operation of pumps and supplies power to the load. Voltage drops during the purge phase are exaggerated by high load (Figure 7-x). Depleted oxygen conditions enhanced this, possibly as air pumps must be worked harder to oxidise excess fuel in the stack (Figure 7-xxv). In non-ambient conditions large drops are also seen, on occasion, for lower loads, there is no pattern for this (Figure 7-xix).

In ambient conditions output power demands are met using both fuel blends and operation in regular and transient cycles. The stability of the output voltage is slightly decreased when using desert fuel in ambient conditions, as seen by the voltage drops during purge in Figure 7-xiii compared to Figure 7-x. This is also highlighted when operating in the fuel cell phase at 15W in Figure 7-xiv against Figure 7-ix.

When operating outside of ambient conditions the stability of output power is the same as in ambient conditions for fuel cell and battery phase operation. The output that changes is the longevity of load. In HH and LH conditions it can be seen in transient cycles that over time the voltage pattern changes, and each purge cycle induces a larger voltage drop (Figure 7-xvii, Figure 7-xx and Figure 7-xxiii). It is possible that the fuel cell is unable to provide the required power output in these conditions and is being supplemented by battery power. After operating in this

transitional mode for up to 2 hours the output voltage falls to that of battery only operation. This mode of operation continues for up to 4 hours before output power is cut. This is supported in the case of the HH HT transient cycle, Figure 7-xxiii, where a restart in power output 2.5 hours after cut out suggests entry into battery mode to recharge internal batteries. This suggests a battery charge 30 minutes longer than stated by SFC, this also suggests that the fuel cell is unable to operate at full output in HH HT conditions. The switch from fuel cell to battery power may have been caused by a thermal cut out of the fuel cell. When removed from the chamber Jenny 600S often displayed high temperature warnings.

In HA2500 (pressure) conditions Figure 7-xxiv, the output power is cut and restarts within 2 minutes. This is because of low air, the fuel cell restarts automatically when low air is detected; this is covered later.

The thermal response from Jenny depends heavily upon the mode in which the unit is operated. The thermal output of the fuel cell tracks the load burden placed on the fuel-cell stack, not the unit as a whole, for instance Jenny can be thermally inactive under a load of 5W, Figure 7-xxix, or thermally active whilst idle, Figure 7-xxxii.

The greatest variance in temperature comes from the exhaust outlet, where at regular intervals the purge cycle causes the fans to shut off and the outlet temperature to fall by up to 10 °C for a matter of seconds, before rising again to former levels on continuation of exhaust fans. In AHAT the peak exhaust temperature is 65.1 °C, Figure 7-xxvii under full load, however for medium and low load the exhaust temperatures never exceed 60 and 50 °C, respectively (see Figure

7-xxviii & Figure 7-xxix). In transient mode the exhaust temperature stays between 40 °C and 50 °C for the majority of operational time, however the exhaust temperature does rise above 50 °C on most cycles, but never exceeds 58 °C (see Figure 7-xxx and Figure 7-xxxi). The temperature of the exhaust tends to be slightly higher when using desert fuel.

Table 4-6. Rough average temperature (excl purge) when active.

MODE	25W	15W	5W
Regular	58	47	39
Desert	61	52	45

In non-ambient conditions the thermocouple used to measure exhaust temperatures suffered from electromagnetic noise and this caused large fluctuations in the readings from the thermocouple. The readings from the thermocouple are therefore not a quantitative measure of temperature; however by 10 second time averaging the data, trends can be followed, showing when the exhaust was thermally active and thermally dormant. In sections identified as transitional in the response section in this report, the thermal output of the exhaust reduces, and continues to reduce into the areas identified as battery dominated. This reduction suggests an increased dependence on battery power to supplement fuel cell power (see Figure 7-xxxix and Figure 7-xx). As the fuel cell exhaust does not cool when entering the transitional mode in HH HT conditions, Figure 7-xlii, here it can be seen that the fuel cell stack is struggling to meet load demands. The exhaust continues to run hot after the load is cut, showing that the fuel cell is in battery mode.

The body temperature also tracks fuel cell stack load, but the effects are less responsive, owing to the plastic casing, which has a high heat capacity. The body temperature does not fluctuate with purge cycling. The peak temperature measured by thermocouple was 41.4 °C for the body. The unit takes 22 minutes to go from ambient temperature (25 °C) to a body temperature of 37 °C under full load. The body temperature remains between 30 °C and 40 °C at all times. Inside the climate chamber the body temperature appears to mirror ambient temperatures more than the load profile. This suggests that the thermocouple is more influenced by the circulating air than the body of the fuel cell unit.

Under low load the thermal signature of the unit is clearly separable into two distinct areas, the times when operating on battery alone and the times when using the fuel cell to recharge the battery. At 5W when using the battery alone both body and exhaust temperatures remain constant. The unit is also silent when operating on battery alone, however when charging the internal battery the unit becomes as loud as the unit at full load and temperatures increase towards those shown at higher loads.

The thermal imaging shows the unit to be warmer than as assessed by thermocouple. After operation at 5W for 1h, Figure 7-xliv shows a peak body temperature of 48.0 °C and a peak exhaust temperature of 52.3 °C. After operation at 1h at 15W, Figure 7-xlv shows that the body temperature has increased to a peak of 53.9 °C and the exhaust to 63.6 °C. After operation at 25W for 1h these temperatures have increased further. Figure 7-xlvi shows temperatures of 56.9 °C and 69.2 °C for body and exhaust, respectively. Taking an exhaust facing image, Figure 7-xlvii, shows peak

exhaust temperatures of 72.6 °C. After shut down the unit takes 5 hours and 23 minutes to reach thermal invisibility, Figure 7-xxviii.

Figure 7-xxix shows the sounds recorded as a frequency sweep, they represent the loudest part of the operational cycle of Jenny 600S and a quiet period of background noise. As each part of the circuitry used in this experiment alters the recording, true decibel readings are not obtainable. Relative measures are instead used to subtract the background from the operational noise, as shown in Equation 22. Data handled by Equation 22 was used to create Figure 7-l and Figure 7-li. Here the relative volume of Jenny is taken against the background noise, from this equation, if the recorded volume of Jenny 600S with background noise is 3dB higher than the background noise alone, then Jenny 600S can be said to have equal loudness to background noise. Any increase in recorded volume below 3dB therefore means Jenny 600S runs more quietly than background noise.

Equation 22. Removing background noise.

$$L_{Jenny} = 10 \log \left[10^{\left(\frac{Jenny_with_background}{10} \right)} - 10^{\left(\frac{background_only}{10} \right)} \right]$$

Relative to background noise, Jenny 600S is loudest at 1766 Hz, 1722 Hz and 1808 Hz at 10 dB above background level. In terms of loudness, overall the loudest point came at 43 Hz, but at this frequency the unit itself was quieter than the background noise.

4.6 Conclusions

Key points from the tests outlined above:

- Jenny 600S is able to run effectively and within specification in standard ambient conditions.
- The internal thermal monitoring appears to over read ambient temperatures, requesting desert fuel before reaching 30 °C.
- The fuel cartridge attachment mechanism is inadequate; a more reliable solution should be implemented.
- The unit is able to track load effectively and rapidly.
- The unit is quiet relative to urban background noise.
- Peak body temperatures exceeding 56 °C leading to thermal visibility in all operating climates.
- The unit appears to be unable to sustain load in simulated alternate climates.
- Desert fuel is no less efficient than regular fuel.
- The LCD display is susceptible to failure.
- Water management is poor outside standard ambient conditions, with water being lost at low humidity and water gained when using desert fuels in ambient conditions.

The following points are qualitative and based on the opinion of the tester.

- The product is sturdy and reliable in standard conditions.
- The units interface can be temperamental; it often required several attempts to reset the fuel gauge.
- The fuel connection is inadequate – it should not have failed in lab based tests.

- The unit may be too hot to carry close to the body.
- Simulated experiments may be unfair on the unit; the equipment used for testing had relatively low volume and may not have been a true representation of real climates.
- Jenny 600S is designed to be used as part of a battery fuel cell hybrid system, some of the problems identified in the report above may be ironed out in such a situation.
- The Glen air connection feels clumsy. The connection seems as if it may break under repeated use.

5 PROJECT SUMMATION

5.1 Industrial Relevance

Whilst the study of fundamental science and narrow focus on niches of fuel cell technology undoubtedly advance the knowledge base of the field, it is not, without knowledge of industrial requirements, possible to advance the technology as a whole. It is important to reflect on the implications of one's research and where it fits into the advancement of the technology, not just the knowledge base.

The work included within this report has aimed to look backwards. In each case, both IP-SOFC and DMFC projects have seen the testing of a fuel cell product, made by Rolls Royce and SFC, respectively. By testing products it is possible to assess the current status of the industry and more importantly target areas that require the most development.

IP-SOFC tubes have a weak point in interconnect materials. The thermal shock capabilities are also poor. Whilst efforts should be made to refine the inks used in the fuel cell, it is the interconnects that should bear the brunt of industrial efforts to advance the technology.

DMFC testing has shown that the fuel cells themselves are stable. BOP systems such as water and thermal management are the systems which need the most attention.

5.2 Presentation of Findings

5.2.1 Conferences

My work on IP-SOFC has been presented as a poster at “Hydrogen & Fuel Cells for Clean Cities, 6th Annual International Conference & Exhibition” in Birmingham, March 2010.

5.2.2 Reports

My work on DMFC was submitted as a confidential report to GDUK.

6 REFERENCES

- [1] *IPCC Third Assessment Report - Climate Change 2001.*
- [2] *IPCC Fourth Assessment Report.*
- [3] R.P. Kane and E.R. de Paula, "Atmospheric CO₂ changes at Mauna Loa, Hawaii," *Journal of Atmospheric and Terrestrial Physics*, vol. 58, Nov. 1996, pp. 1673-1681.
- [4] *UNITED NATIONS FRAMEWORK CONVENTION ON CLIMATE CHANGE*, 1992.
- [5] *Climate Change Act 2008.*
- [6] L. Junfeng, B. Lohani, E.M. Galàn, P. Monga, P. Mubiru, N. Nakicenovic, K. Nassiep, R. Pachauri, W. Palz, H. Pelosse, and others, "Renewable Energy Policy Network for the 21st Century."
- [7] *Air pollution from electricity-generating large combustion plants.*
- [8] R. Shukla, P. Ranjith, A. Haque, and X. Choi, "A review of studies on CO₂ sequestration and caprock integrity," *Fuel*, vol. 89, Oct. 2010, pp. 2651-2664.
- [9] Department of Energy & Climate Change, *Digest of United Kingdom energy statistics 2010.*
- [10] R.S. EG&G Technical Services, Inc., *Fuel Cell Handbook*, National Technical Information Service, U.S. Department of Commerce, 2004.
- [11] J. Larminie, A. Dicks, and M.S. McDonald, *Fuel cell systems explained*, 2003.
- [12] F.H. Holcomb, M.J. Binder, N.M. Josefik, and U.S. ERDC-CERL, "Fuel cell technology demonstrations at DOD installations," *23rd Army Science Conference. Orlando, USA*, 2002.
- [13] B. Somerday, E.B.B. Somerday, P. Sofronis, A.R. Jones, P. Sofronis, and R. Jones, *Effects of Hydrogen on Materials: Proceedings of the 2008 International Hydrogen Conference, September 7-10, 2008, Jackson Lake Lodge, Grand Teton National Park, Wyoming, USA*, ASM International, 2009.
- [14] K. Kendall, B.G. Pollet, A. Dhir, I. Staffell, B. Millington, and J. Jostins, "Hydrogen fuel cell hybrid vehicles (HFCHV) for Birmingham campus," *Journal of Power Sources*, 2009.
- [15] S.C. Singhal and K. Kendall, *High temperature solid oxide fuel cells: fundamentals, design, and applications*, Elsevier Science Ltd, 2003.
- [16] A.B. Stambouli and E. Traversa, "Solid oxide fuel cells (SOFCs): a review of an environmentally clean and efficient source of energy," *Renewable and Sustainable Energy Reviews*, vol. 6, 2002, pp. 433-455.
- [17] R. Payne, J. Love, and M. Kah, "Generating Electricity at 60% Electrical Efficiency from 1 - 2 kW_e SOFC Products," *ECS Transactions*, Vienna, Austria: 2009, pp. 231-239.
- [18] M.C. Williams, J.P. Strakey, and S.C. Singhal, "US distributed generation fuel cell program," *Journal of Power Sources*, vol. 131, 2004, pp. 79-85.
- [19] J. Doyon, H. Ghezel-Ayagh, J. Walzak, S.T. Junker, D. Patel, A. Adriani, P. Huang, D. Stauffer, V. Vaysman, J.S. White, B. Borglum, E. Tang, R. Petri, and C. Sishtla, "SECA Coal-Based Multi-MW SOFC Power Plant Development," *ECS Transactions*, San Antonio, Texas: 2008, pp. 385-389.

- [20] J.L. Lilien and G. Minne, "Performance assessment of a 5 kW SOFC cogeneration fuel cell," *International Journal of Environmental Technology & Management*, vol. 9, 2008.
- [21] F.J. Gardner, M.J. Day, N.P. Brandon, M.N. Pashley, and M. Cassidy, "SOFC technology development at Rolls-Royce," *Journal of Power Sources*, vol. 86, Mar. 2000, pp. 122-129.
- [22] "RRFCS Website."
- [23] L. Magistri, M. Bozzolo, O. Tarnowski, G. Agnew, and A.F. Massardo, "Design and Off-Design Analysis of a MW Hybrid System Based on Rolls-Royce Integrated Planar Solid Oxide Fuel Cells," *Journal of Engineering for Gas Turbines and Power*, vol. 129, 2007, p. 792.
- [24] H. Liu, C. Song, L. Zhang, J. Zhang, H. Wang, and D.P. Wilkinson, "A review of anode catalysis in the direct methanol fuel cell," *Journal of Power Sources*, vol. 155, 2006, pp. 95-110.
- [25] J. Cruickshank and K. Scott, "The degree and effect of methanol crossover in the direct methanol fuel cell," *Journal of Power Sources*, vol. 70, Jan. 1998, pp. 40-47.
- [26] S. Zhang, X. Yuan, J.N.C. Hin, H. Wang, K.A. Friedrich, and M. Schulze, "A review of platinum-based catalyst layer degradation in proton exchange membrane fuel cells," *Journal of Power Sources*, vol. 194, Dec. 2009, pp. 588-600.
- [27] Q. Ye, T.S. Zhao, H. Yang, and J. Prabhuram, "Electrochemical Reactions in a DMFC under Open-Circuit Conditions," *Electrochemical and Solid-State Letters*, vol. 8, 2005, pp. A52-A54.
- [28] G.Q. Lu, F.Q. Liu, and C. Wang, "Water Transport Through Nafion 112 Membrane in DMFCs," *Electrochemical and Solid-State Letters*, vol. 8, 2005, p. A1.
- [29] J. Liu, T. Zhao, R. Chen, and C. Wong, "The effect of methanol concentration on the performance of a passive DMFC," *Electrochemistry Communications*, vol. 7, Mar. 2005, pp. 288-294.
- [30] M.D. Goods, "DEPARTMENT OF TRANSPORTATION," *Omni*, vol. 65, 2009, pp. 0027-0034.
- [31] *Transport security administration*.
- [32] W. Nernst, *U« ber die elektrolytische Leitung fester Ko« rper bei sehr hohen Temperaturen. Z.El ektrochem.*, 6 (1899) 41^43.
- [33] C. Wagner, *U« ber den Mechanismus der elektrischen Stromleitung im Nernststift. Naturwissenschaften*, 31 (1943) 265^268.
- [34] E. Baur and H. Preis, *Z. Electrochem*, 1937, p. 727.
- [35] A.L. Dicks, "Hydrogen generation from natural gas for the fuel cell systems of tomorrow," *Journal of Power Sources*, vol. 61, 1996, pp. 113-124.
- [36] A. Dhir, "Improved Microtubular Solid Oxide Fuel Cells," University of Birmingham, 2008.
- [37] A. Weber, B. Sauer, A.C. M« ller, D. Herbstritt, and E. Ivers-Tiff« e, "Oxidation of H₂, CO and methane in SOFCs with Ni/YSZ-cermet anodes," *Solid State Ionics*, vol. 152-153, Dec. 2002, pp. 543-550.
- [38] R.M. Ormerod, "Solid oxide fuel cells," *Chemical Society Reviews*, vol. 32, 2003, pp. 17-28.
- [39] A. Atkinson, S. Barnett, R.J. Gorte, J.T.S. Irvine, A.J. McEvoy, M. Mogensen, S.C. Singhal, and J. Vohs, "Advanced anodes for high-temperature fuel cells,"

- Nat Mater*, vol. 3, Jan. 2004, pp. 17-27.
- [40] A. Atkinson, "SOFC Anodes, 7th International Solid Fuel Cell Summer School," 2010.
- [41] T. Komatsu, Y. Yoshida, K. Watanabe, R. Chiba, H. Taguchi, H. Orui, and H. Arai, "Degradation behavior of anode-supported solid oxide fuel cell using LNF cathode as function of current load," *Journal of Power Sources*, vol. 195, Sep. 2010, pp. 5601-5605.
- [42] H. Möbius, "On the history of solid electrolyte fuel cells," *Journal of Solid State Electrochemistry*, vol. 1, Jul. 1997, pp. 2-16.
- [43] W.Z. Zhu and S.C. Deevi, "A review on the status of anode materials for solid oxide fuel cells," *Materials Science and Engineering A*, vol. 362, Dec. 2003, pp. 228-239.
- [44] A.S. Joshi, K.N. Grew, A.A. Peracchio, and W.K. Chiu, "Lattice Boltzmann modeling of 2D gas transport in a solid oxide fuel cell anode," *Journal of Power Sources*, vol. 164, Feb. 2007, pp. 631-638.
- [45] C. Tsai and V.H. Schmidt, "Tortuosity in anode-supported proton conductive solid oxide fuel cell found from current flow rates and dusty-gas model," *Journal of Power Sources*, vol. 196, Jan. 2011, pp. 692-699.
- [46] M. Radovic and E. Lara-Curzio, "Mechanical properties of tape cast nickel-based anode materials for solid oxide fuel cells before and after reduction in hydrogen," *Acta Materialia*, vol. 52, Dec. 2004, pp. 5747-5756.
- [47] A.R. Oller, D.T. Kirkpatrick, A. Radovsky, and H.K. Bates, "Inhalation carcinogenicity study with nickel metal powder in Wistar rats," *Toxicology and applied pharmacology*, vol. 233, 2008, pp. 262-275.
- [48] B.C.H. Steele, "Appraisal of Ce_{1-y}Gd_yO_{2-y/2} electrolytes for IT-SOFC operation at 500°C," *Solid State Ionics*, vol. 129, Apr. 2000, pp. 95-110.
- [49] B.C.H. Steele, P.H. Middleton, and R.A. Rudkin, "Material science aspects of SOFC technology with special reference to anode development," *Solid State Ionics*, vol. 40-41, Aug. 1990, pp. 388-393.
- [50] S. McIntosh, J.M. Vohs, and R.J. Gorte, "Effect of Precious-Metal Dopants on SOFC Anodes for Direct Utilization of Hydrocarbons," *Electrochemical and Solid-State Letters*, vol. 6, Nov. 2003, pp. A240-A243.
- [51] C. Sun, R. Hui, and J. Roller, "Cathode materials for solid oxide fuel cells: a review," *Journal of Solid State Electrochemistry*, vol. 14, Jul. 2010, pp. 1125-1144.
- [52] Z. Yang, "Recent advances in metallic interconnects for solid oxide fuel cells," *International Materials Reviews*, vol. 53, pp. 39-54.
- [53] Y. Funahashi, T. Shimamori, T. Suzuki, Y. Fujishiro, and M. Awano, "New Fabrication Technique for Series-Connected Stack With Micro Tubular SOFCs," *Fuel Cells*, vol. 9, 2009, pp. 711-716.
- [54] N. Shaigan, W. Qu, D.G. Ivey, and W. Chen, "A review of recent progress in coatings, surface modifications and alloy developments for solid oxide fuel cell ferritic stainless steel interconnects," *Journal of Power Sources*, vol. 195, Mar. 2010, pp. 1529-1542.
- [55] P. Huczowski, N. Christiansen, V. Shemet, L. Niewolak, J. Piron-Abellan, L. Singheiser, and W.J. Quadackers, "Growth Mechanisms and Electrical Conductivity of Oxide Scales on Ferritic Steels Proposed as Interconnect Materials for SOFC's," *Fuel Cells*, vol. 6, 2006, pp. 93-99.
- [56] P. Huczowski, V. Shemet, J. Piron-Abellan, L. Singheiser, W.J. Quadackers,

- and N. Christiansen, "Oxidation limited life times of chromia forming ferritic steels," *Materials and Corrosion*, vol. 55, 2004, pp. 825-830.
- [57] I. Antepará, I. Villarreal, L.M. Rodríguez-Martínez, N. Lecanda, U. Castro, and A. Laresgoiti, "Evaluation of ferritic steels for use as interconnects and porous metal supports in IT-SOFCs," *Journal of Power Sources*, vol. 151, 2005, pp. 103–107.
- [58] K.J. Yoon, C.N. Cramer, J.W. Stevenson, and O.A. Marina, "Advanced ceramic interconnect material for solid oxide fuel cells: Electrical and thermal properties of calcium- and nickel-doped yttrium chromites," *Journal of Power Sources*, vol. 195, Nov. 2010, pp. 7587-7593.
- [59] J.W. Fergus, "Lanthanum chromite-based materials for solid oxide fuel cell interconnects," *Solid State Ionics*, vol. 171, Jun. 2004, pp. 1-15.
- [60] "Shaffer, S. Development Update on Delphi's Solid Oxide Fuel Cell System. in SECA 2004 Annual Meeting and Core Program Review. 2004. Boston: US DOE NETL."
- [61] P. Tanasini, M. Cannarozzo, P. Costamagna, A. Faes, J.V. Herle, A. Hessler-Wyser, and C. Comninellis, "Experimental and Theoretical Investigation of Degradation Mechanisms by Particle Coarsening in SOFC Electrodes," *Fuel Cells*, vol. 9, 2009, pp. 740-752.
- [62] S. Taylor, "Investigation into the improved dispersion of nickel oxide over the surface of SOFC tubular anodes," Dec. 2010.
- [63] H. Yokokawa, H. Tu, B. Iwanschitz, and A. Mai, "Fundamental mechanisms limiting solid oxide fuel cell durability," *Journal of Power Sources*, vol. 182, Aug. 2008, pp. 400-412.
- [64] W. Bujalski, C.M. Dikwal, and K. Kendall, "Cycling of three solid oxide fuel cell types," *Journal of Power Sources*, vol. 171, 2007, pp. 96–100.
- [65] X.Y. Zhou, A. Pramuanjaroenkij, and S. Kakaç, "A Review on Miniaturization of Solid Oxide Fuel Cell Power Sources-I: State-of-The-Art Systems," *Mini-Micro Fuel Cells*, 2008, pp. 303–318.
- [66] L. Liu, G.Y. Kim, and A. Chandra, "Modeling of thermal stresses and lifetime prediction of planar solid oxide fuel cell under thermal cycling conditions," *Journal of Power Sources*, 2009.
- [67] A. Hagen, P.V. Hendriksen, H.L. Frandsen, K. Thydén, and R. Barfod, "Durability Study of SOFCs Under Cycling Current Load Conditions," *Fuel Cells*, vol. 9, 2009, pp. 814–822.
- [68] W. Bujalski, J. Paragreen, G. Reade, S. Pyke, and K. Kendall, "Cycling studies of solid oxide fuel cells," *Journal of Power Sources*, vol. 157, 2006, pp. 745–749.

7 APPENDICES

7.1 Appendix i - IP-SOFC

7.1.1 Test Conditions

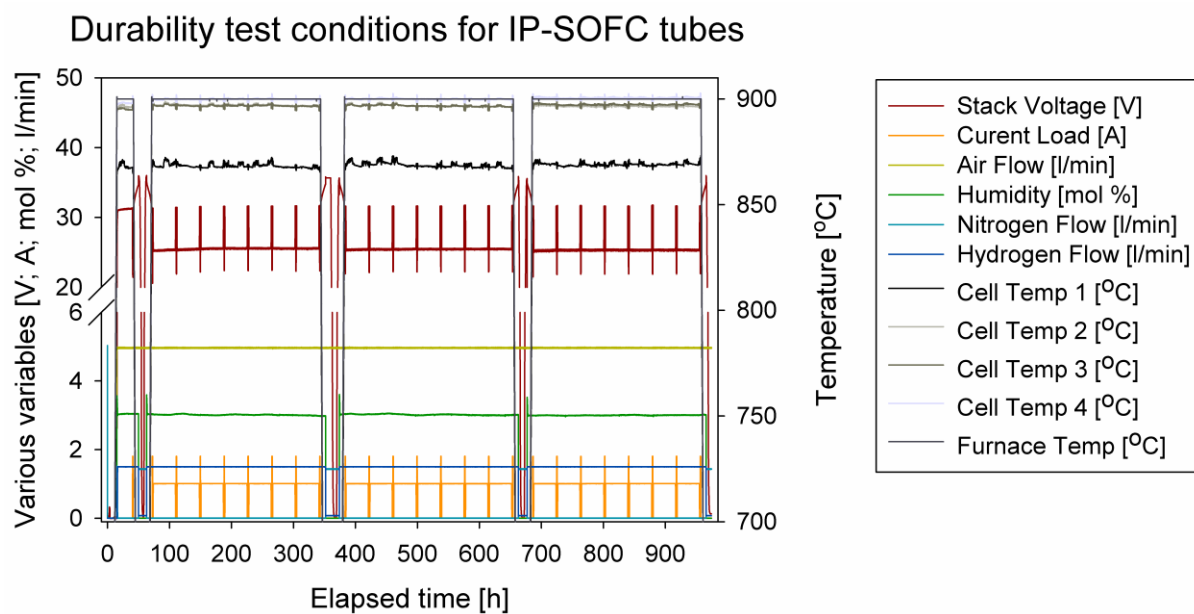


Figure 7-i Test conditions for IP-SOFC over test lifetime

7.1.2 Power output

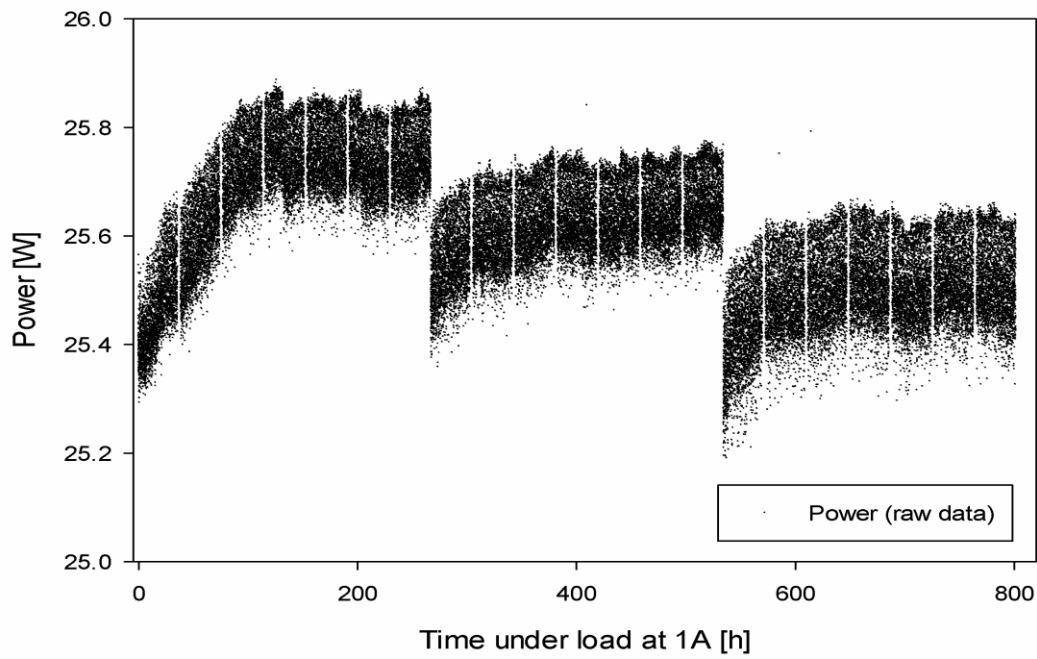


Figure 7-ii Power output from tube 2 at 1A over 801 hours

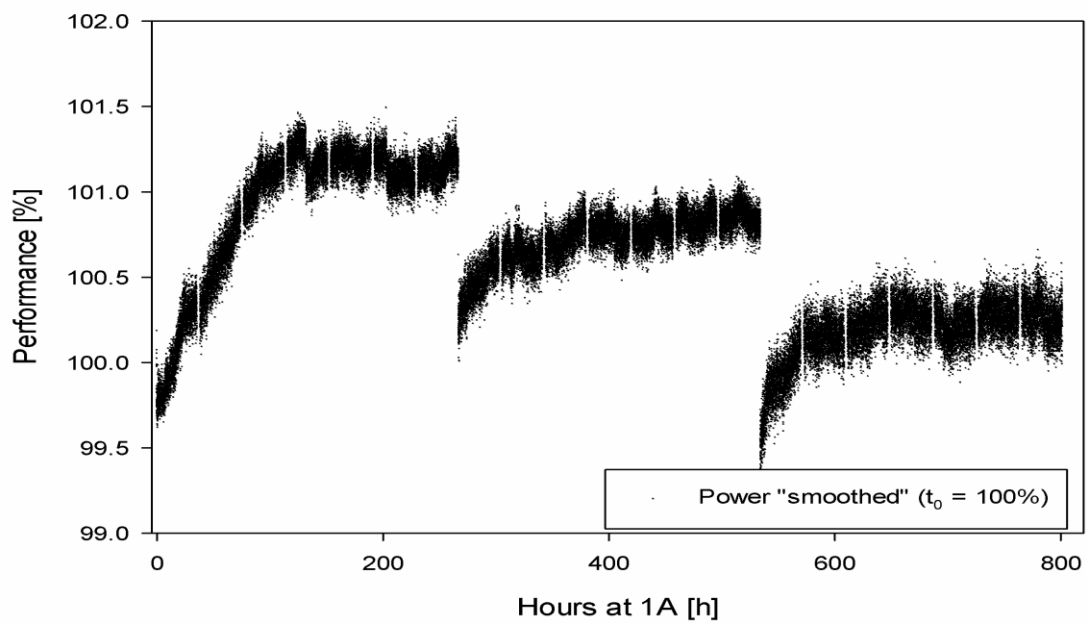


Figure 7-iii "Smoothed" power output from tube 2 at 1A over 801 hours

7.1.3 I-V and Power Curves

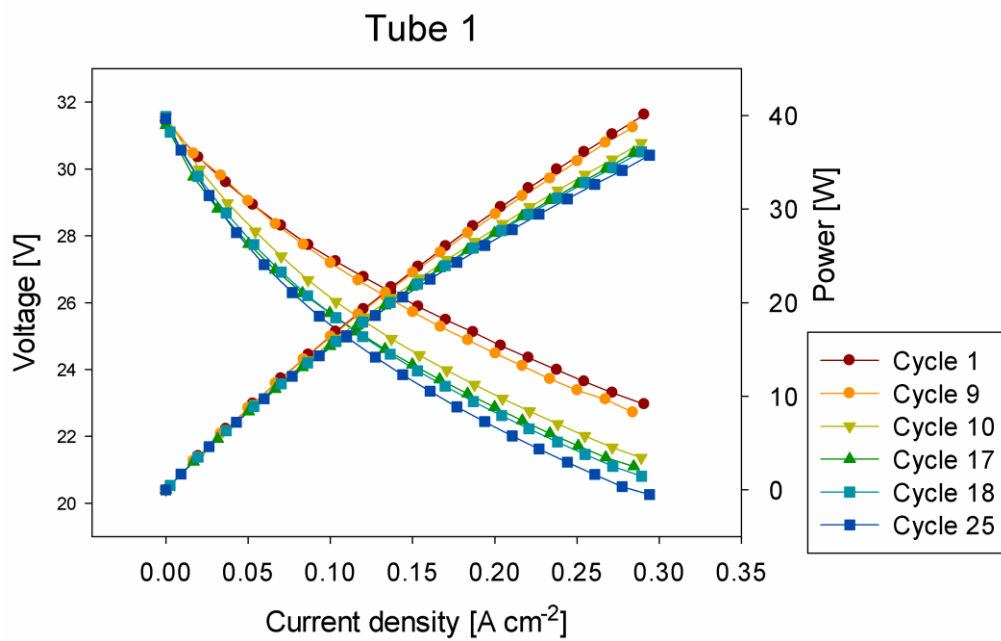


Figure 7-iv IV and power curves for tube 1. From left to right downward sloping lines use left axis, upwards sloping lines use right axis.

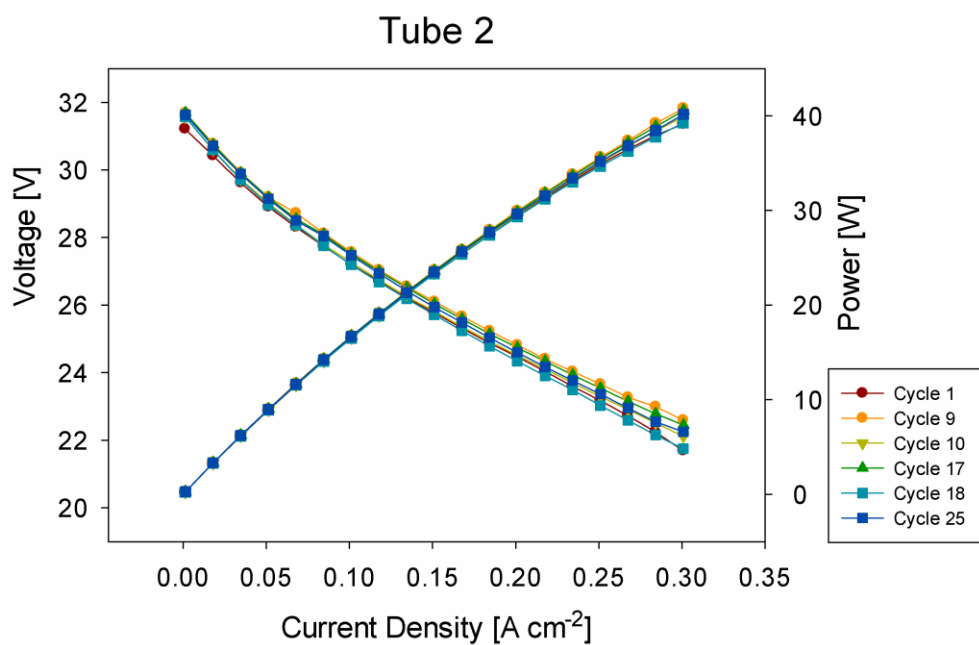


Figure 7-v IV and power curves for tube 2. From left to right downward sloping lines use left axis, upwards sloping lines use right axis.

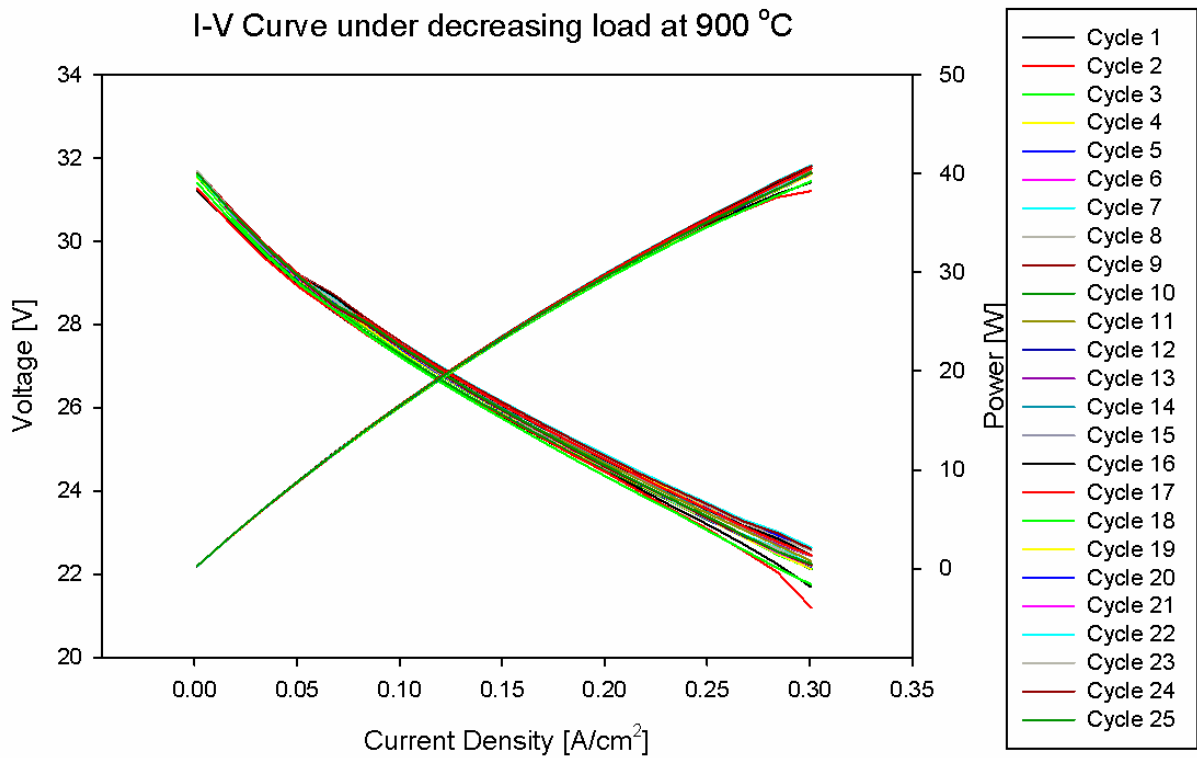


Figure 7-vi IV and power curves for tube 2. From left to right downward sloping lines use left axis, upwards sloping lines use right axis.

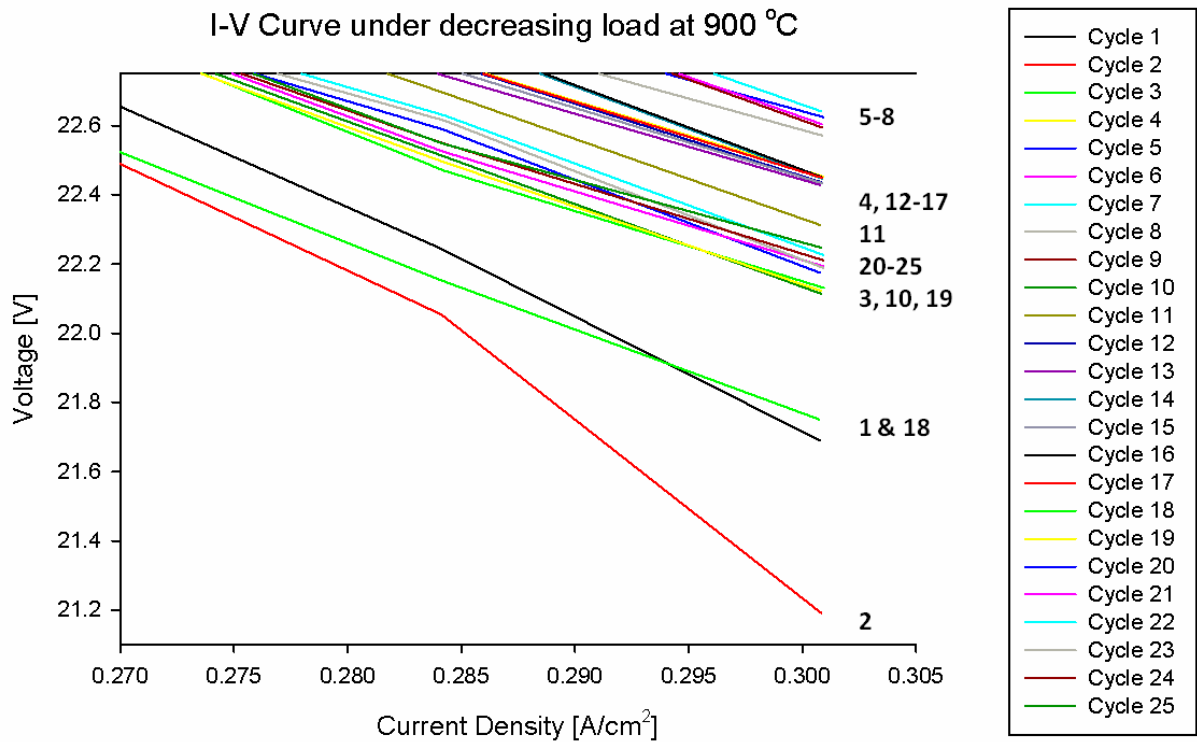


Figure 7-vii Highlighting the difference in voltage at maximum current density in tube 2

7.2 Appendix ii -DMFC

7.2.1 - Voltage response to load

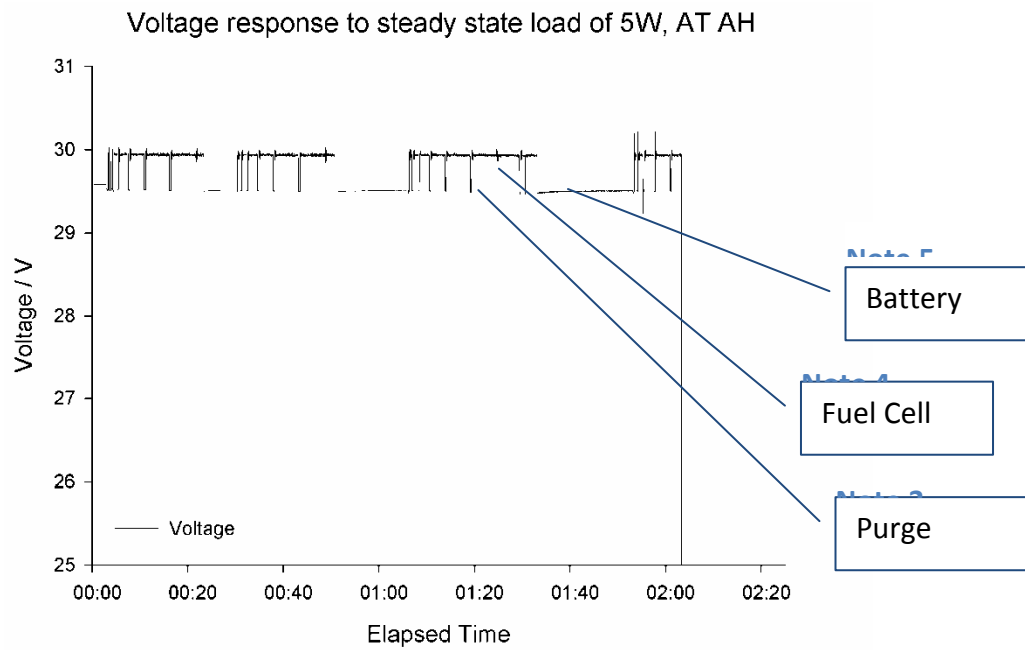


Figure 7-viii. Voltage response to 5W AT AH

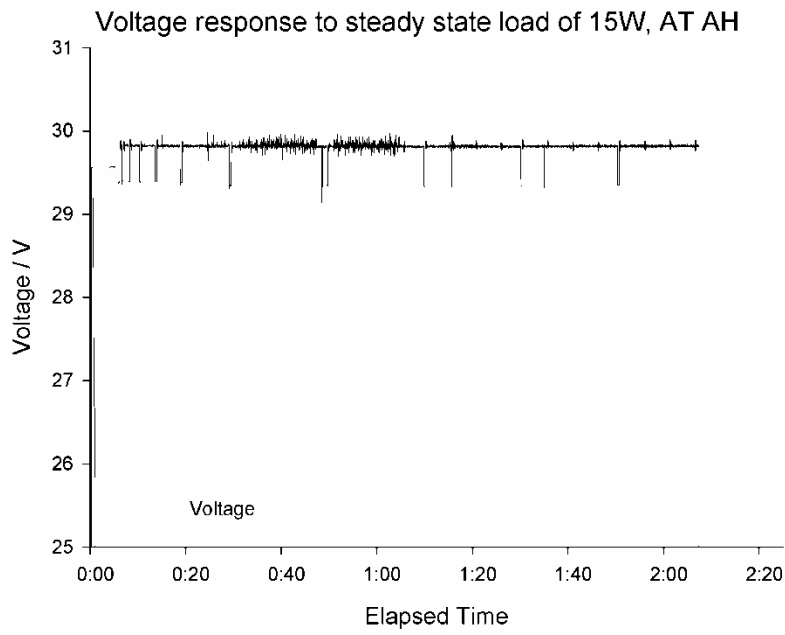


Figure 7-ix. Voltage response to 15W, AT AH, over 2 hours.

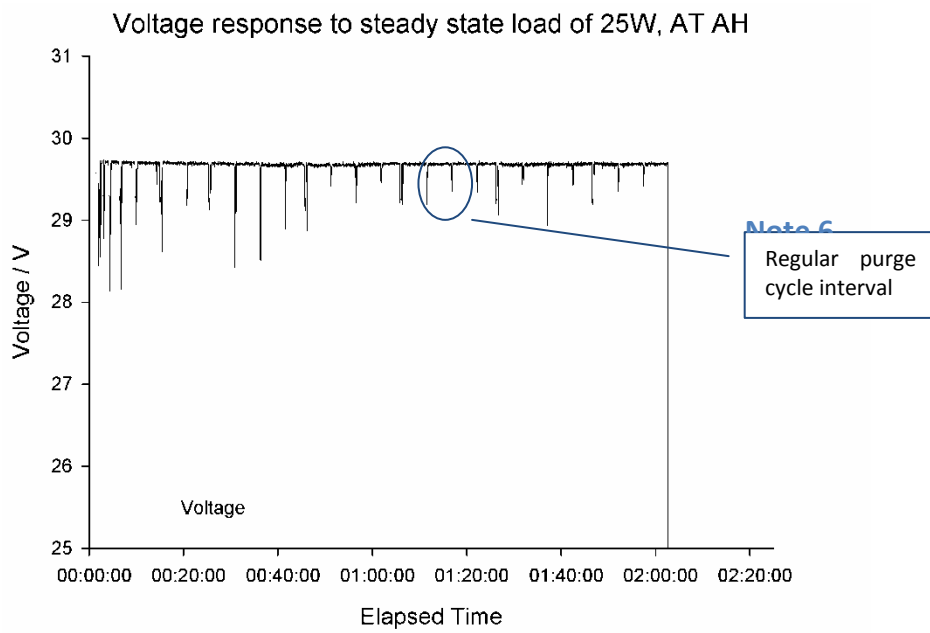


Figure 7-x. Voltage to response 25W AT AH, over 2 hours.

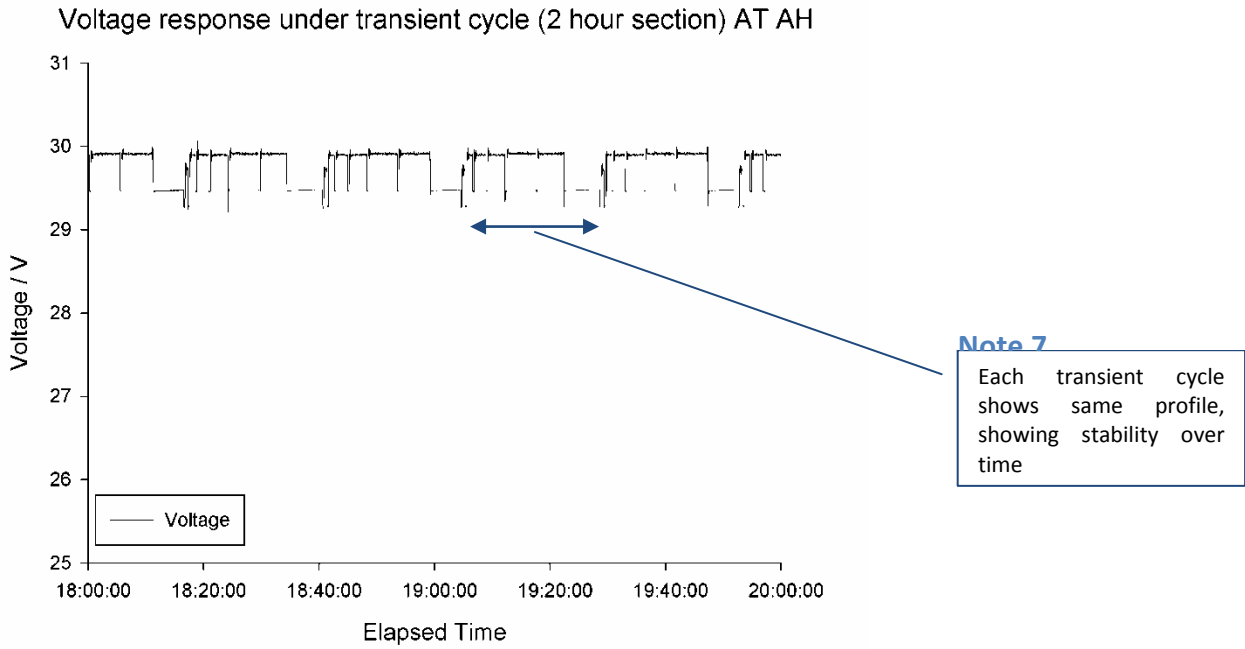


Figure 7-xi. Voltage to response Transient cycle AT AH, over 2 hours.

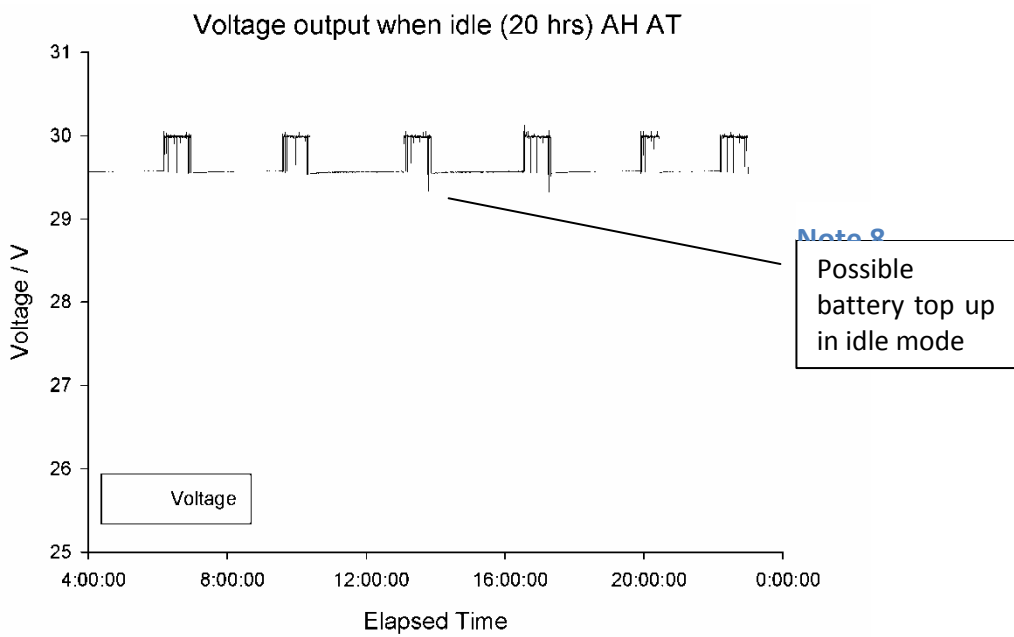


Figure 7-xii. Voltage to response when idle AT AH, over 20 hours.

Voltage response at 25W using desert fuel AH AT

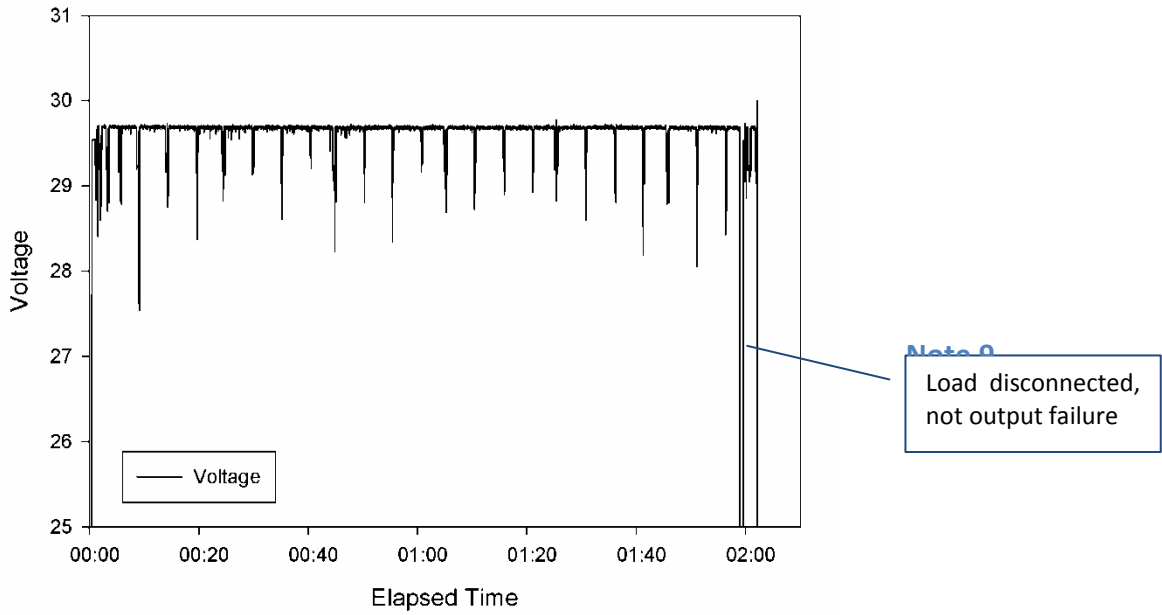


Figure 7-xiii. Voltage to response to 25W, AT AH, over 2 hours, using desert fuel.

Voltage response at 15W using desert fuel AH AT

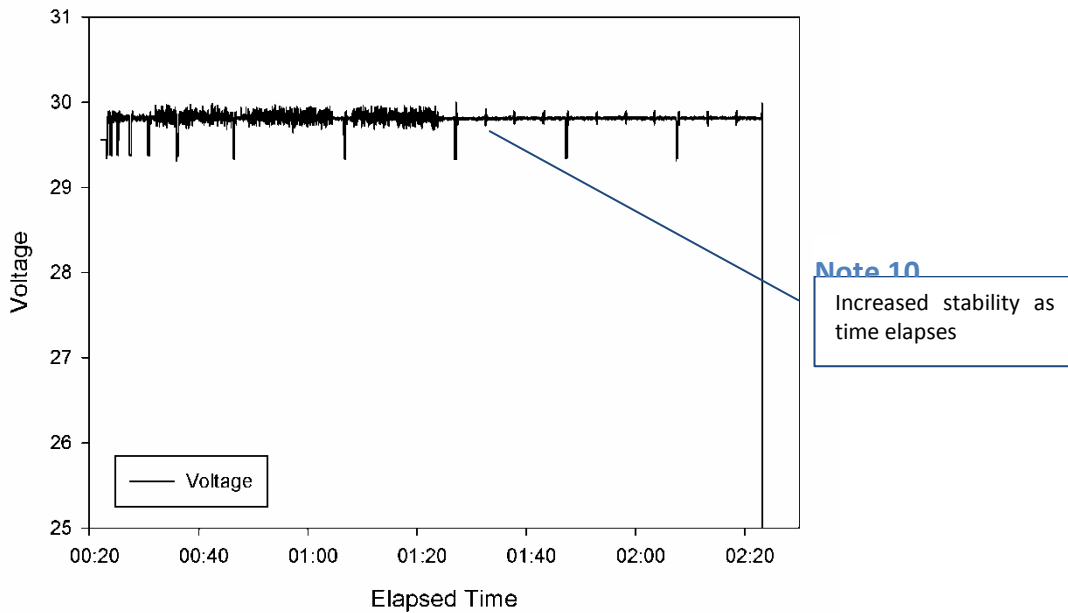


Figure 7-xiv. Voltage to response to 15W, AT AH, over 2 hours, using desert fuel.

Voltage response at 5W using desert fuel AH AT

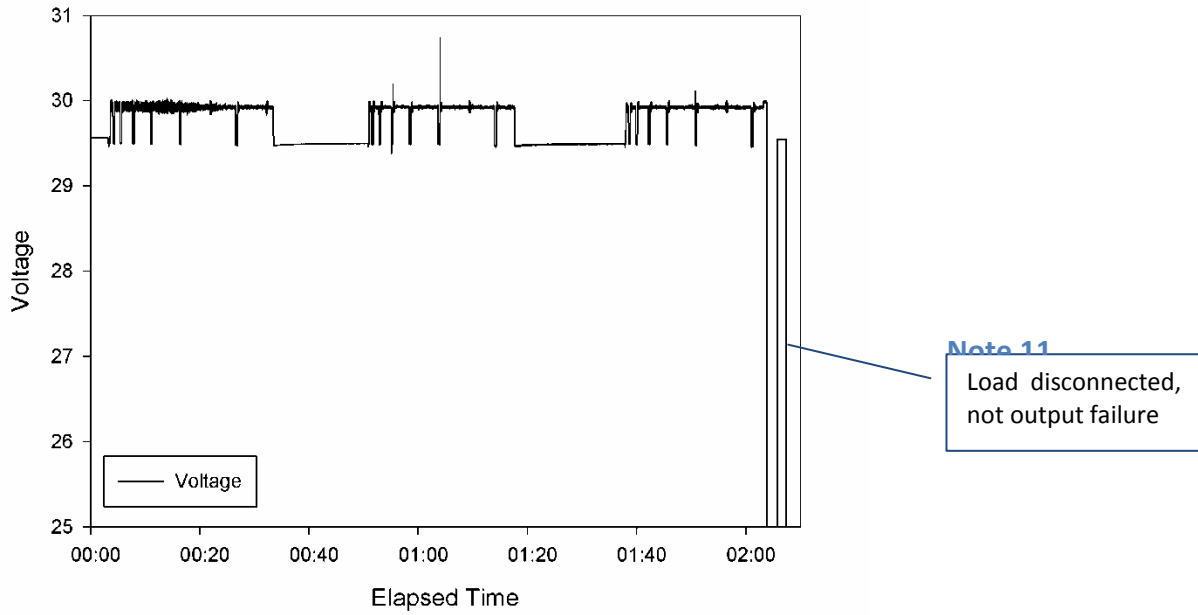


Figure 7-xv. Voltage to response to 5W, AT AH, over 2 hours, using desert fuel.

Voltage response to load (0-4:00 10W, 4:40-6:10 25W, others 0W) AT LH

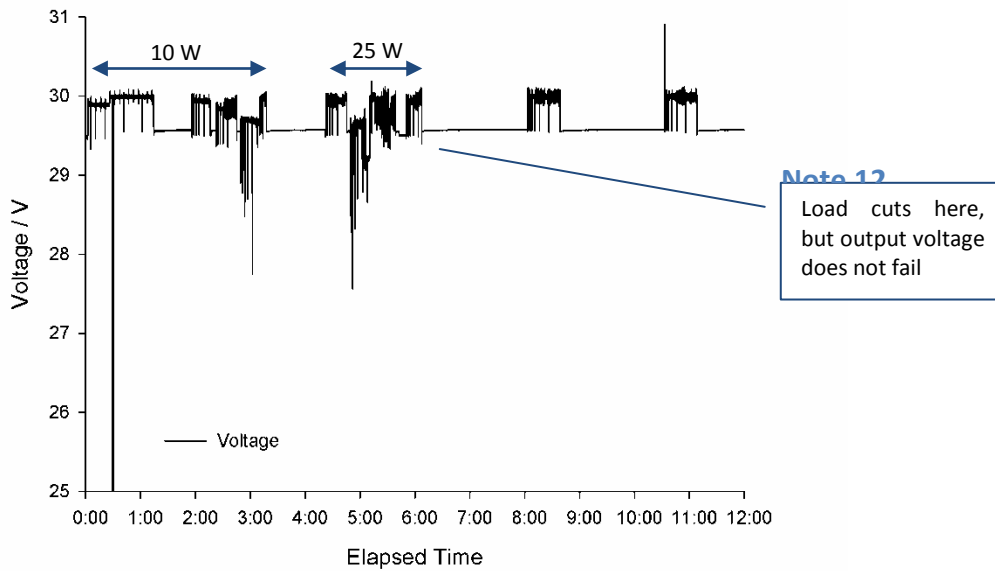


Figure 7-xvi. Voltage to response to 10W, 25W, and idle, AT LH, over 12 hours.

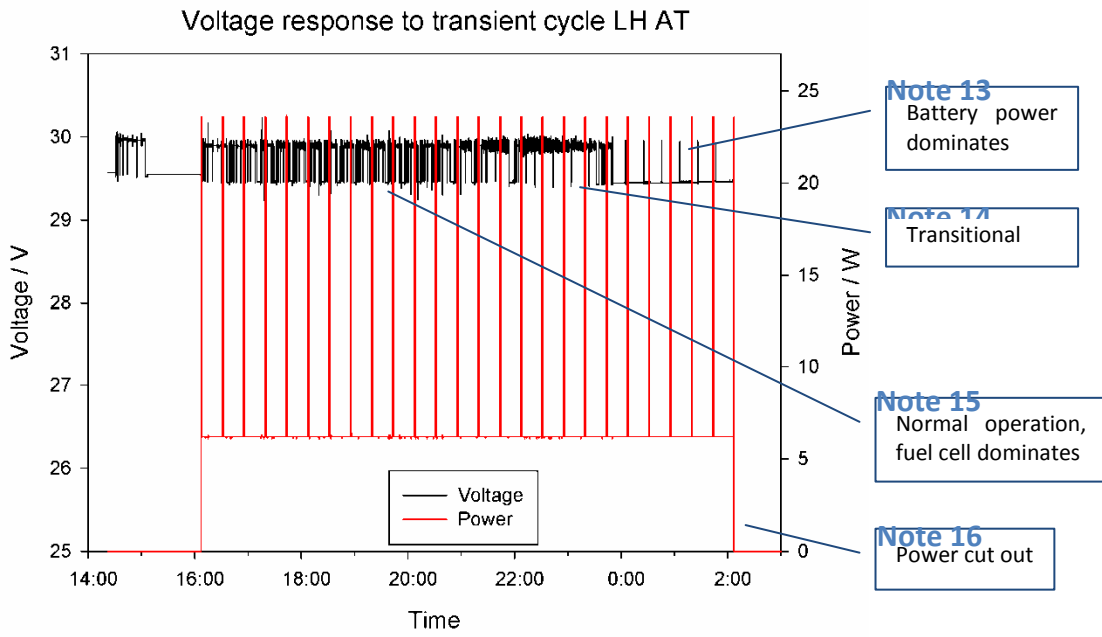


Figure 7-xvii. Voltage to response to transient cycle, AT LH, over 10 hours.

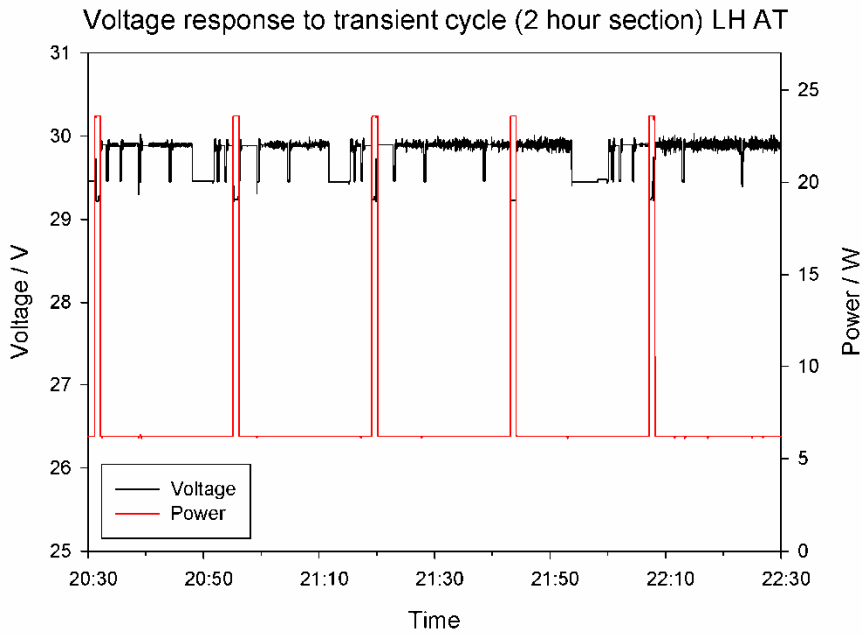


Figure 7-xviii. Voltage to response to transient cycle, AT LH, over 2 hours.

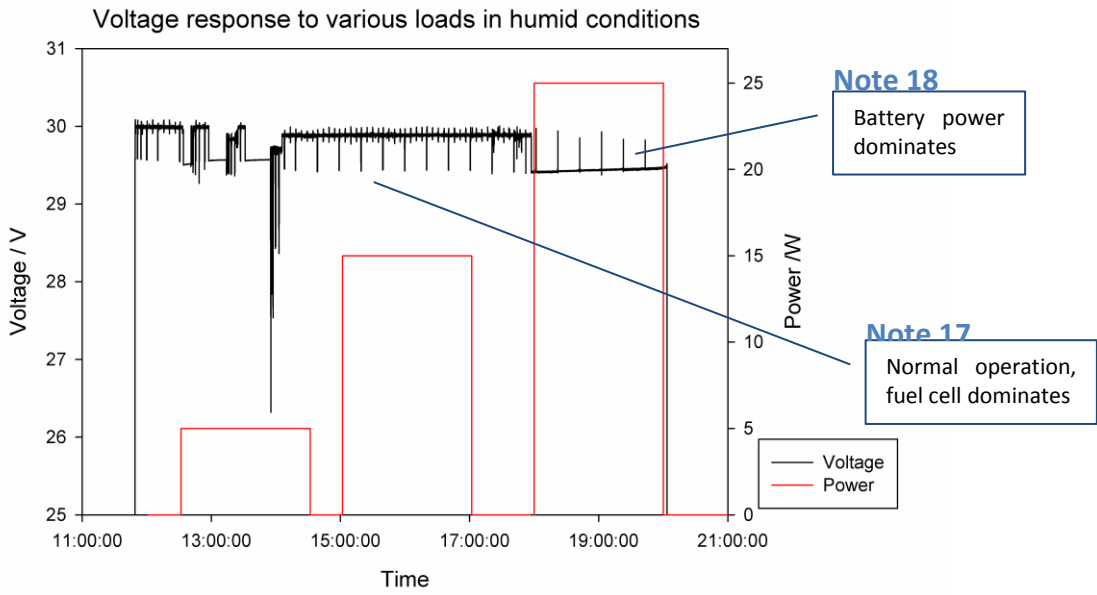


Figure 7-xix. Voltage to response to 5W, 15W and 25W, AT HH, over 10 hours.

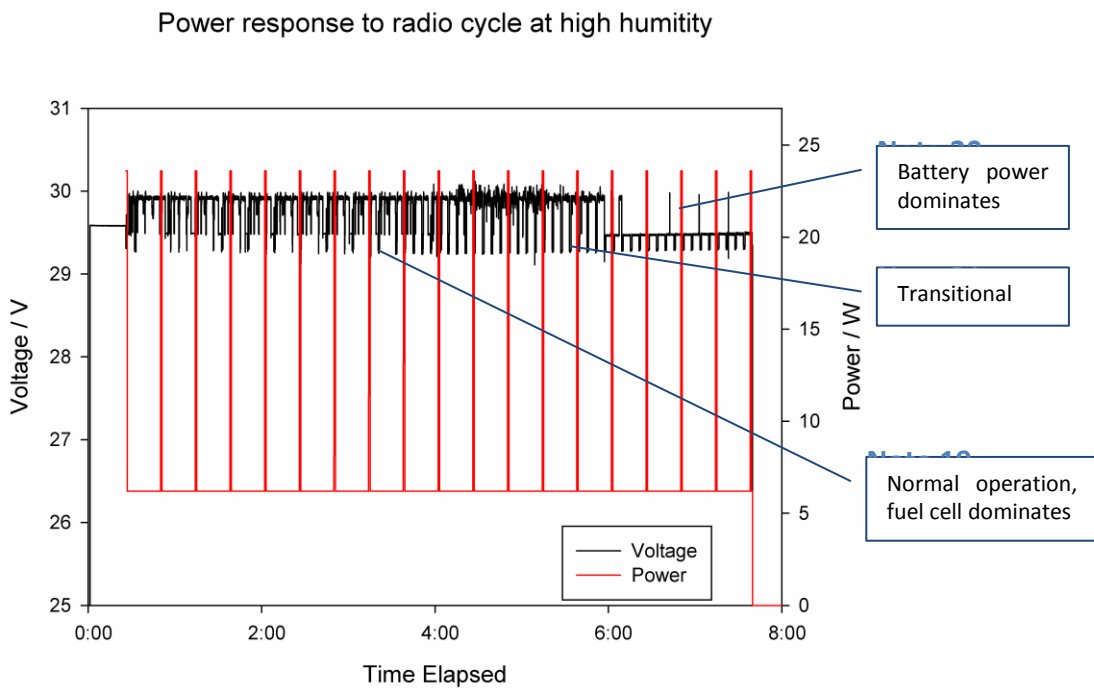


Figure 7-xx. Voltage to response to transient cycle, AT HH, over 8 hours.

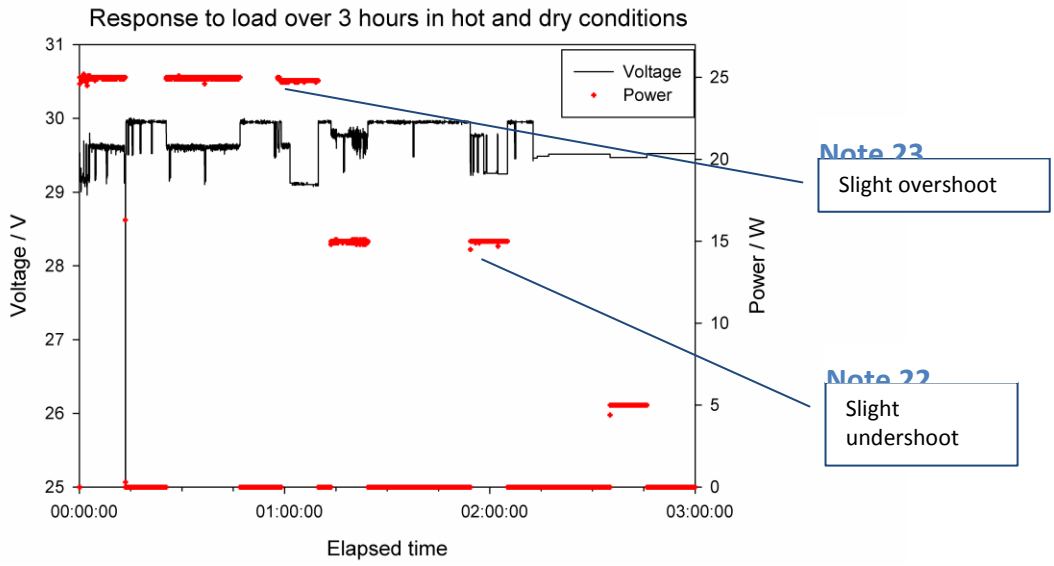


Figure 7-xxi. . Voltage to response to 25W, 15W and 5W, HT LH, over 3 hours. Using desert fuel.

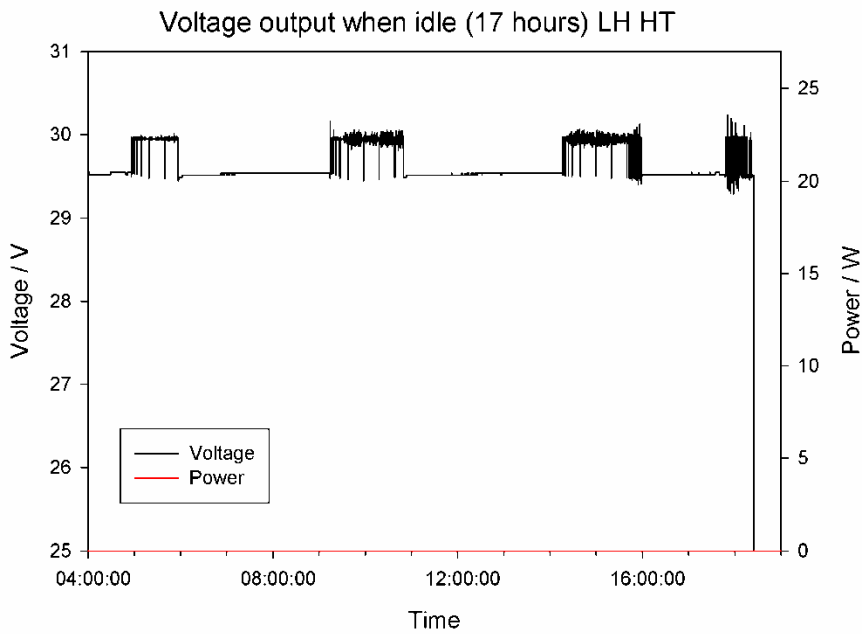


Figure 7-xxii. . Voltage output when idle, HT LH, over 17 hours. Using desert fuel.

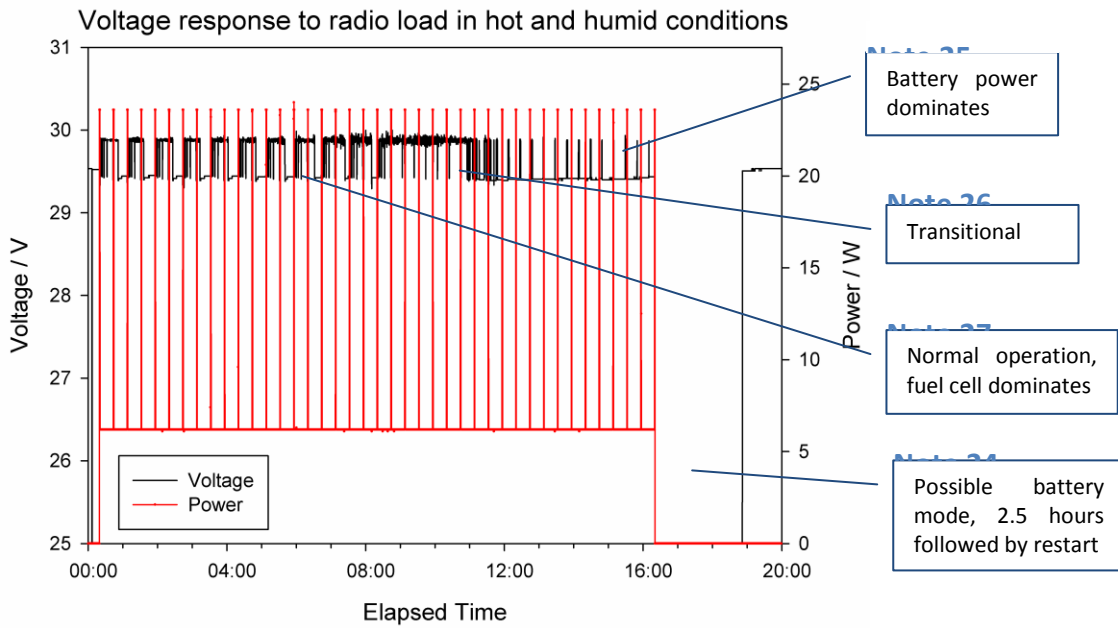


Figure 7-xxiii. Voltage to response to transient cycle, HT HH, over 20 hours. Using desert fuel.

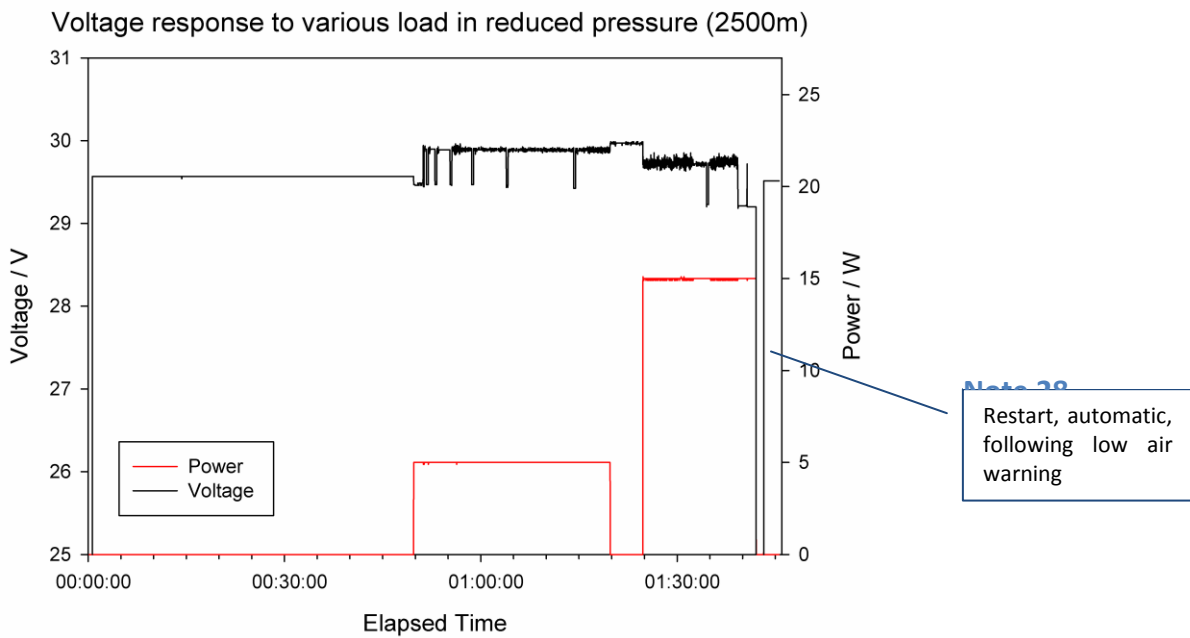


Figure 7-xxiv. Voltage to response to 5W and 15W, HA2500 (pressure), over 2 hours.

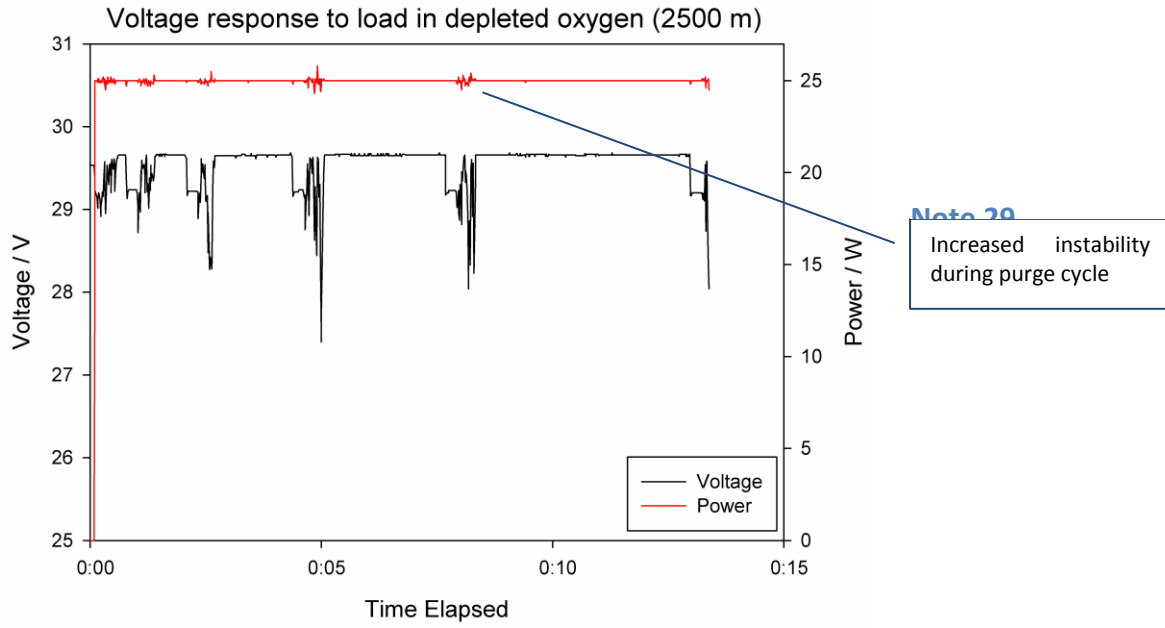


Figure 7-xxv. Voltage response to 25W, HA2500, over 15 minutes.

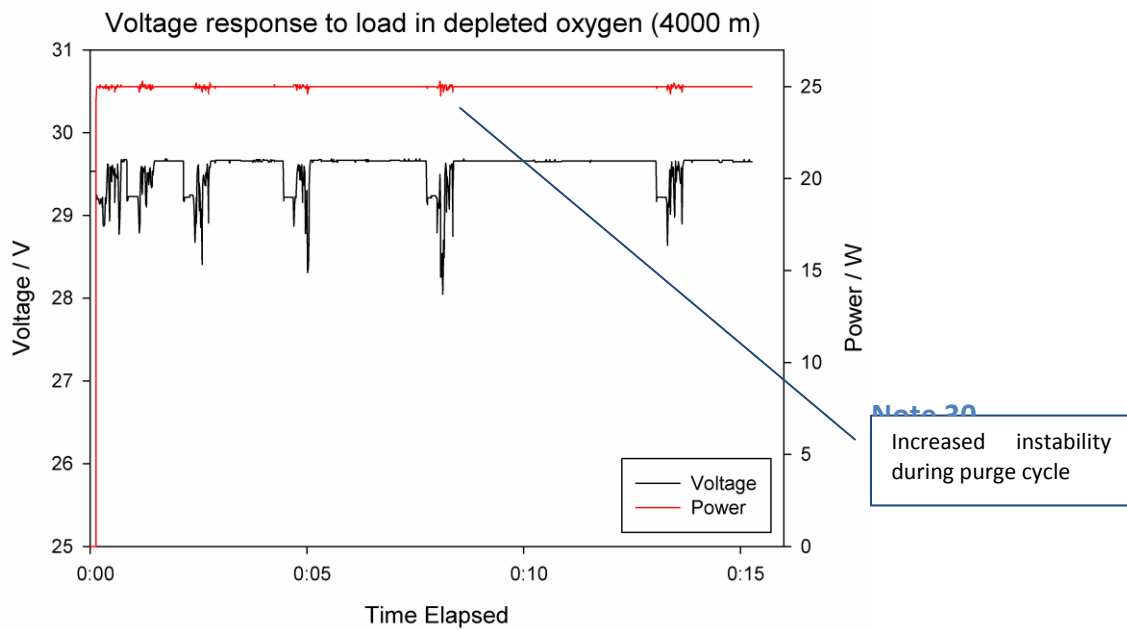


Figure 7-xxvi. Voltage response to 25W, HA4000, over 15 minutes.

7.2.2 Thermal response to load

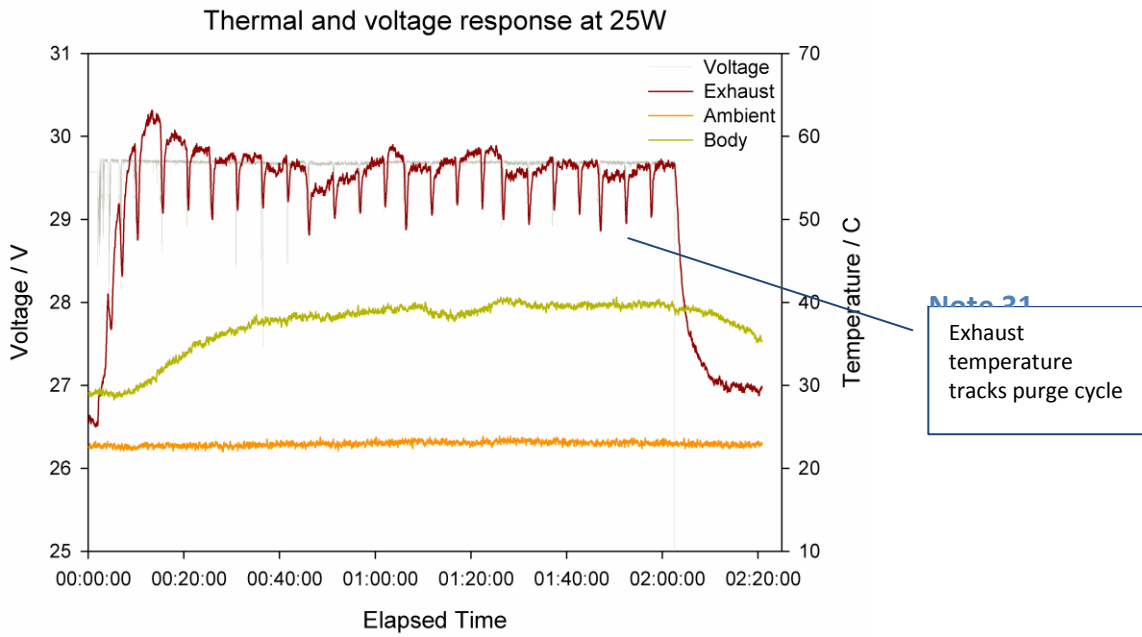


Figure 7-xxvii. Thermal response to load at 25W, AT AH, over 2 hours.

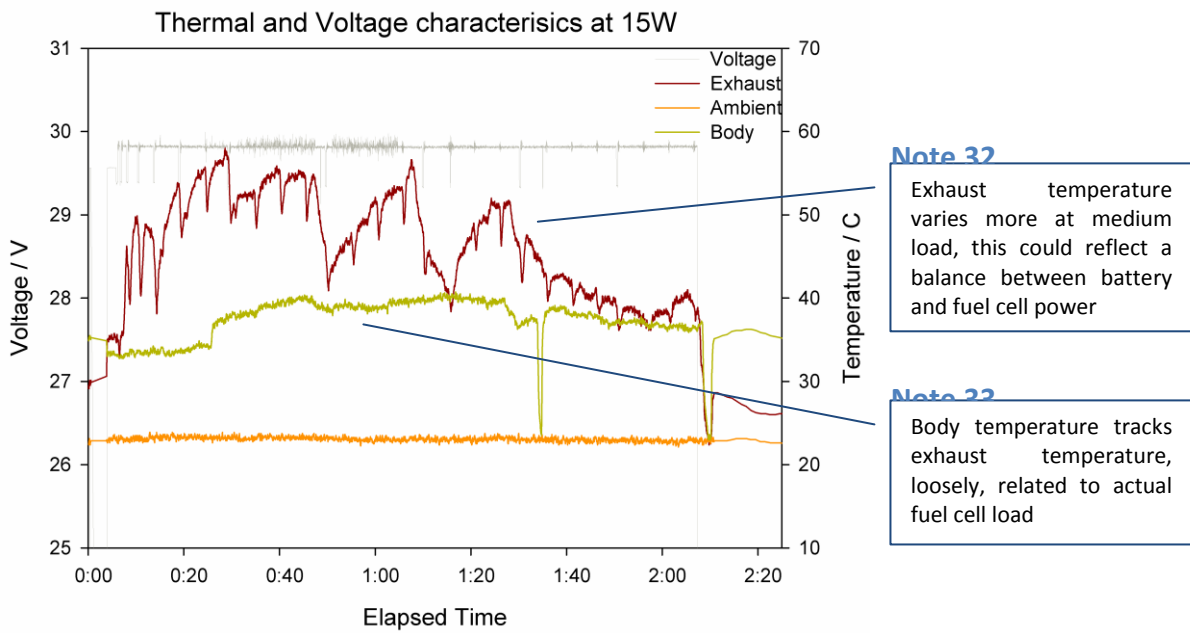


Figure 7-xxviii. Thermal response to load at 15W, AT AH, over 2 hours.

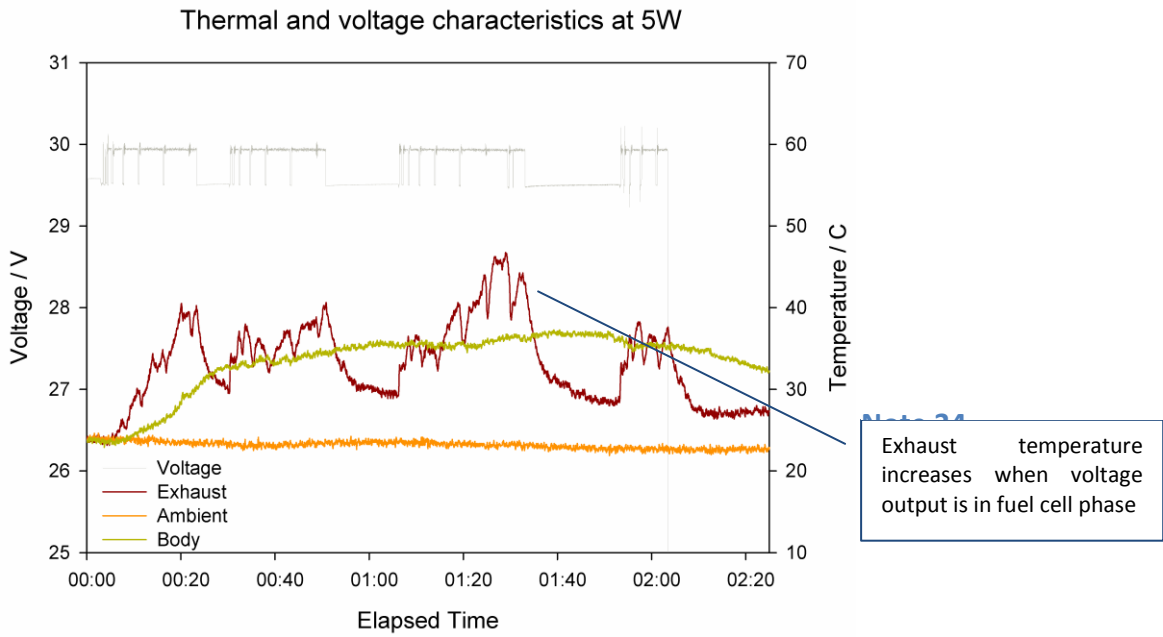


Figure 7-xxix. Thermal response to load at 5W, AT AH, over 2 hours.

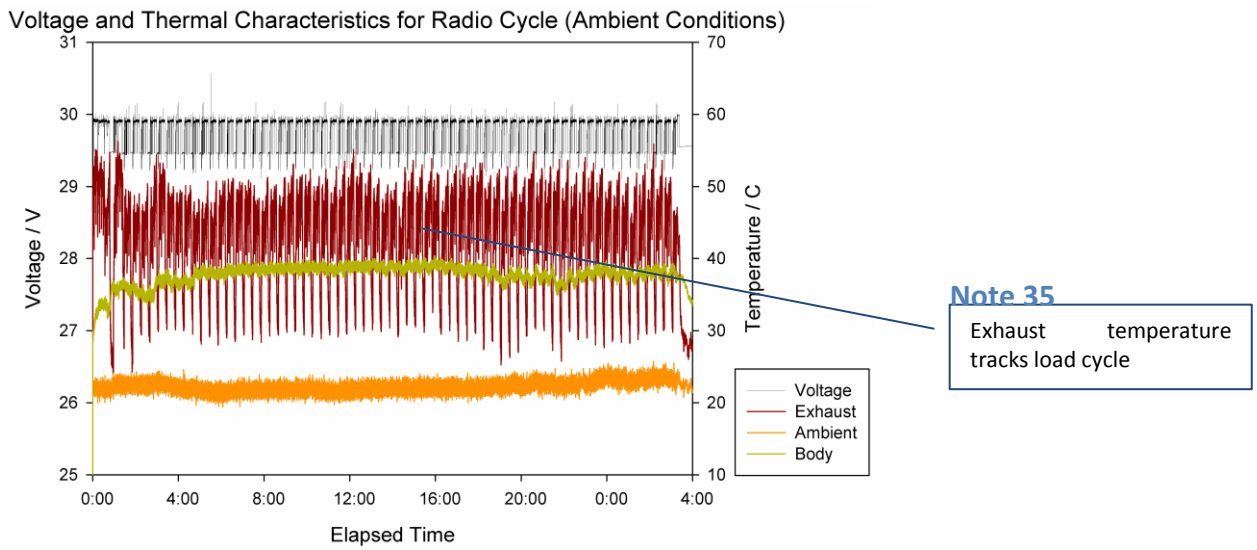


Figure 7-xxx. Thermal response to transient cycle, AT AH, over 28 hours.

Voltage and Thermal Characteristics for Radio Cycle (Ambient Conditions)
Zoomed in to hours 18-20 of continuous operation

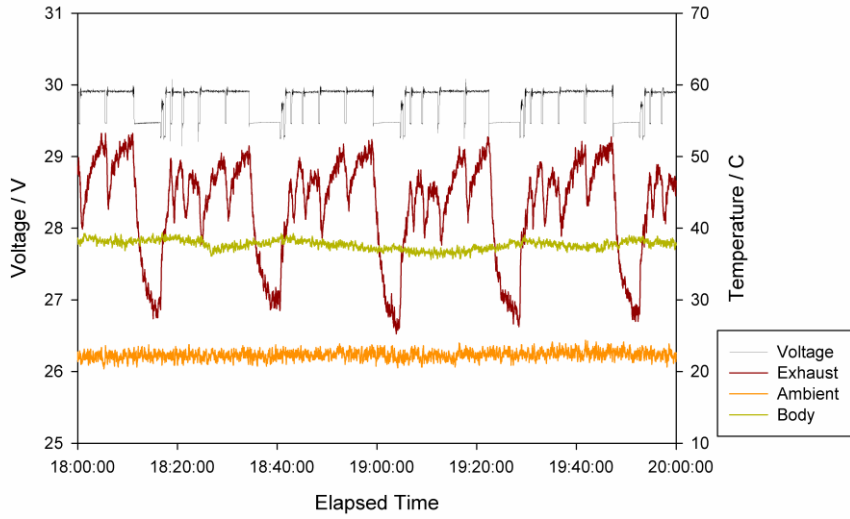


Figure 7-xxxii. Thermal response to transient cycle, AT AH, over 2 hours.

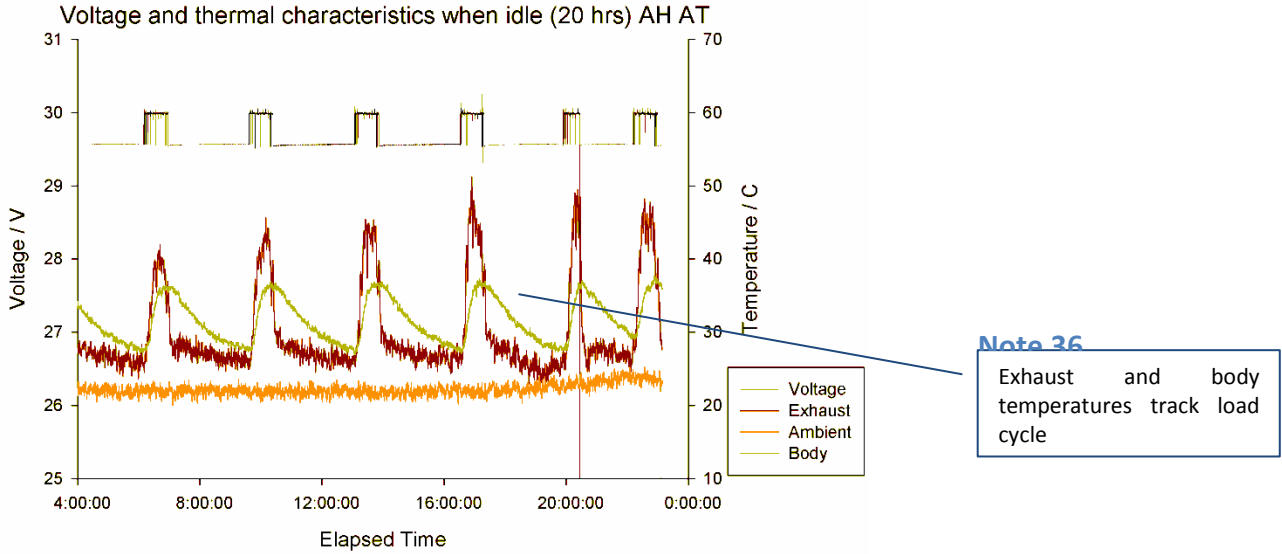


Figure 7-xxxiii. Thermal response when idle, AT AH, over 20 hours.

Voltage and thermal characteristics at 25W using desert fuel AH AT

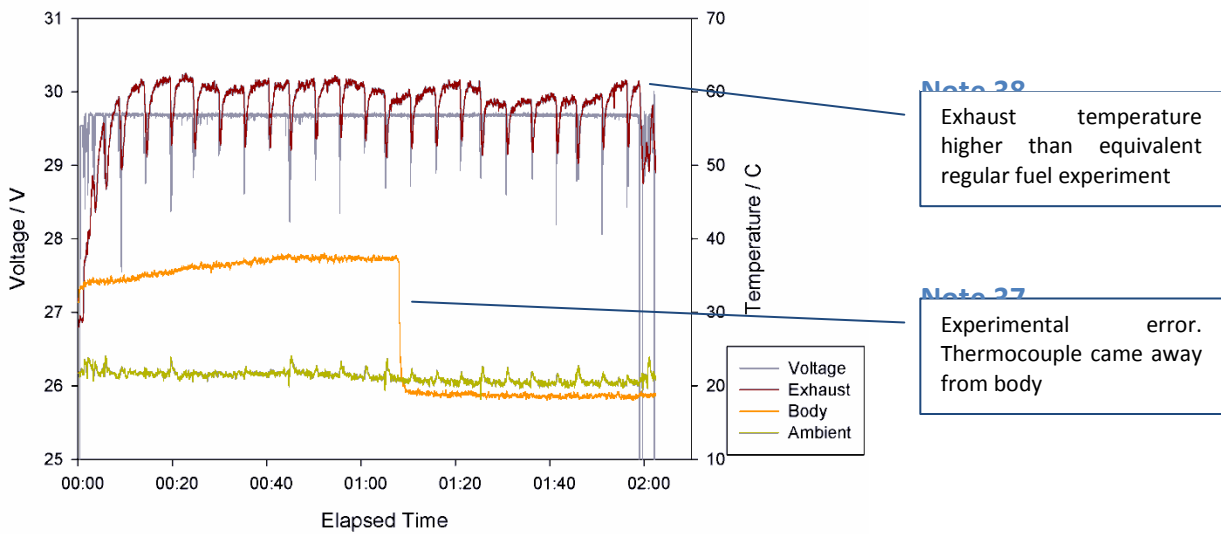


Figure 7-xxxiii. Thermal response to load at 25W, AT AH, over 2 hours. Using desert fuel.

Voltage and thermal characteristics at 15W using desert fuel AH AT

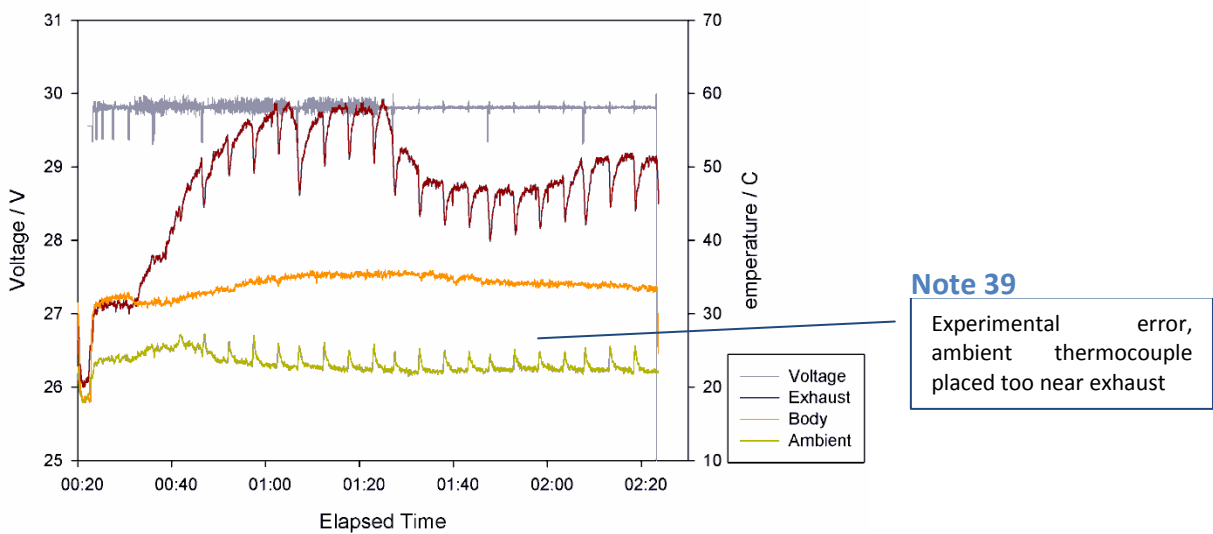


Figure 7-xxxiv. Thermal response to load at 15W, AT AH, over 2 hours. Using desert fuel.

Voltage and thermal characteristics at 5W using desert fuel AH AT

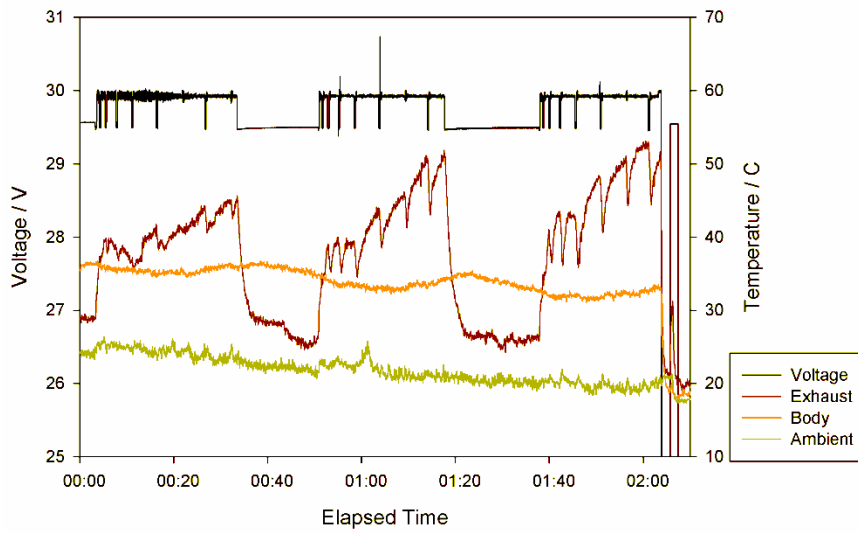
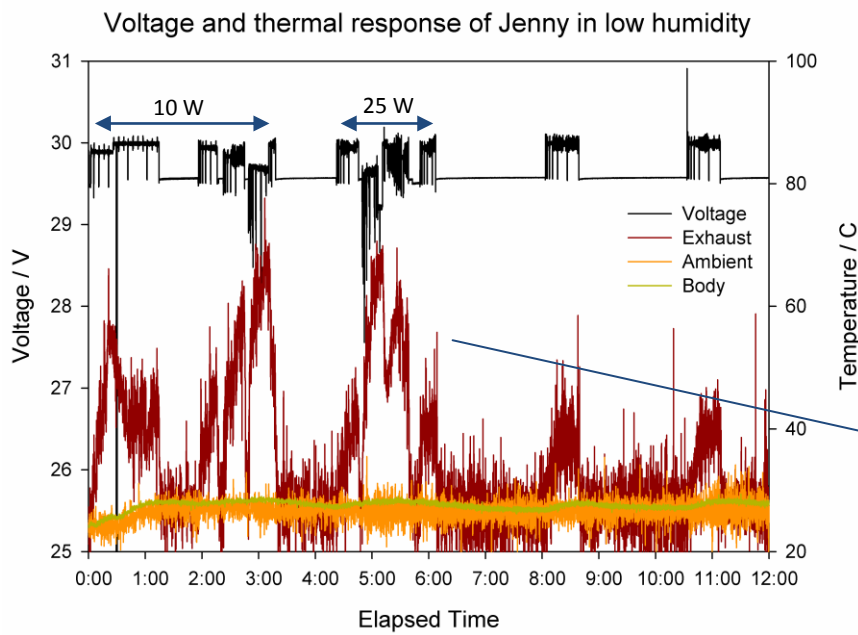
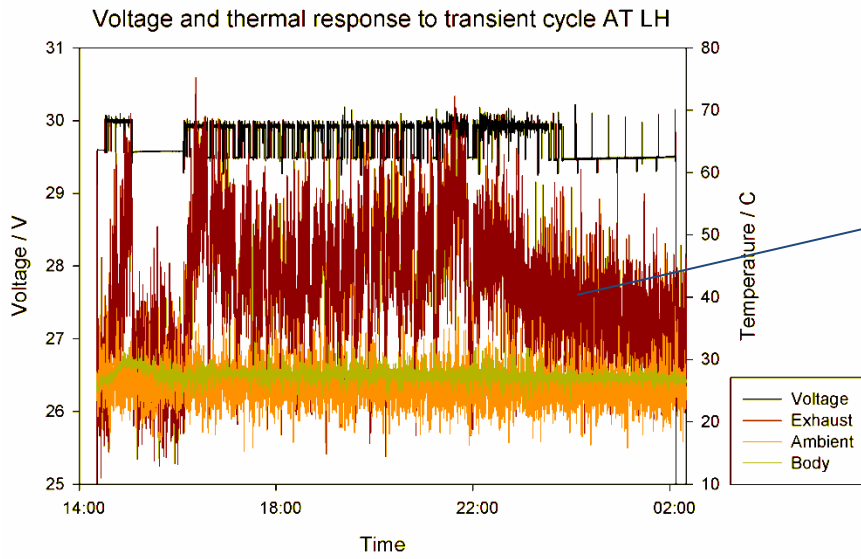


Figure 7-xxxv. Thermal response to load at 5W, AT AH, over 2 hours. Using desert fuel.



Note 40
 Unusual thermal profile for load. Also exhaust rises during active periods when idle

Figure 7-xxxvi. Thermal response to load at 10W, 25W and idle, AT LH, over 12 hours.



Note 41

Noise from climate chamber affected the thermocouple used to monitor exhaust temperatures. Trends may be followed, but values have no meaning.

Figure 7-xxxvii. Thermal response to transient cycle, AT LH, over 2 hours.

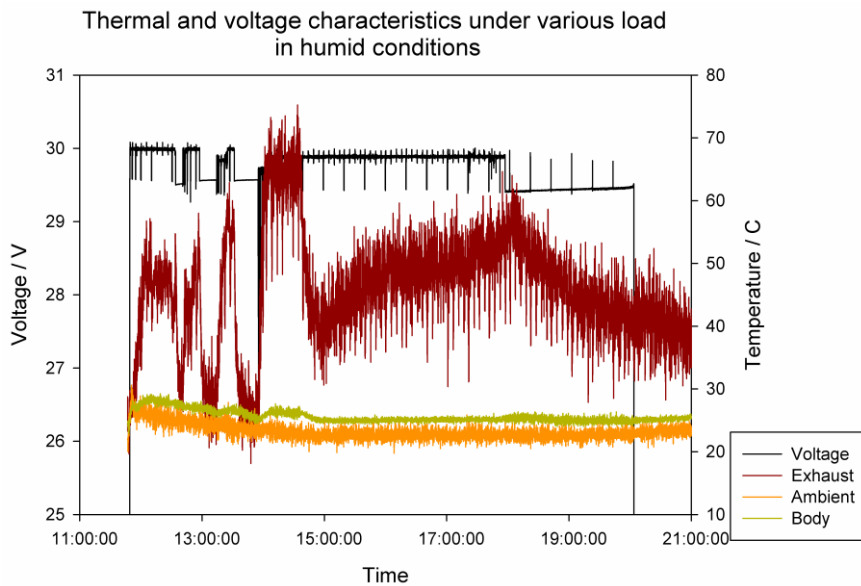


Figure 7-xxxviii. Thermal response to load at 5W, 15W and 25W, AT HH, over 10 hours. See Figure 7-xix.

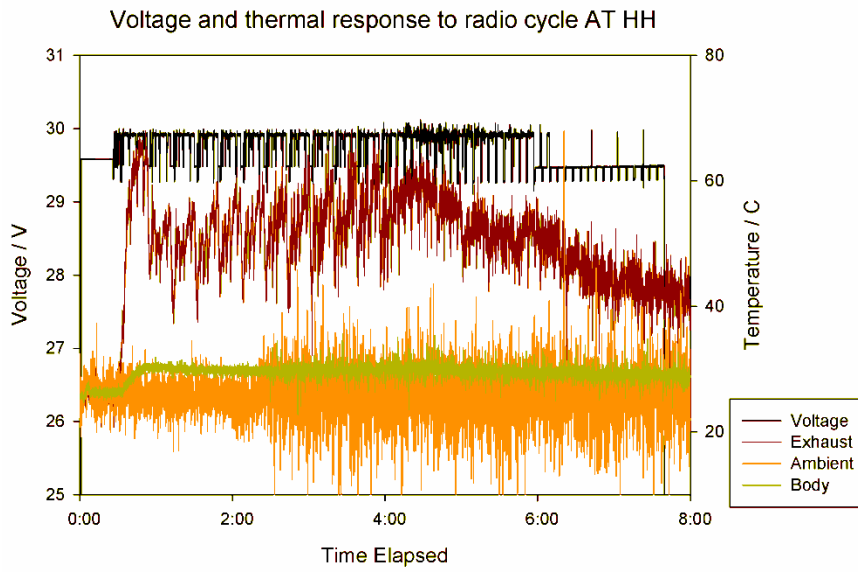


Figure 7-xxxix. Thermal response to transient cycle, AT HH, over 8 hours.

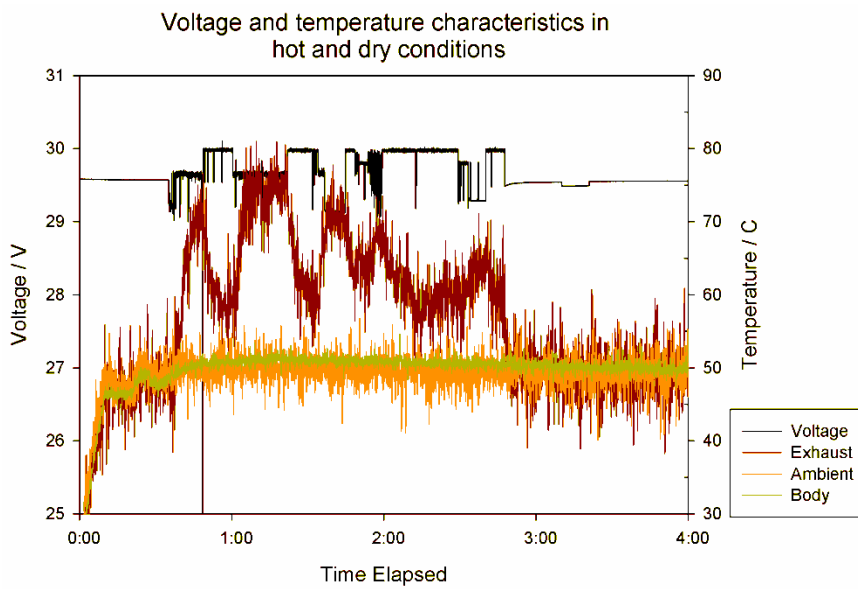


Figure 7-xl. Thermal response to load at 25W, 15W and 5W, HT LH, over 4 hours. Using desert fuel. See Figure 7-xxi.

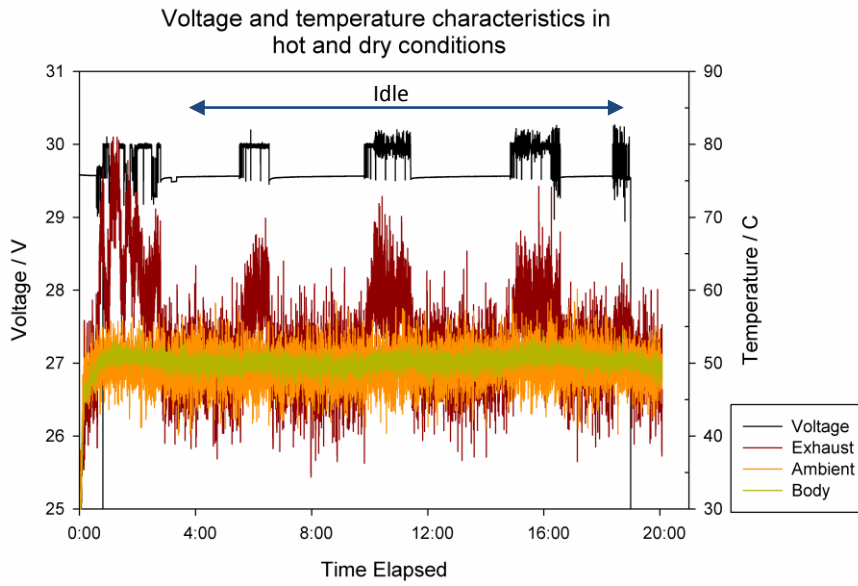


Figure 7-xli. Thermal response when idle, HT LH, over 20 hours. Using desert fuel.

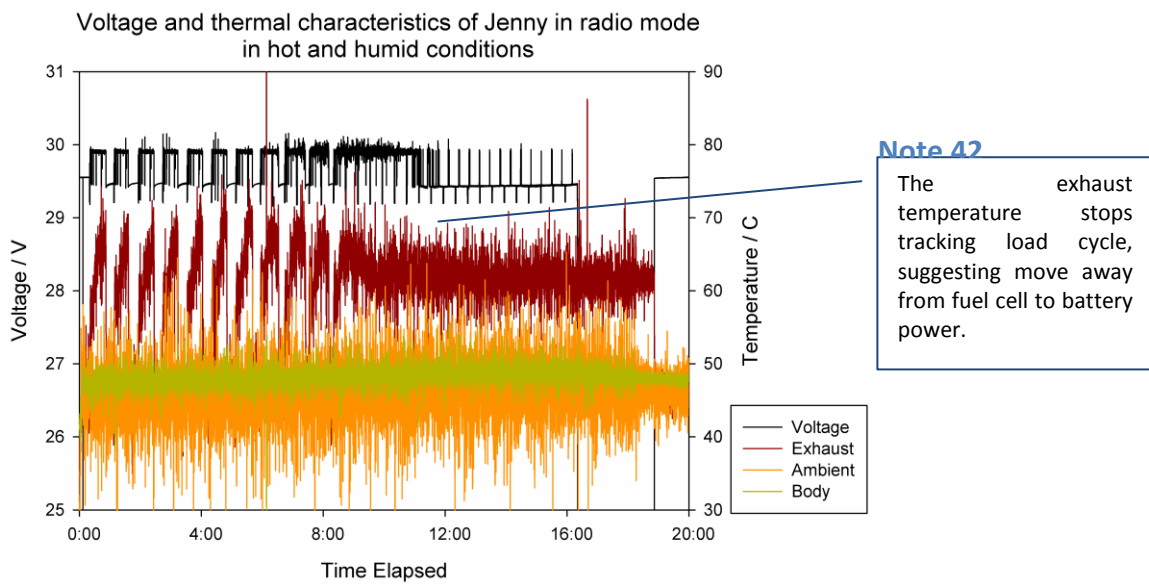


Figure 7-xlii. Thermal response to transient cycle, HT HH, over 20 hours. Using desert fuel.

7.2.3 Thermal imaging



Figure 7-xliii. Thermal image of Jenny 600S before application of load.

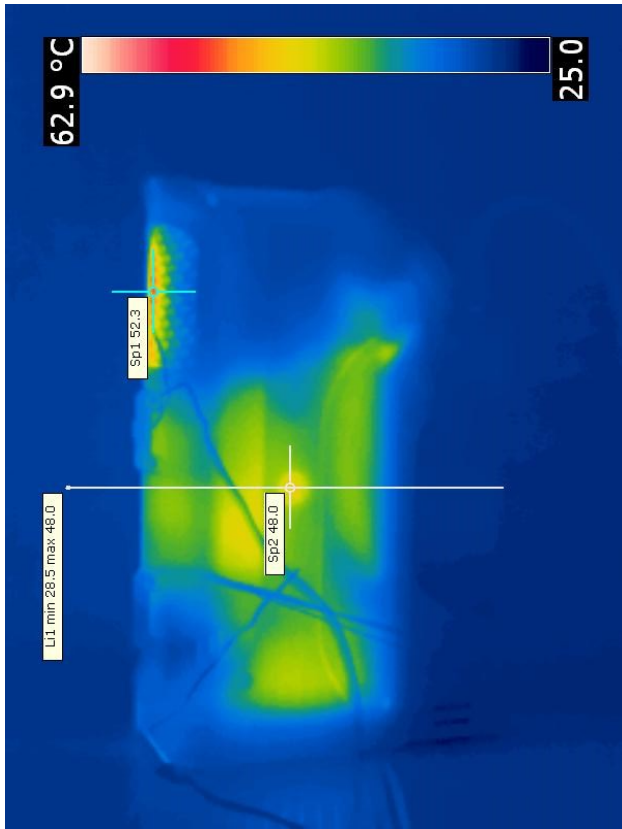


Figure 7-xliv. Thermal image showing peak temperature of Jenny 600S after application of 5W.

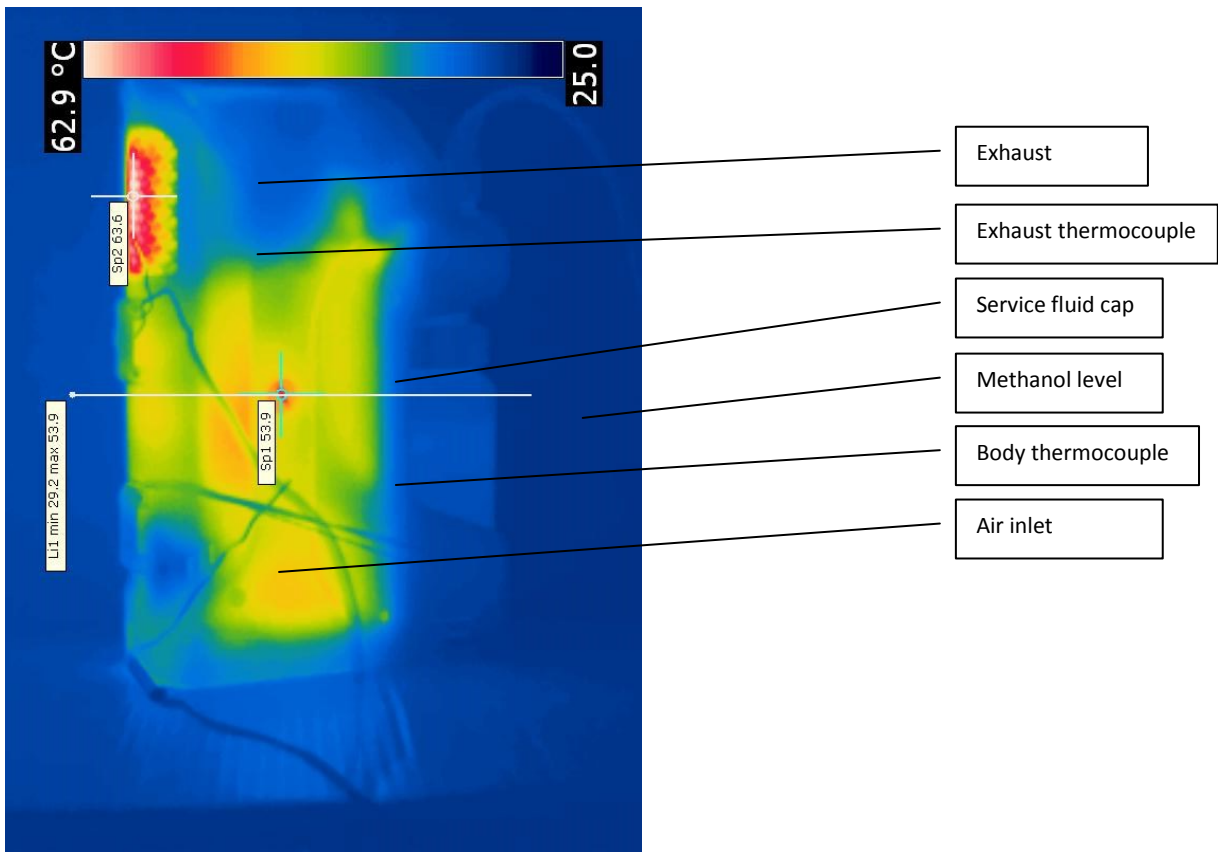


Figure 7-xlv. Thermal image showing peak temperature of Jenny 600S after application of 15W.

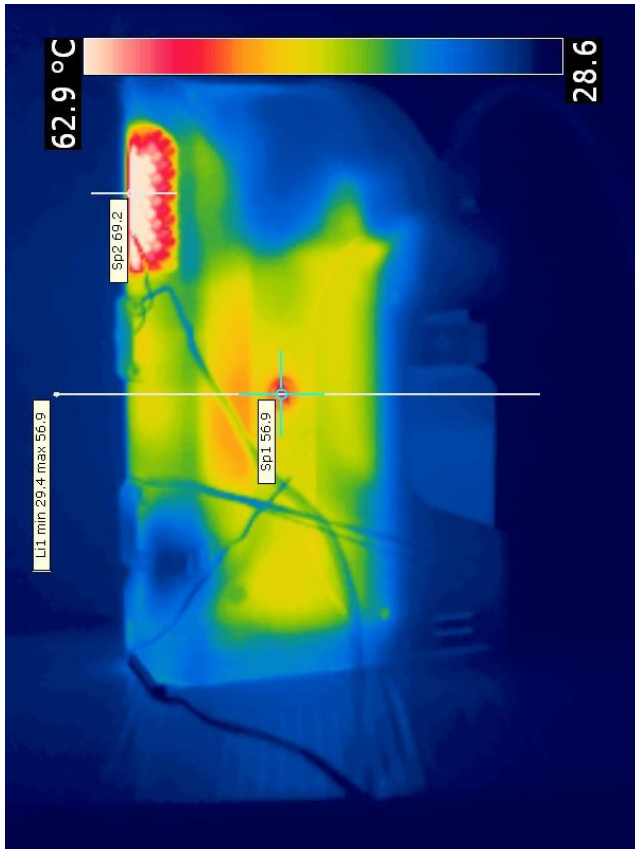


Figure 7-xlvi. Thermal image showing peak temperature of Jenny 600S after application of 25W. (Orientation 1)

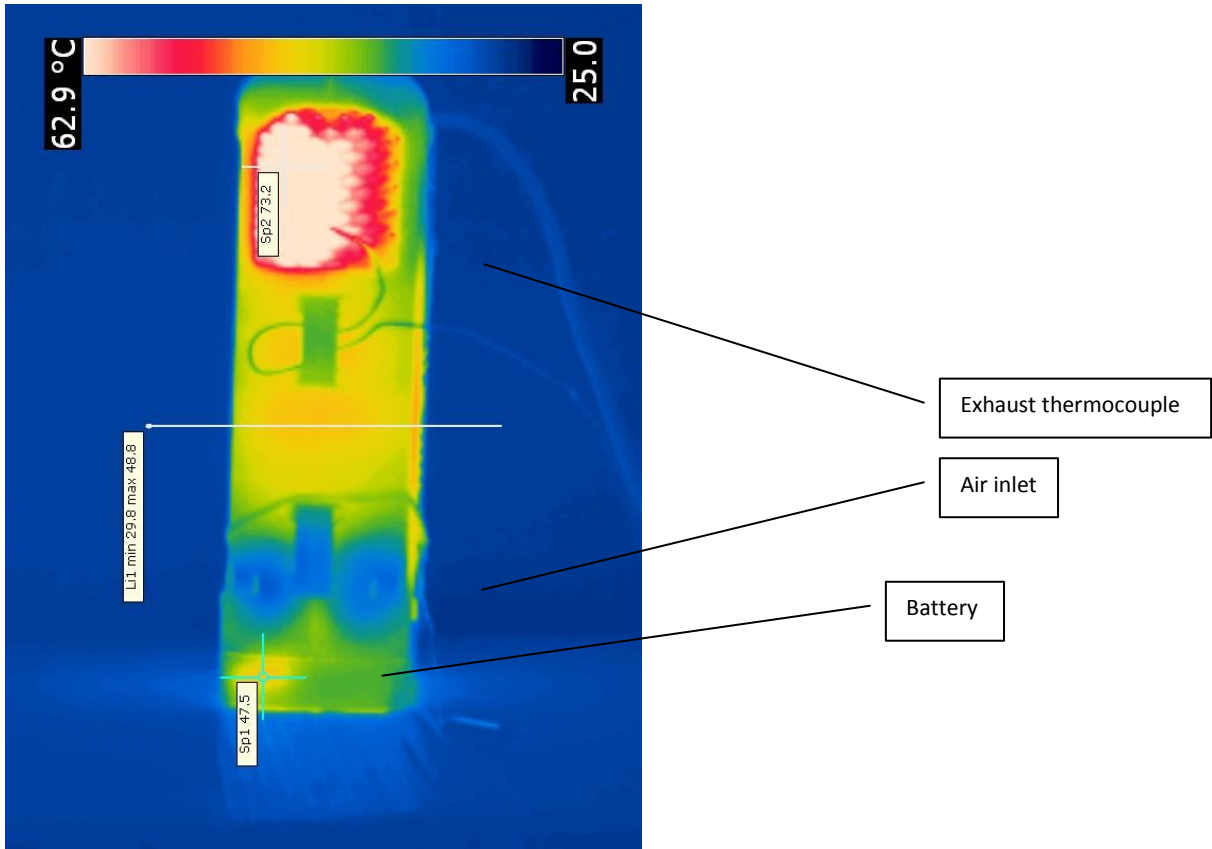


Figure 7-xxvii. Thermal image showing peak temperature of Jenny 600S after application of 25W. (Orientation 2)

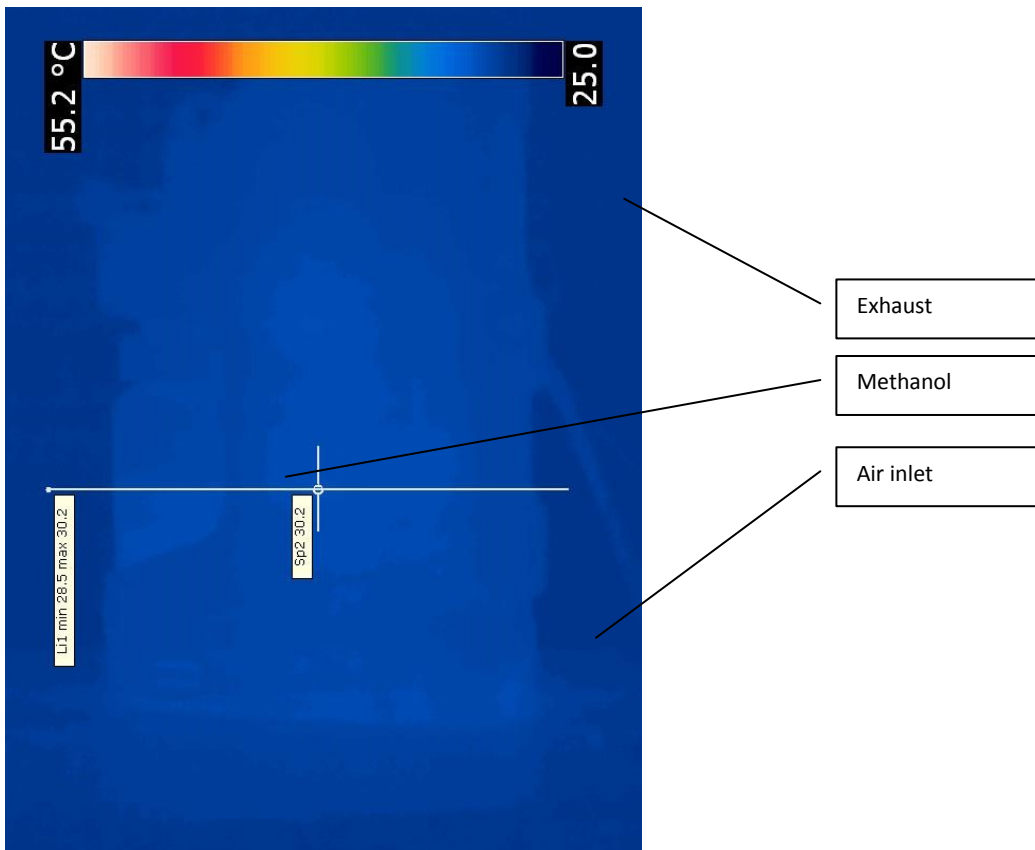
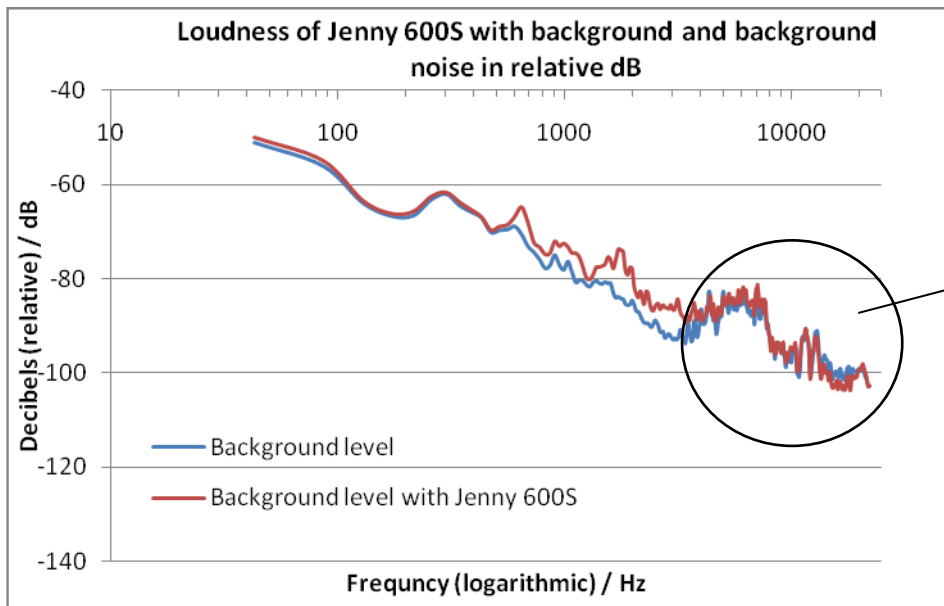


Figure 7-xxviii. Thermal image showing Jenny 600S as thermally invisible after cooling.

7.2.4 Acoustic signature



Note 43
 In this region there is a low signal to noise ratio, Jenny 600S may not emit in this region, this will cause unusual looking results in Figure 7-l and Figure 7-li

Figure 7-xlix. Sound levels recorded for background and Jenny 600S

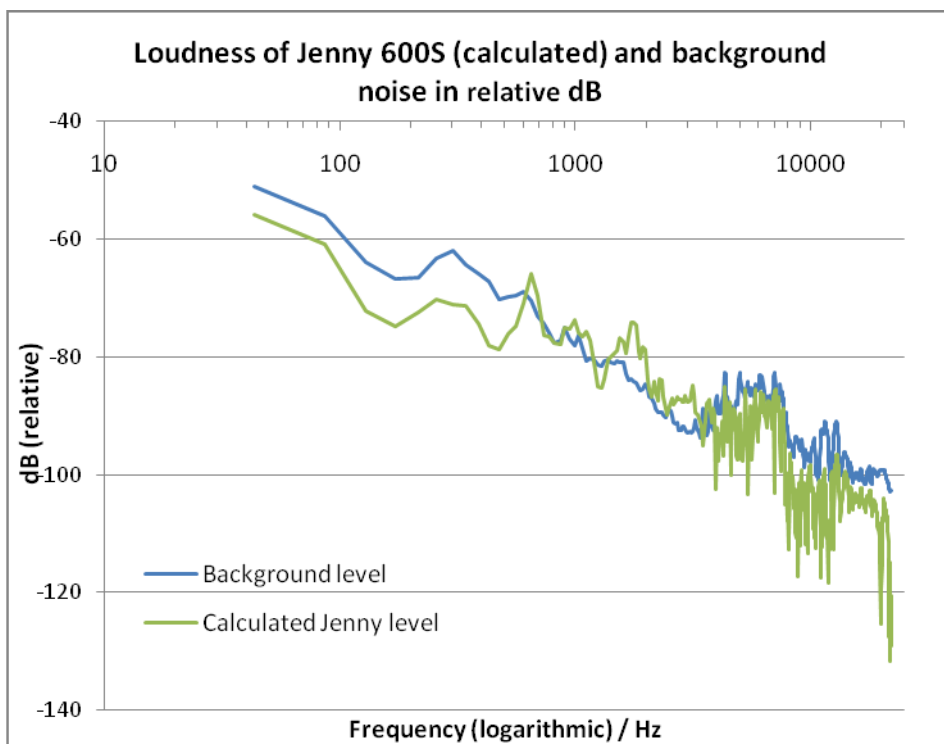


Figure 7-l. Sound levels recorded for background and calculated for Jenny 600S.

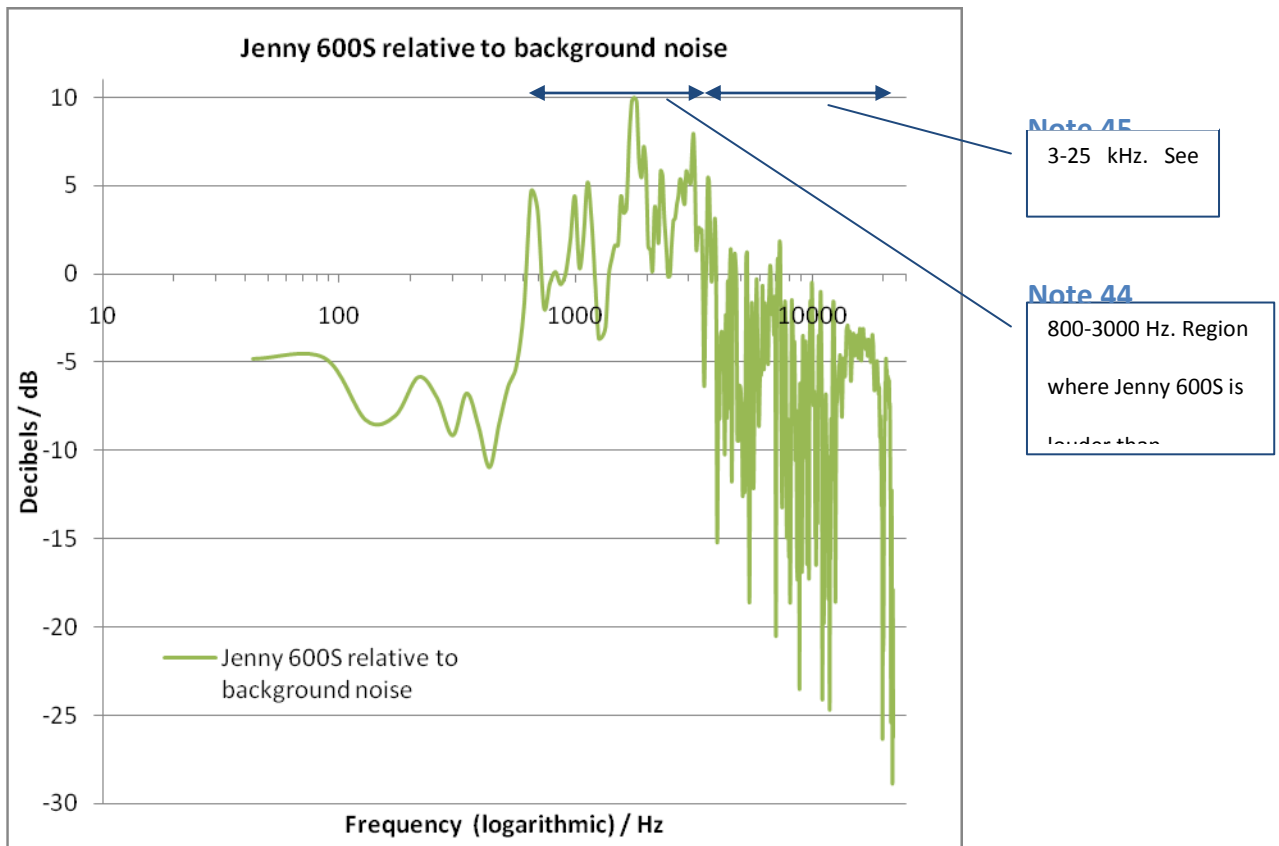


Figure 7-ii. Sound levels calculated for Jenny 600S with background noise set as baseline.

7.2.5 Fuel consumption

7.2.5.1 Regular Fuel, Steady State, Ambient Conditions

Table 7. Regular fuel consumption in ambient conditions

Mode	25W	15W	5W
Fuel Consumption (g/h)*	19.5	12.5	5
Fuel consumption (ml/h)#	24.6	15.8	6.3
Fuel consumption (l/kWh)#	0.98	1.05	1.26
Cartridge depletion time (h)#	14.2	22.2	55.6

*Measured #Calculated

7.2.5.2 Desert Fuel, Steady State, Ambient Conditions

Table 8. Desert fuel consumption in ambient conditions

Mode	25W	15W ¹	15W ²	5W
Fuel Consumption (g/h)*	34	19.5	24	8.5
Fuel consumption (ml/h) [#]	37.4	21.4	26.4	9.3
Fuel consumption (l/kWh) [#]	1.50	1.43	1.76	1.87
Cartridge depletion time (h) [#]	9.4	16.4	13.3	37.6

*Measured [#]Calculated ¹Unit mass change method ²Cartridge mass change method

Desert fuel is gravimetrically 13% more dense than regular fuel. Desert fuel is also 40% less energetically dense than regular fuel. As such the energetic efficiency was calculated to allow direct comparison.

Table 9. Conversion of desert fuel consumption into pure methanol consumption.

Mode	25W	15W ¹	15W ²	5W
Fuel Consumption (g/h)*	34	19.5	24	8.5
Pure methanol consumption (ml/h) [#]	22.4	12.9	15.8	5.6
Pure methanol consumption (l/kWh) [#]	0.90	0.86	1.06	1.12

*Measured [#]Calculated ¹Unit mass change method ²Cartridge mass change method

7.2.5.3 Steady state, ambient conditions, Fuel Comparison.

Table 10. Comparison of energetic efficiencies of regular and desert fuels

Mode	25W	15W ¹	15W ²	5W
Regular (methanol l/kWh) [#]	0.98	1.05	1.05	1.26
Desert (methanol l/kWh) [#]	0.90	0.86	1.06	1.12
Efficiency Δ ^{#+‡}	+8% (±2%)	+18% (±3%)	-1% (±3%)	+11% (±7%)

[#]Calculated ⁺Errors relate to max error in mass calculation [‡]Efficiency is that of desert fuel

over regular fuel

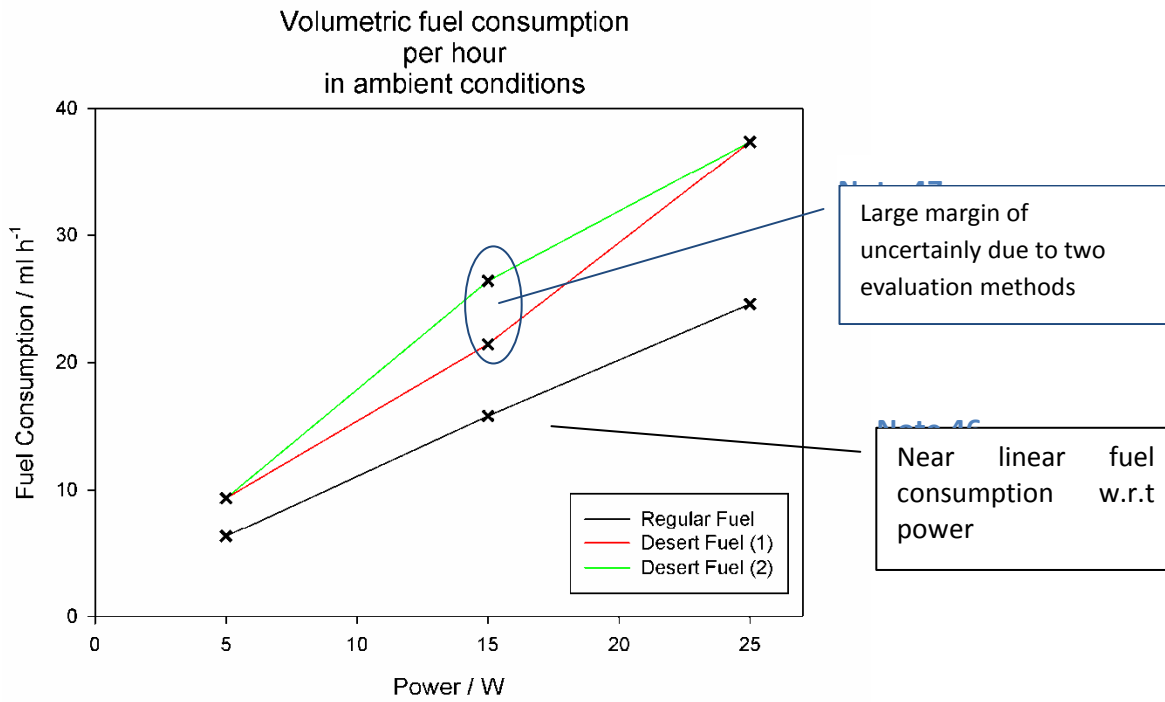


Figure 7-iii. Hourly volumetric consumption of fuel. Desert fuel consumption measured 2 ways.

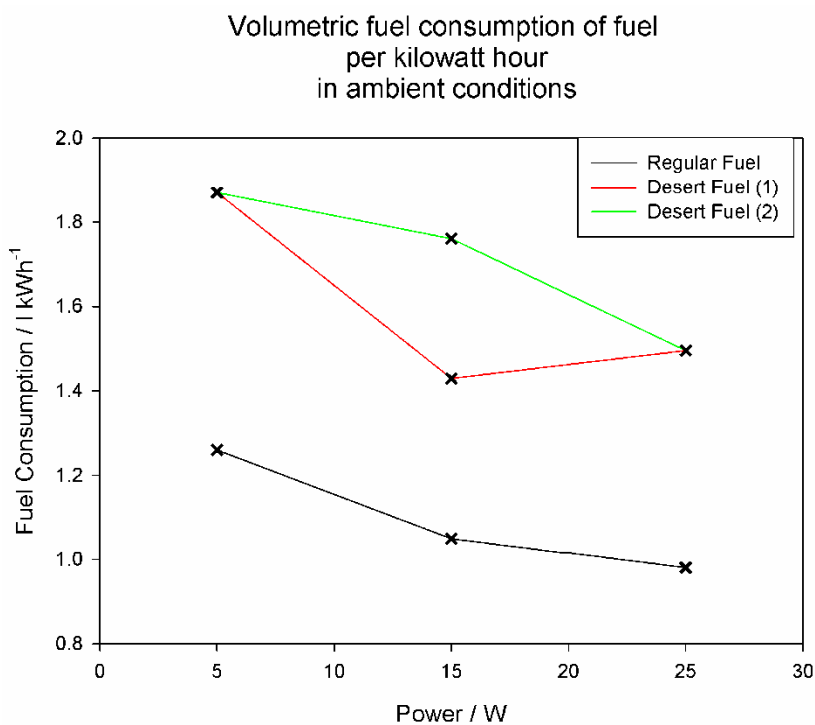


Figure 7-iii. Volumetric consumption of fuel per kilowatt hour. Desert fuel consumption measured 2 ways.

Volumetric consumption of pure methanol
per kilowatt hour
in ambient conditions

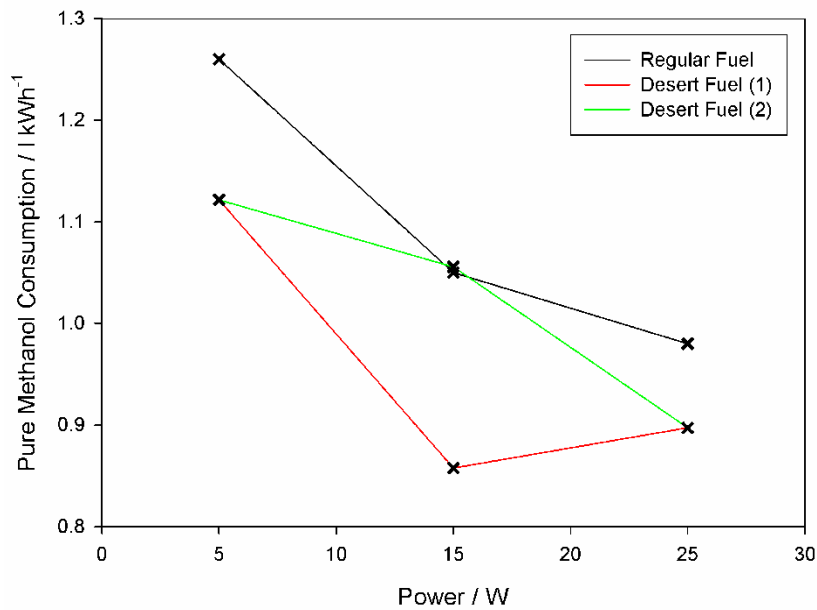


Figure 7-iv. Volumetric consumption of pure methanol per kilowatt hour. Desert fuel consumption measured 2 ways.

7.2.5.4 Regular Fuel, Transient State

Table 11. Regular fuel consumption in transient state

Mode	Ambient	AT LH [@]
Fuel Consumption (g/h)*	8.8	10.5
Fuel consumption (ml/h) [#]	11.1	13.3
Fuel consumption (l/kWh) [#]	1.34	1.85
Cartridge depletion time (h) [#]	31.5	26.3

*Measured [#]Calculated [@]Based on assumption (%)

7.2.5.5 Regular Fuel, Idle State, Ambient Conditions

Table 12. Regular fuel consumption when idle

Mode	0W [%]
Fuel Consumption (g/h) [#]	2
Fuel consumption (ml/h) [#]	2.5
Cartridge depletion time (h) [#]	140

Results [#]Calculated [%]Basis for assumption

7.3 Appendix iii -Poster

